Interaction of Metal Nanoparticles with Fluorophores and Their Effect on Fluorescence

Dissertation

zur Erlangung des akademischen Grades
Doktor der Naturwissenschaften
(Dr. rer.nat.)

eingereicht an der
Fakultät Mathematik und Naturwissenschaften
der Technischen Universität Dresden

von
Fuat Yigit Aksoy
aus Ankara

Gutachter:	1. Prof. Dr. Wolfgang Pompe
	2. Prof. Dr. Gerhard Rödel
	3. Prof. Dr. André Gorbunoff
Eingereicht am:	15.01.2009
Tag der Disputation:	27.03.2009

Part of this work was presented in:

Mkandawire M., Lakatos M., Krause-Buchholz U., Aksoy F.A., Springer A., Rödel G., Pompe W., 2008, Intracellular Delivery of Au nanoparticle labelled proteins, Nano-objetcs in living cells: from physics to physiology, Villeneuve d'Ascq, France

Lakatos M., Appelhans D, Aksoy F., Pompe W., 2008, Fluorescent Au clusters surrounded by dendritic oligosaccharide shells and their optical properties in water, Particles 2008, Orlando, USA

Aksoy F.Y., Gorbunoff A., Krause-Buchholz, U., Lakatos M., Pompe W., Rödel G., 2005, Bioconjugated metal nanoparticles for biophotonic studies, Biophotonik Symposium, Jena/Germany

Contents

Abbreviations

A	Ampere
acTEV protease	Enhanced Tobacco etch virus protease
AFM	Atomic force microscopy
Ag	Silver
AOT	bis(2-ethylhexyl)sulfosuccinate
Au	Gold
Au/AgNP	Gold/silver alloyed nanoparticle
AuND	Gold nanodot
AuNP	Gold nanoparticle
bp	Base pairs
CFP	Cyan fluorescent protein
Cu	Copper
Cy3/5	Cyanine3/5
Da	Dalton
DMEM	Dulbecco's Modified Eagle's Medium
DNA	Deoxyribonucleic acid
dNTP	Deoxynucleosidetriphosphate
eGFP	Enhanced green fluorescent protein
F	Farad
Fig	Figure
FM	Fluorescence microscopy
FP	Fluorescent protein
FPLC	Fast-performance liquid chromatography
FRET	Förster (or fluorescence) resonance energy transfer
g	Gravitational acceleration
GST	Glutathione S-transferase
HA	Hemagglutinin
HPLC	High-performance (or pressure) liquid chromatography
h	hour

HRP	Horseradish peroxidase
IgG	Immunoglobulin G
LB	Luria-Bertani broth
LSM	Laser scanning microscopy
LSPR	Localised surface plasmon resonance
min	Minute
ND	Nanodot (nanosphere with a diameter less than 2 nm)
NIR	Near-infrared
nm	Nanometer
NMR	Nuclear magnetic resonance
NP	Nanoparticle (nanosphere with a diameter more than 3 nm)
OD	Optical density
PCR	Polymerase chain reaction
pI	Isoelectric point
PPI	Poly(propyleneimine)
rPhiYFP	Recombinant yellow fluorescent protein from *Phialidium* species
RT	Room temperature
SbsC	Surface-layer protein from *Geobacillus stearothermophilus* species
SDS-PAGE	Sodium dodecyl sulphate polyacrylamide gel electrophoresis
SEM	Scanning electron microscopy
SOC	Super optimal broth, catabolite repression medium
TBE	Tris Borate EDTA
TBS	Tris-buffered saline
Tris	Tris(hydroxymethyl)aminomethane
UV/Vis	UV/Visible light
V	Volt
v/v	Volume per volume
W	Watt
w/v	Weight per volume
Ω	Ohm

Amino Acid Abbreviations

1-Letter	3-Letter	Name
A	Ala	Alanine
C	Cys	Cysteine
D	Asp	Aspartic acid (Aspartate)
E	Glu	Glutamic acid (Glutamate)
F	Phe	Phenylalanine
G	Gly	Glycine
H	His	Histidine
I	Ile	Isoleucine
K	Lys	Lysine
L	Leu	Leucine
M	Met	Methionine
N	Asn	Asparagine
P	Pro	Proline
Q	Gln	Glutamine
R	Arg	Arginine
S	Ser	Serine
T	Thr	Threonine
V	Val	Valine
W	Trp	Tryptophan
Y	Tyr	Tyrosine

Aim of the work

Usage of the peculiar properties of gold nanoclusters dates back as far as centuries B.C., when colloidal gold was used to decorate ceramics and later polychromatic glasses, and employed in medical treatments for various pathologies ranging from unstable mental and/or emotional states, to arthritis and tuberculosis. [Shaw C.F., 1999]. In 1857, Faraday reported the synthesis of "small" gold clusters via reduction from gold ions and a study about the optical properties of such clusters. In the recent decades, not only various synthesis methods for metallic nanoclusters have been developed, but also most of their optical and electronical properties have been illuminated. It is now clear that nanosized noble metal clusters demonstrate very different characteristics compared to bulk metals. Moreover, these properties earned them a place in many industrial applications. Perhaps the most notable and mostly researched property is the demonstration of surface plasmon resonance (SPR) and the strong absorption of electromagnetic radiation as a result of SPR. SPR has been so far utilised in chemical and bio-sensing, imaging, spectroscopy, and in targeted therapy [Phillips K.S. and Cheng Q., 2007].

Molecular fluorescence based measurements and devices are widely employed in fields such as chemistry, molecular biology, materials science, photonics, and medicine. Applications as varied as single molecule detection, automated DNA sequencing and examination of circulation in the heart and retina [Frangioni J.V., 2003] represent the vastness of the potential applications of fluorescence. Regardless of the nature of the application, most of such systems rely directly on the inherent brightness of the molecular fluorophore for the detection sensitivity [Tam F., *et al.*, 2007]. Especially, fluorophores with emission in the range between 500-700 nm have been proven to be valuable tools in biosensing/imaging for disease screening, diagnosis, and monitoring due to the fact that most biological systems generate autofluorescence noise minimally at these wavelengths [Berlier J.E., *et al.*, 2003]. The ability to enhance the emission of such fluorophores is greatly desired in order to increase the sensitivity of detection and to reduce the signal to noise ratio. On the other hand, the ability to turn off or to quench the signal from a certain fluorophore might be advantageous in the case of multiple fluorescent tag employing assay systems.

It was first suggested by Purcell in 1946, that spontaneous emission could be modified by resonant coupling to the external electromagnetic field. Since then amplified and inhibited spontaneous emission have been observed from semiconductor quantum wells integrated into microstructures, photonic crystals, and fluorophores near metal surfaces and nanoparticles [Härtling T., *et al.*, 2007].

For the detection of a biological molecule (an antigen) there are two mechanisms: the change of fluorescence signal from the bioconjugated nanoparticle, and the shift of the localised surface plasmon resonance (LSPR) of the gold nanoparticle. However, in such a hybrid system there are various additional processes which have a potential to influence the above mentioned signals. Firstly, the overlap of the excitation spectrum of the fluorophore and LSPR of the nanoparticle can cause an energy transfer which in turn can create additional resonances or cause the quenching of the fluorophore. Furthermore, the high electric field around the gold nanoparticle could yield to an enhancement of both mechanisms. Finally, there is also the possibility, that a change in the environment can pose an additional influence on the measured signal(s). A very critical application in that sense would be the application of such a bioconjugated gold nanoparticle employing assay for intracellular measurements, where the stability of the bioconjugates during intracellular delivery becomes important.

In this work I tried to observe the effects of various noble metal nanoparticles on the emission of two fluorescent proteins, namely the enhanced green fluorescent protein (eGFP) and the yellow fluorescent protein (rPhiYFP); and to develop an example for an application of such a nanoparticle based fluorescence modifying *in vitro* system. Additionally the final part deals with the intracellular delivery and use of nanoparticles as fluorescence reporters *in vivo*.

Formulated bioassay method

The main intention of this work is to study the potential of bioconjugated gold nanoparticles for biosensing/bioassay applications, in which the interaction of an antigen is monitored in terms of plasmon peak shift and fluorescence change. The model is illustrated in the following scheme (Fig. 1).

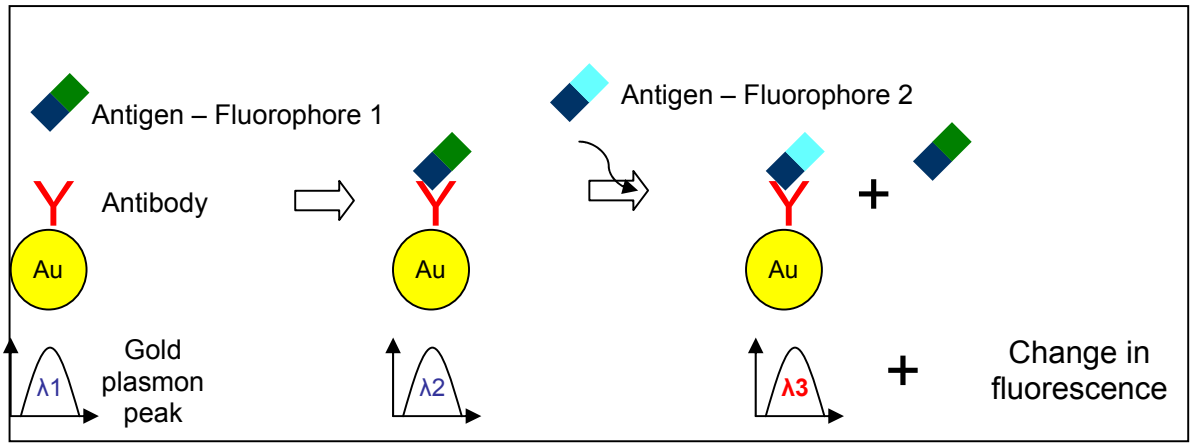

Figure 1. Gold nanoparticles are functionalised with a specific antibody and the antigen is labelled with a fluorophore. Binding of the labelled antigen to the antibody will cause a shift in the plasmon peak. Upon introduction of the same antigen labelled with a different fluorophore, it is expected to get a further change in the plasmon peak and a change in the fluorescence signal.

1 Introduction

1.1 Nanobiotechnology and Metallic Nanoparticles

The word nanobiotechnology describes the use of nanotechnology in biological systems. Although the field itself is considered to be relatively new, nanotechnology is already having an impact in bioanalysis, where nanoparticles of various sizes, shapes, and compositions are being used to replace "traditional" bioanalysis schemes [Penn S.G., *et al.*, 2003]. The field nanobiotechnology spans a vast area of application, and not all of the subfields necessarily involve the use of nanoparticles, which constitutes the backbone of this thesis.

As stated above, the field of nanotechnology deals with research and technology development in the length scale range approximately 1 to 100 nm and designing and using systems and devices characterised by novel properties arising from their size and shape. Applicative uses of nanotechnology are in general still very limited, but nanoparticles have already found many industrial applications including: electronic, optoelectronic, biomedical, pharmaceutical, cosmetic, catalytic, and material areas and made their way into various products.

The impressive range of interests and applications of nanoparticles arises from the versatility and tunability of their properties. It is well known that properties of bulk materials change as their size goes down to small aggregates, even down to a few atoms [Kubo R., 1962]. Metal and semiconductor bulk properties can be explained referring to electrons that occupy energy bands, whereas in single atoms electrons are distributed in discrete energy levels. When only a few atoms are linked together forming very small clusters with dimensions in the range of a few nanometers, their electronic configuration lays somewhat in between; it dramatically depends on the size of nanoparticles and can only be explained by quantum mechanics. In other words, the electronic (optical, electrochemical, magnetic, and catalytic) properties of nanoparticles differ from those of bulk materials because their valence electrons experience different energies and distributions [Li X.-B.., *et al.*, 2007]. These properties of such small clusters depend not only on the material but also on their size and shape, besides the environmental conditions that their

surfaces experience. Furthermore, many different capping agents can be used to derivatise their surface tailoring their properties such as solubility or affinity [Bakshi M.S., *et al.*, 2007].

Among the different kinds of nanoparticles, the ones consisting of gold are extensively studied for several reasons. First of all, their synthesis is straightforward. Secondly, they are very stable; perhaps the most stable among metallic colloids. Finally, they present very peculiar electronic, magnetic, and optical properties related to their size.

1.1.1 Synthesis of gold and silver nanoparticles

The first systematic synthesis of pure nanosized Au was introduced by Michael Faraday in 1857. In his classical work, Faraday reduced AuCl with phosphorous into Au nanoparticles. On the other hand, unlike the synthesis of Au nanoparticles, synthesis of Ag nanoparticles is conceptually rather new. As of now, a large number of well established methods for the synthesis of both nanoparticles have been made available [Biju V., *et al.*, 2008]. Some of the most commonly used methods for NP synthesis are shown in Fig. 2.

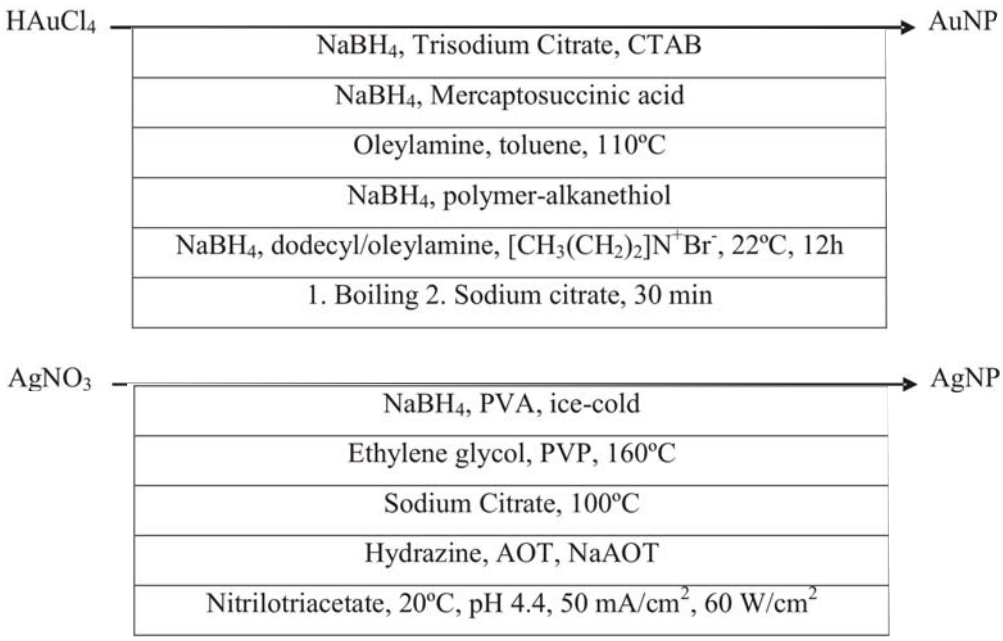

Figure 2. Some selected methods for Au and Ag nanoparticle synthesis.

1.1.2 Optical Properties of metallic nanoparticles and localised surface plasmon resonance (LSPR)

Interaction of light with nanostructured metal films and nanoparticles, i.e. light waves coupled to free electrons on a metal surface, can give rise to hybrid surface waves, broadly termed as surface plasmons. The so-called surface plasmons demonstrate the ability to confine light at a metal/dielectric interface, which can either localise or propagate depending upon the dimensionality of the nanostructured material. The confinement of light, which is responsible for the peculiar optoelectronical properties of such nanomaterials, results from the collective oscillation of conduction electrons at the metal surface. The surface of a metallic nanoparticle contains free and mobile conduction electrons. In the presence of electromagnetic radiation, the free electrons are displaced by the electric vector and the columbic attraction between the electron cloud and nuclei becomes the main restoring force. As a result of the oscillating nature of the electric field of light, the electron clouds coherently oscillate over the surface with a ceratin resonance frequency. Nanostructured systems of noble metals such as silver and gold are of great interest since their localised surface plasmons resonate at the optical wavelength of electromagnetic radiation [Pastoriza-Santos I., *et al.*, 2006 and Talley C.A. *et al.*, 2005].

The surface plasmons are broadly classified as propagating surface plasmons and localised surface plasmons. Propagating surface plasmons (often called surface polaritons) are associated with smooth, thin films of gold and silver wherein the plasmon feels a boundary due to the planar surface. The surface plasmon in such a metal/dielectric interface has a combined electromagnetic wave as well as surface charge character and is highly bound to the surface (Fig. 3A). As a result of the combined character, an enhanced field is observed near the surface in the perpendicular direction, the amplitude of which decays exponentially with the distance from the surface and is said to be evanescent or near-field in nature. Once surface plasmons are generated on a flat metal surface they can propagate, however they gradually attenuate due to the loss arising from the absorption in the metal. This can be minimised using several methods, however, since this type of surface plasmons are not within the scope of this work, more detail will not be presented. The phenomenon of propagation, serving the basis behind the ability of such nanostructures to trap, concentrate, and channel light has potential applications in optical devices, spectroscopy, chemical and biosensing [Barnes W.L., Dereux A. and Ebbesen T.W., 2003].

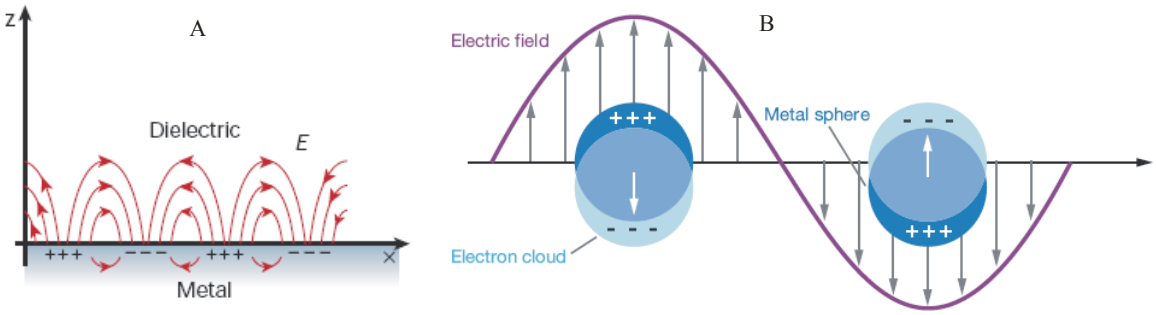

Figure 3. Surface plasmons at the interface between a metal and a dielectric material having a combined electromagnetic wave and surface charge character. Picture taken from Barnes W.L., Dereux A. and Ebbesen T.W., 2003 (A); Schematic illustrating a localised surface plasmon. Picture taken from Willets K.A. and Van Duyne R.P., 200/ (B).

In contrast to the propagating nature of surface plasmons on a planar metal/dielectric interface, the electron plasma in metal nanoparticles is contained in a finite volume, which is smaller than the wavelength of light. Localised surface plasmons originate from the collective oscillation of free electrons, confined at the surface of metallic nanoparticles, when excited with electromagnetic radiation (figure 3B). Unlike bulk materials, the surface plasmons in metallic nanoparticles, especially Ag, Au, and Cu, can be directly excited by light in the visible region. Absorption of electromagnetic radiation occurs when incident photon frequency is in resonance with the collective oscillation of the conduction electrons, resulting in unique optical properties. In 1908, Gustav Mie provided a quantitative description of the resonance for spherical particles [Liou K.-N., 1977]. According to Mie theory, the total cross section consists of scattering and absorption (often referred to as extinction) and is given as summation over all electric and magnetic oscillation. The contribution of absorption and scattering mainly depends on the size and shape of the particles and the dielectric constant of the medium (Fig. 4 and 5) [Pal A., *et al.*, 2004].

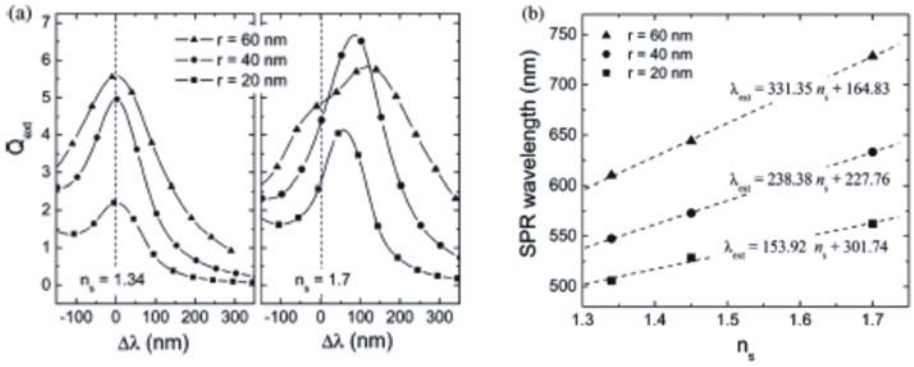

Figure 4. (a) Calculated spectra of optical extinction efficiencies for gold nanoparticles with three different radii (20, 40, and 60 nm) as a function of the relative wavelength shift in response to the refractive index change in surrounding medium from 1.34 to 1.7. (b) Size dependence of the SPR wavelength response to change in the refractive index of the surrounding medium. The sensitivity is estimated from the slope of this linear plot. [Figures taken from Lee K-S. and El-Sayed M.A., 2006]

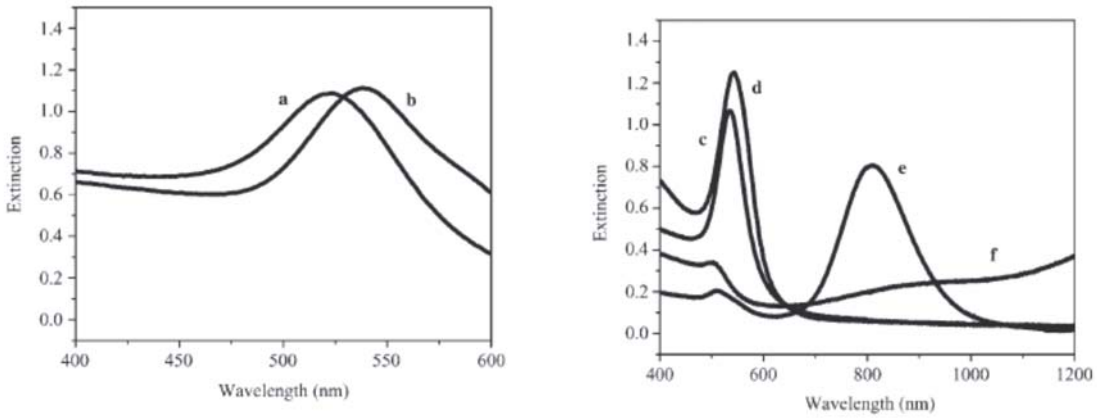

Figure 5. Extinction spectra of gold nanoparticles: a) 23-nm-diameter spheres, b) 70-nm-diameter spheres, c) hexagons, d) cubes, e) rods (aspect ratio ~4.4), f) rods (aspect ratio ~16) [Figures taken from Orendorff C.J., *et al.*, 2006].

1.1.3 Binding proteins to nanoparticles and evidencing the binding event

With the recent development of biotechnology, bioconjugates of nanoparticles have received considerable research interests because the obtained hybrid biomaterials own unique properties provided by the gold nanoparticles. The stabilization and functionalisation of gold nanoparticles with a biomolecular recognition motif have provided flexibility for a variety of applications, including bioassays, bioimaging and biosensing. As a result, the ability to synthesize aqueous-stabilized nanoparticles of controlled size and shape that can be easily functionalized with biomolecules (peptides, enzymes, antibodies, DNA) is highly desirable.

It is well established that many functionalities can bind to metallic gold, including sulphur-containing moieties such as thiols, thioethers, thioesters, disulfides, isothiocyanates, and then phosphines, amines, citrate, carboxylates, yielding, in all cases, a passivation of the surface that stabilizes nanoparticles preventing their coalescence, although each of these confer a different degree of stability.

For the validation and demonstration, of whether above-mentioned organic molecules used as capping agents are actually bound to the nanoparticle surface, several methods are available. These methods rely on the fact that the capping process is based on the interaction of the approaching molecules with the electrons of the external atoms of the nanoparticles, inducing rearrangements of their electron density. Therefore, upon successful binding, the NMR spectra of the molecules adsorbed on the surface are altered [Thomas K.G. *et al.*, 2002].

However, the most straightforward ways to probe molecular binding to the surface are photophysical techniques, i.e. UV/Visible absorption measurements. The ligands on the nanoparticle surface demonstrate a refractive index or dielectric constant change in the immediate vicinity of the nanoparticle surface and therefore perturb the shape and position of the localised surface plasmon band (LSPB), which - as explained above - is determined by free electrons occupying the outer conduction band [Kreibig U. and Vollmer M, 1995]. The capping moieties are expected to cause a shift of the LSPB as compared to uncapped nanoparticles, and the changes are expected to be larger with increasing strength of the binding event. There are two ways to evaluate changes in the plasmon spectra caused by target binding: wavelength change of the plasmon peak or extinction/absorption intensity change at a fixed wavelength [Englebienne P., *et al.*, 2000]. In the case the plasmon peak upon target binding is very small due to low signal/noise ratio the latter is often used as an indicator. However, the second approach has an inherent problem: the change in extinction intensity could also occur due to a change in particle concentration, i.e. because of several washing steps, contributing to the noise. Therefore, the wavelength shift of the plasmon band has a greater potential for biosensing [Marinakos S.M., *et al.*, 2007]. For an example of this kind of a sensor and plasmon band shift please refer to section 1.3.1.2

1.1.4 Formular expression of dependency of LSPR peak on the dielectric constant of the medium

The LSPR peak depends on the refractive index of the surrounding medium (n) and can be determined by the following equation [Mulvaney. P., 1996]:

$$\frac{\lambda^2}{(1+\frac{\varpi_d^2 \cdot \lambda^2}{4\pi^2 c^2})} = \lambda_p^2 \left(\varepsilon^{\infty} + 2\varepsilon_m\right) \qquad \text{(Eq. 1)}$$

where, λ_P is the bulk plasma wavelength, ε^{∞} is the high-frequency dielectric constant due to interband and core transitions, ϖ_d is the relaxation or damping frequency, c is the vacuum light velocity, and ε_m is the dielectric constant of the medium, which is related to the refractive index of the medium by the following formula:

$$n = (\varepsilon_m)^{1/2} \qquad \text{(Eq. 2)}$$

The particle size R influences the damping frequency ϖ_d. It depends on an effective radius R_{eff} as

$$\varpi_d = \frac{v_{Fermi}}{R_{eff}} \qquad \text{with} \qquad \frac{1}{R_{eff}} = \frac{1}{R} + \frac{1}{R_{MFP}} \qquad \text{(Eq. 3)}$$

where R_{MFP} is the mean free path of the electrons in the bulk material.

For small damping frequency (large particles) with $\frac{v_{Fermi}\lambda}{2\pi c R_{eff}} << 1$ equation 1 tends to

$$\lambda^2 = \lambda_P^2(\varepsilon^{\infty} + 2\varepsilon_m) \qquad \text{(Eq. 4)}$$

describing the plasmon resonance for the bulk material. Equation 1 and equation 4 hold true for Au nanoparticles lacking a capping agent. However, in most of the cases Au nanoparticles are stabilised by capping agents in solutions. By involving the contribution of the monolayer, equation 4 was modified as follows [Templeton A.C. *et al.*, 2000]:

$$\lambda^2 = \lambda_P^2\{\varepsilon^{\infty} + 2\varepsilon_m + [2g(\varepsilon_s - \varepsilon_m)/3]\} \qquad \text{(Eq. 5)}$$

where, ε_s is the dispersionless optical dielectric function of the shell (capping agent), g is the volume fraction of the shell layer. For very small Au nanoparticles, the equation relating to the

position of the LSPR peak is given by equation 5; and according to that formula the size of the core and organic shell becomes comparable and g value is large. Therefore, the solvent refractive index effect is quite small for Au nanoparticles with a diameter less than ~2 nm and it becomes more important with increasing nanoparticle diameter.

$$\lambda^2 = \lambda_P^2\{\varepsilon^\infty + 2\varepsilon_s + [2f\,\varepsilon_s(\varepsilon_m - \varepsilon_s)/(\varepsilon_s + 2\varepsilon_m)]\} \quad \text{(Eq. 6)}$$

where, f is the core volume fraction and is represented by:

$$f = (1 - g) \quad \text{(Eq. 7)}$$

For values of f = (1 – g) = 0.05, the surface plasmon mode remains constant at a certain value and loses its sensitivity to solvent refractive index changes.

1.1.5 Bimetallic silver-gold alloy nanoparticles

Alloy nanoparticles exhibit unique electronic, optical, and catalytic properties that are different from those of the corresponding individual metal nanoparticles [Kariuki N.N., *et al.* 2004]. Their chemical and physical properties can be tuned by varying the composition and atomic ordering as well as the size of the clusters. Nanoalloys may not only demonstrate “magic sizes” but also “magic compositions”, i.e., sizes and compositions at which the alloy nanoparticles present a special stability. Surface structures, compositions, and segregation properties [Ruban A.V., *et al.*, 1999] of nanoalloys are also of interest as they are important in determining chemical reactivity and especially catalytic activity.

Nanoalloys might also exhibit certain properties due to finite size effects, e.g., pairs of elements (such as iron and silver) which are immiscible in the bulk but readily mix in finite clusters [Andrews M.P. and O’Brien S.C., 1992].

Bimetallic nanoalloys can be generated with, more or less, controlled size and composition (figure 6). The nanoparticle structures and degree of segregation of the atoms making up the nanoalloy or mixing may depend on the method and conditions of cluster generation (type of

cluster source, temperature, pressure, etc.). Nanoalloys can be generated in a variety of media, such as cluster beams, colloidal solutions, immobilized on surfaces, or inside pores.

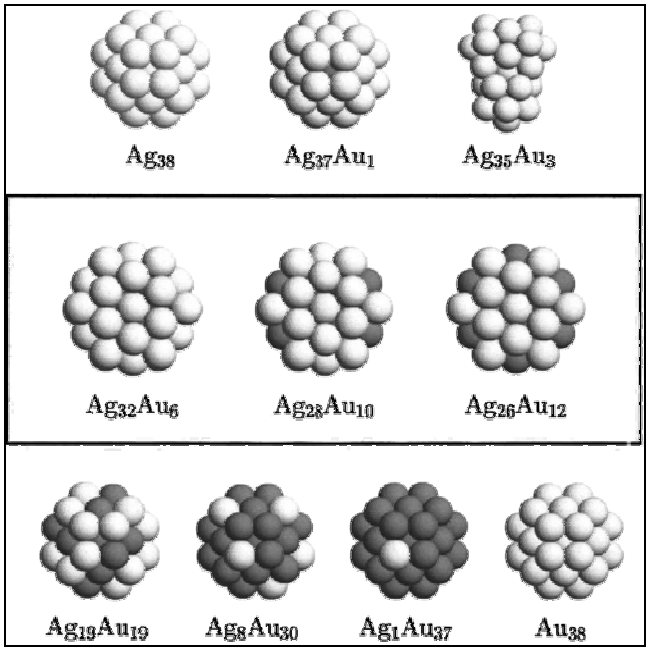

Figure 6. Snapshots from the 38-atom Ag-Au sequence. Light and dark gray spheres correspond to Ag and Au atoms, respectively. In the first row, the first two global minima of the sequence are truncated octahedral structures, while a core-shell disordered structure is located at $Ag_{35}Au_3$. In the box, the cluster $Ag_{32}Au_6$ is the perfect sixfold pancake, and this perfect structure is the best up to $Ag_{26}Au_{12}$. Thereafter, all the global minimum structures are truncated octahedra, with silver atoms preferentially occupying vertex or edge positions [picture taken from Rossi G., *et al.*, 2005].

Most of the experimental interest has centered on the optical properties of silver-gold nanoalloys; for example, how the shape and frequency of the plasmon resonance of Ag-Au nanoparticles vary with composition and the degree of segregation or mixing [Kreibig U. and Vollmer M., 1995]. In addition to the optical applications, there is also interest in improving the selectivity of the activity of silver or gold counterpart, for instance the differences in the DNA binding capability of silver and gold counterparts of an alloyed nanoparticle. Core-shell type particles can also be generated by chemical or electrochemical deposition of one metal onto a preformed cluster of the other. Optical measurements on these core-shell nanoparticles have revealed that the surface plasmons of the bimetallic nanoparticles are broad and complex. On the other hand, intermixed Ag-Au nanoparticles show a single plasmon resonance, as for pure metals. For intermixed clusters of fixed size, experiment and theory agree that the plasmon peak varies smoothly with

composition between that of pure Ag and pure Au nanoparticles: red shifting with increasing Au content (figure 7) [Bruzzone S., *et al.*, 2003]. Alloyed Ag-Au nanoparticles also demonstrate increasing plasmon frequency with decreasing size, with the rate of increase of frequency being intermediate between that of pure large Au and pure small Ag nanoparticles [Voisin C., *et al.*, 2000].

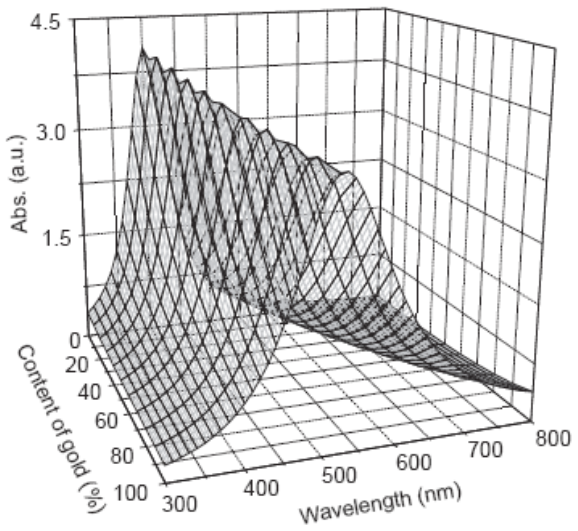

Figure 7. Calculated absorption cross-section versus wavelength for Au-Ag alloyed nanoparticles with different relative Au composition. With the increasing Au content, the absorption peak shifts towards red [picture taken from Jian Zhu, 2005].

Experimentally, it is challenging to obtain detailed internal structural information for bimetallic Ag-Au nanoparticles. Due to the small difference in the lattice constants of Ag and Au, direct lattice imaging using high resolution electron microscopy is not very informative. For particles with a diameter of 10 nm or above, chemically sensitive diffraction contrast can be used to determine the elemental separation inside the particles by making use of the difference in the extinction distances in Ag and Au metals [Srnová-Sloufová I., *et al.*, 2000].

1.1.6 Autofluorescent gold nanodots

Autofluorescence from gold nanoparticles was predicted to some degree as early as in 1969 [Mooradian A., 1969]. After some studies relating the fluorescence to roughness and other factors [Boyd G.T., *et al.*, 1986], the phenomenon was finally correlated to the electronic structure only in 1988 [Penn D.R. and Apell P., 1988]. Excitation was then related to transitions from occupied

d bands to states higher in energy. On the other hand, emission was related to the reoccupation of the hole created by the excitation of the d band electron with another from an occupied sp band.

In one of the earliest synthesis of autofluorescent germanium colloids stabilized with nonfluorescent moieties, a quantum yield of 10^{-4}-10^{-5} for the emission observed at 440 nm upon excitation at 230 nm was reported [Wilcoxon J.P., *et al.*, 2001]. By the use of size-exclusion liquid chromatography, size-dependency of the fluorescence was investigated, showing that no fluorescence was detectable for clusters exceeding a diameter of 5 nm; which suggests that quantum effects are important in the autofluorescence of such metallic nanoparticles.

Higher quantum fluorescence efficiency was reported for water soluble, 1.8 nm diametered gold nanoclusters, which are protected with tiopronin thiolate [Huang T. and Murray R.W., 2001]. The same authors also investigated the fluorescence by varying the thiolate ligands in order to relate the fluorescence to the protecting agent. It was found that the fluorescence band energy and intensity were affected by the nature of the protecting agent.

Although certain parameters, on which the fluorescence of gold nanoclusters depends, have been identified, the exact mechanism of this phenomenon is yet to be clarified. Most of the systems reported in the literature, even the apparently similar ones, present very different photophysical properties and the various authors explain them suggesting different models. However, it is believed that the phenomenon is due to the transitions within different electronic levels in the broadest sense.

1.2 Optical Interaction of Nanoparticles with Fluorescent Molecules

Metallic nanoparticles are known to drastically modify the spontaneous emission of nearby fluorescent molecules and materials [Tam F., *et al.* 2007]. Over the past few years, research has focused on determining the form, the extent, the fundamental properties underlying, and the parameters affecting the modification. Especially enhancement of molecular fluorescence has been of great interest due to the widespread popularity of molecular fluorescence based measurements and devices. Applications spanning diverse range of fields such as chemistry, molecular biology, materials science, photonics, and medicine all rely directly on the inherent brightness of the molecular fluorophore for detection sensitivity [Weiss S., 1999 and Painter O.,

1999]. Two examples to such methods are single molecule detection and automated DNA sequencing.

The fluorescent emission of molecules can be influenced by metallic nanoparticles in several ways:

1. By enhancing the optical intensity incident on the molecule via near field enhancement: At the plasmon resonance wavelength of a metallic nanoparticle, the light intensity in the near field of the nanoparticle is enhanced strongly relative to the incident optical wave [Dulkeith, E., 2002].
2. By modifying the radiative decay rate of the molecule [Kitson S.C., *et al.*, 1995 and Aslan K., *et al.*, 2005].
3. By increasing the coupling efficiency of the fluorescence emission to the far field through nanoparticle scattering [Szmacinski H., *et al.*, 2005].

1.2.1 Quenching of fluorophores linked to nanoparticles

One of the best defined types of fluorescent signal modification documented in the literature is the quenching of fluorescence by the presence of nanoparticles in the vicinity. In 1999, Murray and co-workers demonstrated the strong quenching of the emission from the fluorescein moiety by spectrofluorometric measurements when 5-(aminoacetoamido)-fluorescein was bound to tiopronin protected gold nanoparticles. One year later in the same group the dependence of quenching on the distance between the fluorophore and gold nanoparticle was demonstrated, simply by stabilizing the gold nanoparticles with a mixed monolayer of alkanethiolate and alkanethiolate derivatised with fluorescent dansyl groups and then varying the length of the alkyl linker and monitoring the fluorescence. [Templeton A.C., *et al.*, 1999] Their results indicated a less efficient energy transfer and hence a reduced quenching with increasing linker length. Several other similar reports eventually indicated that the fluorescence quenching is neither due to competitive absorption by the gold cluster nor to an enhanced intersystem crossing efficiency, but to a quick deactivation of the excitation energy through electronic coupling of the excited fluorescent group with the nanoparticle [Canepa M., *et al.*, 2003].

Another group worked with the fluorescent dye Cy5 attached to gold nanoparticles by single stranded DNA oligonucleotides functionalized with thiol groups. By time-resolved

photoluminescence spectroscopy they determined the values of radiative and nonradiative decay rates of the fluorescence that was suppressed by 95%. The photoluminescence quantum efficiency is distance dependent, and the radiative rate decreases monotonically with decreasing distance while the nonradiative one increases [Dulkeith E., *et al.*, 2005]. These experimental results demonstrate that in the case of Cy5 dyes the luminescence quenching is almost exclusively due to a phase induced suppression of the radiative rate while energy transfer is of minor importance.

Other studies have concerned the core size effects on the photophysical properties of appended chromophores [Imahori H., *et al.*, 2003; Canepa M., *et al.*, 2003]. They all agree that for gold nanoclusters, the efficiency of their electronic coupling with fluorophores does not depend on the size of the metal core, as long as it spans over at least 5 to 10 nanometers.

It is worth underlying that it is possible to influence the different excited state deactivation pathways in these nanosystems by changing the appended chromophore. This means that each single system has its own specific properties arising from its components and their peculiar interactions in the assembly. Therefore, it is not possible to spot general behaviours but, at the same time, this is the basis of their versatility, one of the most valuable characteristics of metallic nanoparticles.

1.2.2 Nonquenched fluorophores linked to nanoparticles

The phenomenon which takes place when fluorophores are linked to or reside in the vicinity of metallic nanoparticles is not only quenching of the fluorescence; enhancement of the fluorescent signal by the metallic nanoparticles is another widely investigated event.

One of the first reported observations of fluorescent signal enhancement by nanoparticles was by Thomas and Kamat in 2000 [Thomas K.G. and Kamat P.V., 2000]. 1-Methylaminopyrene was attached on gold clusters (with diameters ranging from 5 to 8 nm), weakly stabilized by tetraoctylammonium bromide moieties. In the resulting system, an intense emission was detected, while the nanoparticles are nonfluorescent and the 1-methylaminopyrene in the buffer used was weakly luminescent. It was then hypothesized that the interaction of the amino lone pair electrons of the fluorophore with the metal decreases the donating ability of the fluorophore and hence

suppresses the photo-induced electron transfer responsible for the main nonradiative decay process.

Another interesting observation was the increase of the fluorescence lifetime of a fluorophore strongly bound to gold nanoparticle surface [Hernandez F.E., *et al.*, 2005]. Fluorophore, 4-acetamido-4'-maleimidylstilbene-2,2'-dithiol (AMDT)-functionalized gold nanoparticles (with average diameter of 3.5 nm) were synthesized by following the method proposed by Brust and Schiffrin (1994). The fluorescence lifetime of the excited state of the AMDT was enhanced when it was very close to the noble metal nanoparticle surface. No decrease of the fluorescence quantum yield could be measured and this indicates a weak energy transfer between the metal and AMDT in this organic-inorganic system.

1.3 S-Layer Protein SbsC

Surface layers, termed S-layer, comprise the outermost cell envelope component of most archaea and many bacteria; and serve various functions, including protective coats, molecular sieves (in the ultrafiltration range), ion or molecule traps, structures involved in cell surface interactions, and as antifouling coats. Furthermore, they are involved in determining the cell shape, and they contribute to virulence [Sara M., *et al.*, 2005]. S-layers are composed of a single protein or glycoprotein species, which crystallize into oblique, square, or hexagonal symmetry demonstrating lattices [Pavkov T., *et al.*, 2008]. The S-layer subunits are held together and linked to the underlying cell envelope by non-covalent bonds. Those lattices are highly porous and the pores are of identical size and morphology with diameters in the range of 2 – 8 nm [Sara M., *et al.*, 2005]. After isolating from the cell wall, S-layer subunits mostly maintain the ability to self-assemble in suspension, at air-water interface, on artificial solid supports, and on substrates covered with secondary cell wall polymers *in vitro* [Sleytr U.B., *et al.*, 2007]. The ability to assemble *in vitro* and to form isoporous structures with functional groups located on the surface in an identical position and orientation, have led to the applications of S-layers as ultrafiltration membranes, immobilization matrices for functional molecules, conjugate vaccines, and as patterning elements in molecular nanotechnology [Sleytr U.B., *et al.*, 1994].

A gram-positive bacterial species, *Geobacillus stearothermophilus*, representing one of the best studied S-layer systems, can produce at least five different S-layers depending on the

environmental conditions. The cell surface of *G. stearothermophilus* strain ATCC 12980 is completely covered with an oblique lattice formed by the S-layer protein SbsC [Egelseer E.M., *et al.*, 1996]. The protein precursor includes a 30 amino acid signal peptide typical for gram-positive bacteria, and consists of 1099 amino acids, with a molecular mass of 112.5 kDa and an isoelectric point of 5.5 [Jarosch M., *et al.*, 2000].

1.4 Bioassays Employing Plasmon Shift and Fluorescence

1.4.1 Use of metallic nanoparticles in biosensing

The unique properties of noble metal particles, which have been explained above and which have attracted much attention in certain research fields such as medicinal imaging, thermal and/or nonthermal therapy, drug delivery, etc. have also attracted interest in biosensing. The main advantages are the precision, simplicity, and rapidity of such tests. Historically speaking, aggregation based detection have enjoyed much clinical and commercial succees since the development of the latex agglutination test (LAT) in 1956 [Singer J.M. and Plotz C.M., 1956]. In the LAT and similar agglutination based tests, specific antibodies are conjugated to latex microspheres or gold nanoparticles which, when mixed with a solution containing the target antigen, cause the microspheres/nanoparticles to form visible aggregates. Whereas this type of analysis is effective and rapid, it is relatively insensitive, relying on high concentrations of analytes and on human eye as the detector [Stuart D.A., *et al.*, 2005].

Another means of detection utilising gold nanoparticles takes advantage of localised surface plasmon resonance (LSPR) of gold nanoparticles. This type of measurement is dependent on the strong UV/Vis absorption band at the LSPR wavelength. The assay we tried to prepare in this study lies in this category, and therefore a more detailed background will be given. However, it is noteworthy to discuss about a relatively newer approach, namely the scatter based sensing, before going deeper into LSPR based detection, which still is the backbone of nanoparticle based detection/biosensing.

1.4.1.1 Scattering-based properties of plasmonic nanoparticles and scatter-based biosensing

When a metallic nanoparticle is exposed to an electromagnetic wave, the plasmons (i.e. the electrons on the outer surface) start to oscillate at the same frequency as the incident wave; which

is followed by the emission of electromagnetic radiation by the oscillating electrons at their frequency of oscillation. This reradiation of light at the same incident wavelength is often referred to as plasmon scatter [Yguerabide J. and Yguerabide E.E., 1998].

As stated above, the number of reports on plasmon light scattering based sensing is smaller than on absorption-based sensing. Similar to absorbance-based measurements, plasmon supporting colloids also red-shift their scattering spectra as a function of coupling to other close proximity colloids. By taking the ratio of the scattered intensities at two different wavelengths, it is possible to measure, whether a given biospecies causes the aggregation or dissociation of the nanostructures. An example of such a system for glucose sensing was described by Aslan K. and Lackowicz J.R. in 2005.

1.4.1.2 Absorption-based (or LSPR-based) biosensing

The first type of signal transduction in this type of sensing depends on the sensitivity of the surface plasmon to interparticle coupling. When in a solution, interparticle spacing becomes less than the nanoparticle diameter, nanoparticles are able to interact electromagnetically by a dipole coupling mechanism. This readily leads to a broadening and red-shifting of the LSPR. Several papers have been published on a gold nanoparticle based UV/Vis technique for the detection of DNA. This detection method relies on the absorption spectra as particles are brought together by the hybridisation of complementary strands of DNA [Elghanian R., *et al.*, 1997]. More recently, gold nanoshells functionalised with specific antibodies have been used to detect antigens in whole blood. Upon addition of the nanoshell conjugates to whole blood containing the antigen, the plasmon resonance broadens, the intensity decreases and a red-shift in the LSPR occurs [Hirsch L.R., *et al.*, 2003]. The group reports this system to be capable of detecting pictogram/millilitre quantities of antigens within 30 minutes. However, the main disadvantage of the system is the risk of aggregation of nanoparticles, which is often irreversible, difficult to quantify, and interferes with the measurement.

The first report of using an LSPR wavelength-shift measurement for sensing the local refractive index change owing to antigen-antibody binding came in 1998 from Englebienne. In that study, anti-human heart fatty acid binding protein (hFABP) monoclonal antibodies were adsorbed onto gold nanoparticles with various diameters by charge adsorption at pH 8.5; followed by incubating

the gold-connected antibodies with recombinant hFABP and the UV/Vis spectra were measured. They observed a significant LSPR shift, which cannot be attributed to agglomerization, which was the case in the above two examples, since the antibodies used were monoclonal and the recombinant hFABP contains a single epitope, ruling out the possibility of the formation of nanoparticle-protein matrices (figure 8). The LSPR shift is therefore hypothesized to result from the refractive index change of the individual particles upon antigen-antibody binding [Englebienne P., 1998]. This demonstrates that a significant spectroscopic change, i.e. LSPR shift, in a bioassay employing nanoparticles does not necessarily require the agglutination of nanoparticles; refractive index or dielectric constant change of the surrounding medium upon antigen-antibody binding is strong enough to yield a significant change. The sensitivity of measurement is still retained without giving up the simplicity and rapidity of the measurement. Furthermore the unknown contribution introduced by the agglutination is eliminated.

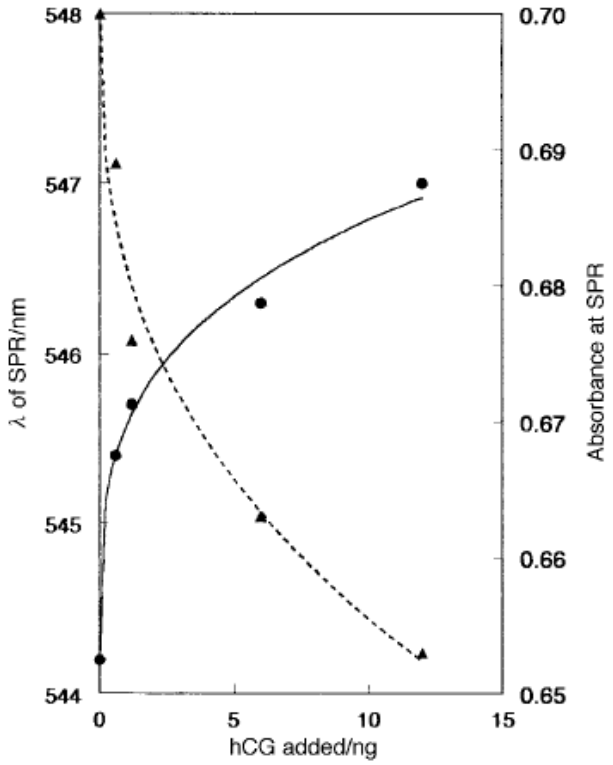

Figure 8. Shift of the SPR (closed circles, solid curve, left axis) peak and absorbance decrease (closed triangles, dotted curve, right axis) of colloidal gold particles coated with a monoclonal anti-hCG antibody, calculated from visible spectra recorded after incubation of a fixed amount of the colloidal gold reagent with samples containing increasing concentrations of hCG [figure taken from Englebienne P., *et al.*, 1998].

Another extension of LSPR sensing is carried out by aligning nanoparticles into well-defined arrays on solid support. Since this type of assays does not lie within the scope of this study a detailed description will not be presented here.

1.4.2 Use of fluorescence in biosensing

After discovery of the green fluorescent protein (GFP) in *Aequorea Victoria* [Prendergast F.G. and Mann K.G., 1978], cloning and subsequent expression in heterologous systems and generation of recombinant variants exhibiting stronger emission, stability, etc., GFP has become one of the mostly employed reporters for the analysis of gene expression and protein localisation among many other possible uses in a variety of experimental systems.

One of the remarkable features of GFP is that it is a naturally fluorescent protein, encoding the light-emitting chromophore within its primary amino acid sequence. The GFP chromophore consists of a cyclic tripeptide derived from Ser-Tyr-Gly at positions 65-67 in the protein and is only fluorescent when embedded within the fully folded complete GFP molecule [Cody C.W., *et al.*, 1993]. A number of variants of wild type GFP have been described by several authors, most of which contain one or more amino acid substitutions in the chromophore region of the protein [Kain S.R., 1999]. One of the two most commonly used GFP variant, which we also used in our study, is enhanced GFP (eGFP). It contains two amino acid substitutions: Phe at position 64 substituted by Leu and Ser at position 65 by Thr. eGFP coding sequence has been further modified with 190 silent base changes to contain codons that are preferentially found in highly expressed human proteins. Advantages of eGFP include improved sensitivity of detection, improved solubility, more efficient protein folding, faster chromophore oxidation to form the fluorescent form of the protein and reduced rates of photobleaching [Patterson G.H., *et al.*, 1997]. The following image (Fig. 9) shows the excitation and emission maxima of some GFP variants including eGFP.

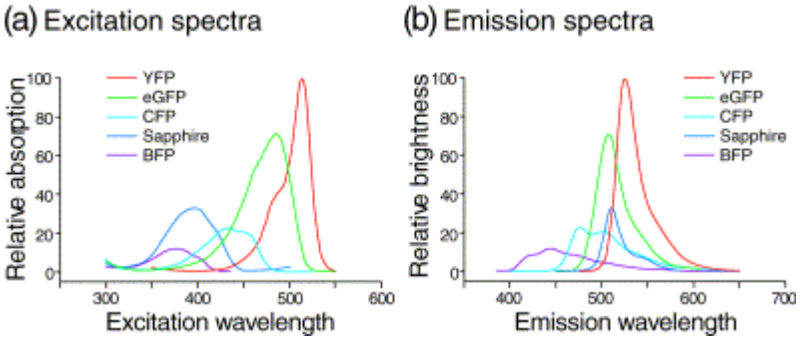

Figure 9. Relative excitation (absorption) and emission (brightness) spectra for the five green fluorescent protein (GFP) mutant classes. Purified recombinant protein was used to generate the spectra. Y-axis values are set relative to rPhiYFP (100%) [picture taken from Cubbitt A.B., Woollenweber L., and Heim. R., 1999].

However, long before the discovery of GFP and its variants, fluorescence (for instance fluorescent dyes) has been used in biosensing due to several advantages:

- High sensitivity
- Non-invasiveness
- Measurements can be made not only of fluorescence intensity but also of fluorescence decay times. Time-resolved fluorescence has the special advantages for *in vivo* sensing of being relatively independent of light scattering in the tissues and of fluorophore concentration, thus correcting for photobleaching or fluorophore loss mediated by diffusion or degradation [Szmacinski H., *et al.*, 1994].
- Special fluorescence techniques can provide information about the structure and micro-environment of molecules, and how these change in response to analyte variations in health and disease [Zhang Q., *et al.*, 2004].
- The structure and distribution of biomolecules can also be probed by the phenomenon of fluorescence (or Förster) resonance energy transfer (FRET).

Currently, there is no universally accepted classification system for sensor systems employing fluorescence; according to a recent review by VanEngelenburg and Palmer (2008) such systems can be divided into three classes: (i) Sensors in which protein activity or ligand binding alters FRET between two fluorescent proteins (fig 10 a, b, c, and d). (ii) Sensors which rely on modulation of the optical properties of a single fluorescent protein upon ligand binding (fig 10e). (iii) Sensors in which ligand binding causes the translocation of the fluorescent reporter (fig 10b). The following figure (Fig. 10) highlights the differences in these classes.

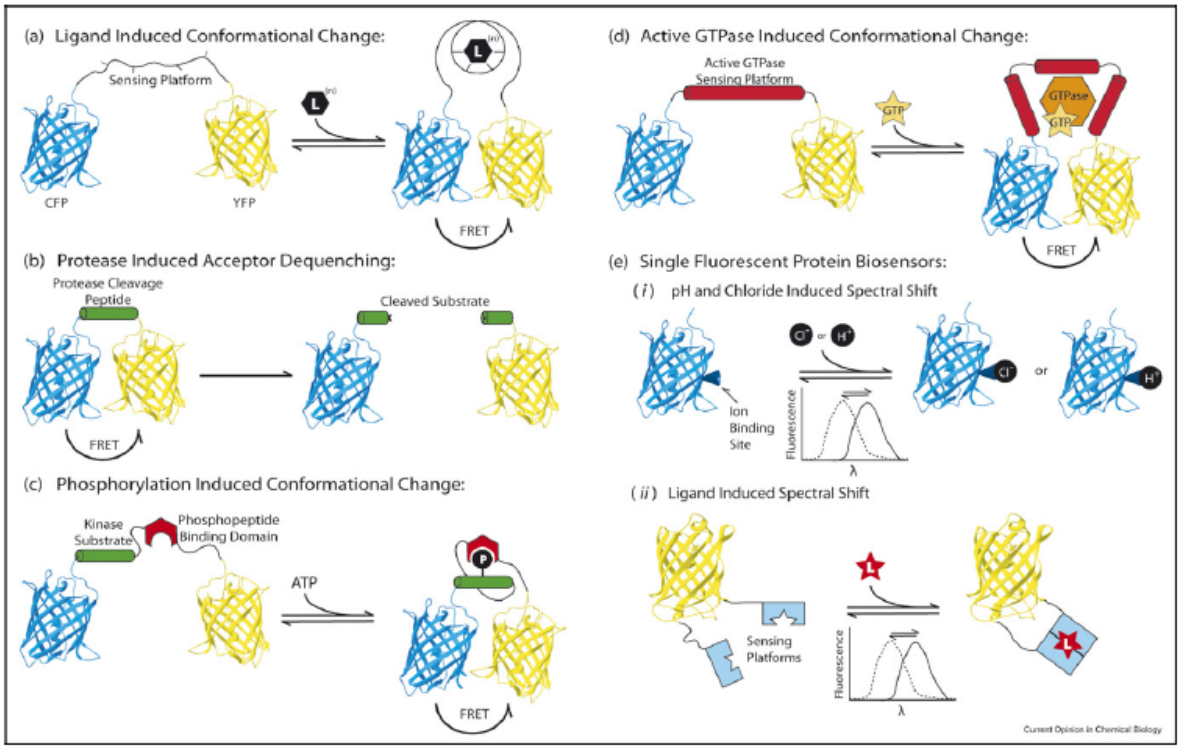

Figure 10. Platforms for fluorescent biosensor design. (a) Ligand induced conformational change platforms respond to intracellular ligand concentrations and 'hinge' open or closed to bring the fluorescent proteins (FP) in close proximity for FRET. (b) Sensors responding to specific protease activity contain a consensus peptide motif recognized by their cognate protease and dequench fluorescence from the donor FP. These sensors represent an essentially irreversible class of biosensor. (c) Kinase biosensors report the phosphorylation status of a model kinase substrate. Phosphorylation of a consensus peptide motif promotes intramolecular binding to a phosphopeptide-binding domain. (d) GTPase sensors utilize protein domains which selectively interact with the GTPase in the 'ON' or GTP bound state yielding FRET changes. (e) Biosensor designs using single fluorescent protein platforms: (i) pH and halide detection using fluorescent proteins engineered such that ligand-binding induce a spectral shift in the chromophore and (ii) circularly permuted fluorescent protein sensor appended to proximal ligand-binding domains which induces a spectral shift upon ligand-binding [picture taken from VanEngelenburg S.B. and Palmer A.E., 2008].

1.5 Intracellular Delivery of Gold Nanoparticles

Intracellular delivery of gold nanoparticles has gained interest in the ongoing research in the nanotechnology field. Gold nanoparticles have been extensively studied as carriers of various bio-active molecules (peptides, proteins, DNA, etc.) through the cell membrane into the cells due to the importance of such delivery of bio-active molecules in medicine and drug delivery. Vehicles for intracellular delivery can be broadly classified into four major groups: viral carriers, organic cationic compounds, recombinant proteins, and inorganic nanoparticles. Although the former three have been investigated for a longer time, they have some disadvantages such as

being expensive, (highly) toxic, or immunogenic. On the other hand inorganic nanoparticles possess versatile properties suitable for this task, including availability, functionality, high biocompatibility, potential capability of targeted delivery and controlled release of cargo [Xu Z.P., *et al.*, 2006].

1.5.1 Motivations of intracellular delivery of nanoparticles

Recent advances in the nanotechnology field is causing a slow replacement of photothermal therapy methods, which employ light absorbing dyes for achieving photothermal damage to tumors, and photodynamic methods, which employ chemical photosensitizers that generate singlet oxygen that is capable of tumor destruction, by noble metal nanoparticles. Nanoparticles demonstrate a very strong absorption at their plasmon resonance peak, which is at least several times higher than that of conventional photoabsorbing dyes. This enables the use of laser irradiations at lower intensities, making the therapy minimally invasive. Furthermore gold nanoparticles have higher photostability and do not suffer from bleaching [Huang X., *et al.*, 2007; Gannon C.J., *et al.*, 2008]. One of the pivotal examples of this application is the *in vitro* selective killing of breast cancer cells treated with gold/silicon dioxide nanoshells targeted against them and irradiated at near infrared [Lowery A.R., *et al.*, 2005].

A rather recently emerging application of gold nanoparticles is in the cancer treatment field, still different from the photothermal therapy explained above. It was documented that gold nanoparticles inhibit the proliferation of endothelial cells induced by VPF/VEGF (vascular permeability factor/vascular endothelial growth factor – the main protein factor responsible for the growth of new blood vessels into the tumorigenic tissue *in vivo*). Gold nanoparticles bind to the VPF/VEGF to inhibit its activity, successfully blocking neovascularisation [Mukherjee P., *et al.*, 2005]. The exact mechanism of inactivation is not yet clear. In the case of VPF/VEGF, it has been determined that for the interaction between the protein and nanoparticle as well as for the inactivation of the protein, the heparin binding domain of VEGF/VPF is crucial. However, it is still not known, whether the effect is due to the charge distribution change of the whole protein, or the charge distribution change within the heparin binding domain upon binding of nanoparticles, or the interaction between cysteine residues in the heparin binding domain and the nanoparticles [Bhattacharya R. and Mukherjee P., 2008].

Another important use of intracellular delivery of metallic nanoparticles is for bioimaging, where the main role is either as contrast agents or as autofluorescent reporters. As explained above, another very promising application is the enhancement of molecular fluorescence of various fluorophores by nanoparticles. Conventional contrast agents suffer from photobleaching, having broad overlapping emission spectra making multicolour imaging troublesome, and excitation/emission spectra susceptible to environmental changes. On the other hand nanoparticles demonstrate increased *in vivo* and *in vitro* stability, resistance to photobleaching, high quantum yield and high absorbance, resistance to metabolic breakdown, non-toxicity, and adequate dispersibility in the biological environment [Sharma P., *et al.*, 2006]. The most widespread employed nanoparticles for imaging are dye-doped silicon nanoparticles, quantum dots, and gold nanoparticles. In the first two cases the basis of imaging relies on the dye or the fluorescence of the quantum dot particles, respectively. As explained above, autofluorescent gold nanoparticles are now readily available for direct use as fluorescent tags. However, still the majority of the reports in the literature depend on using gold nanoparticles as contrast agents.

1.5.2 Methods of delivery

It is now clear that metallic nanoparticles among with other products of nanotechnology offer a wide range of possibilities for biological sciences, ranging from detection, sensing, and imaging to therapeutics. One critical step in such processes is the intracellular delivery of nanoparticles, and there are already several methods available for that purpose. The most straightforward and the simplest method is perhaps the use of "naked" nanoparticles, i.e. nanoparticles not coupled to any type of carrier. Nanoparticles have been used as carriers of nucleic acids and proteins into the cells for some time already [Sokolova V. and Epple M., 2008]. This ability of nanoparticles arise from their size which is small enough to penetrate the plasma membrane, their biostability, non-toxicity, and their ability to bind to various types of molecules as cargo. The other methods of delivery include usage of liposomes, dendrimers, or fullerenes. Every method has its advantages and disadvantages. Since in this study dendrimers were employed for the intracellular delivery, a more detailed description will be presented here.

Dendrimers represent a class of polymers characterised by their well-defined structure, with a high degree of molecular uniformity and low polydispersity, which is a measure of the distribution of molecular weights in a given polymer. Dendrimers – consisting of a central core

branched cell, interior branch cells possessing surface groups – are synthesized either by a divergent (radial synthesis from a central core through stepwise repetitive reactions) or a convergent (construction of branched subunits followed by their attachment to a multifunctional core) approach [Tomalia D.A., *et al.*, 1985; Hawker C. and Fréchet J.M.J., 1990]. Both approaches lead to a dendritic architecture with properties amenable to modifications of shape, size, polarity, surface properties and internal structure. Due to such versatility dendrimers have attracted great interest as potential drug delivery systems in biomedical applications, and in metal complexation, magnetic resonance imaging, host-guest chemistry, and glycomics [Wolinsky J.B. and Grinstaff M.W., 2008].

The ability of dendrimers to enter cells is one of their key properties, which make them good candidates in the above mentioned potential applications. A detailed understanding of the mechanisms by which dendrimers are taken up by, and transported within cells is required in order to optimise dendrimer-based delivery systems [Najlah M. and D'Emanuele A., 2006]. Such mechanisms depend strongly on the surface properties of the dendrimers in question. Kannan and co-workers studied the dynamics of cellular entry of four different dendrimers into cultured human lung epithelial carcinoma cells: one with amine groups, one with hydroxyl groups, and one covered with PEG, and a hyperbranched polymer (polyol). The species carrying amine surface groups entered the cells faster than the other ones. The rapid entry of the amine containing dendrimers suggests that an electrostatic interaction between the positively charged amino group and the negatively charged epithelial cells leading to fluid phase pinocytosis is the underlying process [Kannan S., *et al.*, 2004; Kohle P., *et al.*, 2004].

Depending on the intended use, the cargo has to be carried within the dendrimers or on their outer surface. Cargo complexing with surface of the dendrimer might not only limit the internalisation process, but also is subject to easy detachment e.g. by enzymes, pH, temperature, ionic strength for *in vivo* as well as *in vivo* experiments. Therefore, it might be reasonable to embed the cargo within the interior of the dendrimer, when it is important not to lose the cargo in a complex buffer system, as for instance in the body. The following figure (Fig. 11) illustrates the available ways of cargo complexation with the nanoparticles, where the cargo in this particular example is metal.

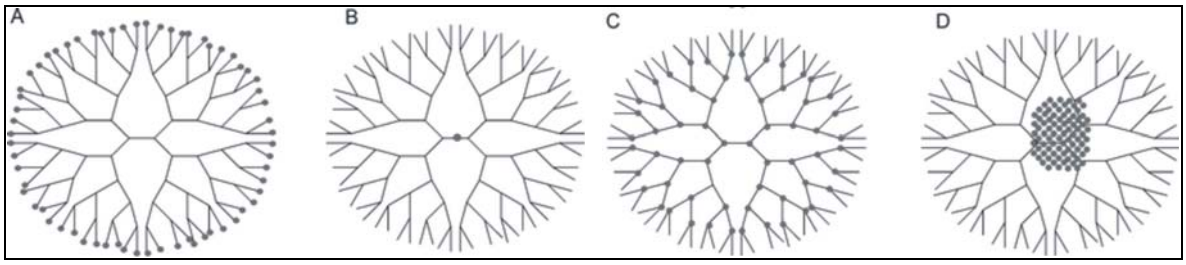

Figure 11. Dendrimers can have metal containing end groups (A), metal containing cores (B) or metal containing branches (C). Dendrimers can also encapsulate metal nanoparticles (D) [figure taken from Ravoo B.J. 2008].

In this study, oligosaccharide-modified poly(propyleneimine) dendrimers (PPI) were employed. PPI dendrimers were synthesized via reductive amination for the introduction of di- or trisaccharide units as surface groups with minimal synthetic steps [Baigude H., *et al.*, 2004]. This reaction results in the simultaneous coupling of two oligosaccharide units for one amino surface group, which in turn results in not only a higher rigidity of the molecular structure but also an improved biocompatibility conferred by the oligosaccharide groups [Appelhans D., *et al.*, 2007]. The synthesis is shown in fig. 12.

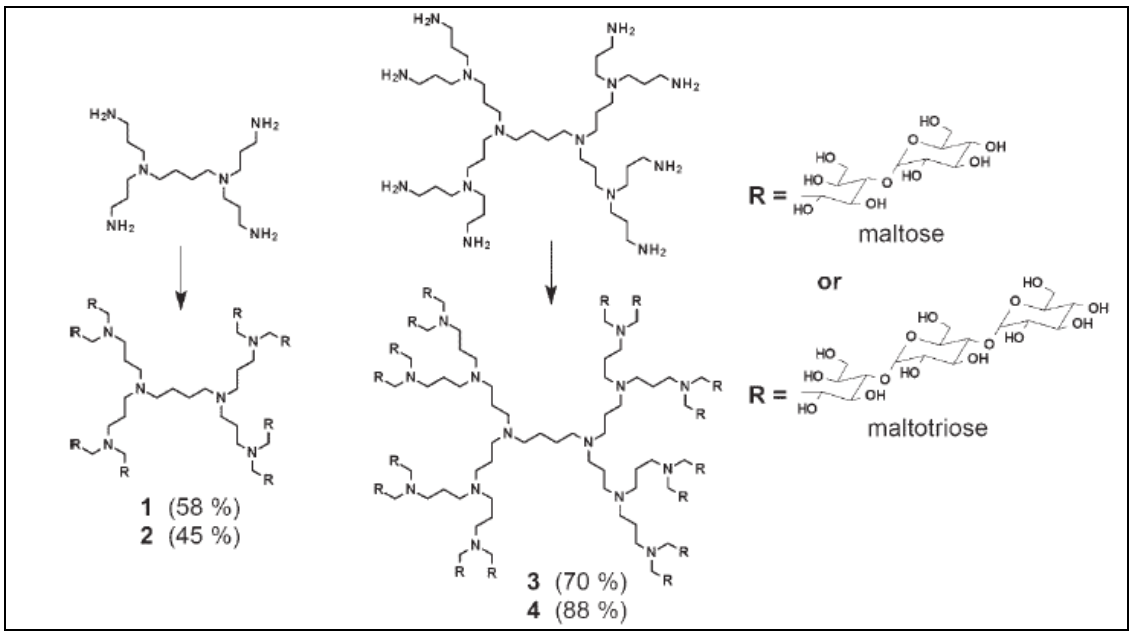

Figure 12. Synthesis of first and second generation PPI dendrimers (1–4) with oligosaccharide units. The values in parentheses show the yield of the synthesis process [figure taken from Appelhans D., *et al.*, 2007].

In biological research, metal complexed dendrimers are extensively used as sensors, catalysts, contrast agents in magnetic resonance imaging (MRI), carriers of therapeutic nanoparticles, and many more applications which require a strict control over the geometry of the metallic nanoparticle and the carrier system [Ravoo B.J. 2008]. Furthermore, dendrimers are attractive protective agents for metallic nanoparticles, especially gold ones, because: (i) the dendrimer templates themselves are of fairly uniform composition and structure, and therefore they yield well-defined nanoparticle replicas; (ii) the nanoparticles are stabilized by encapsulation within the dendrimer, and therefore they do not agglomerate; (iii) the dendrimer branches can be used as selective gates to control access of small molecules (substrates) to the encapsulated nanoparticles; (iv) the gold nanoparticles protected by dendrimer own very small size, typical 1–5 nm, which will find application in catalysis due to their high activity and surface-to-volume ratio and as autofluorescent gold nanoparticles. In their paper Appelhans and co-workers describe the complexation of the dendrimers with copper. In our study we used them for carrying autofluorescent gold nanodots into cultured human cells.

2. Materials and Methods

2.1 Equipment

2.1.1 Consumables and equipment

Consumable/equipment	Type	Brand
6- and 96-well plates		TPP or Nunclon
Amber coloured reaction tubes	1.5 ml	Eppendorf
Centrifuge tubes	5 ml, 50 ml, 500 ml	Beckman
Coverslips	22 x 22 or 24 x 24	Menzel Gläser
Dialysis membranes	0.025 µm, VS type	Millipore or Roth
Erlenmeyer flasks	50 ml, 100 ml, 250 ml, 500 ml, 1L, 2L, 3L, 5L	Schott or Simax
Gel blotting paper	GB-002, GB-003	Schleicher and Schuell
Glass slides		Menzel Gläser
Immobilon™-P	Polyvinylidene difluoride (PVDF) Membranes	Millipore
Neubauer cell counting chamber	2 x 0.1 mm^3	Brand
Petri dishes		Greiner
Pipette tips	1000 µl, 200 µl, 10 µl	TPP
Pipettes	P1000, P200, P20, P10	Gilson
Poly-L-lysine collated glass slides		Roth
Reaction tubes	0.5 ml, 1.5 ml, 2.0 ml	Eppendorf or Plastibrand
Reaction tubes	15 ml, 50 ml	Greiner or TPP
Spectrophotometer cuvettes	special optical glass or quartz 3500 µl, 1400 µl	Hellma
T75 cell cluture flasks		TPP
X-ray films		GE Healthcare or Kodak

2.1.2 Devices

Device	Model	Brand
Centrifuge	Biofuge pico	Heraeus
Centrifuge	Biofuge fresco	Heraeus
Centrifuge	5417R	Eppendorf
Centrifuge	3K30	Sigma
Centrifuge	Avanti™ J25	Beckman
Thermo cycler	Cyclone 96	PeqLab
Light microscope	H 600 Wilo-Prax Archo	HUND WETZLAR
Fluorescence microscope	Axiovert200M	Zeiss
Filter sets	09, 10, 15	Zeiss
Camera	Cascade 512B	Roper Scientific
Scanning electron microscope	Leo982 digital	Zeiss
Scanning Probe Microscope connected with a fluorescence microscope	BioScope™ axiovert 100M	Digital Instruments Inc. Zeiss
Laser scanning microscope mounted on a wide field microscope	LSM 510 meta Axioscope 2 mot FS	Zeiss
FPLC System	500 series	Pharmacia Biotech
Water bath	1083	GFL
Incubator		Binder or Heraeus
UV/Vis spectrophotometer	Ultrospec 3000	Pharmacia Biotech
UV/Vis spectrophotometer	Cary 50	Varian
Microplate reader	Infinite® 200	Tecan
Fluorescence spectrometer	FluoroMax-3	HORIBA Jobin Yvon GmbH
Plasma Etcher	Plasma-Prep™ II	Spi Supplies
Concentrator	5301	Eppendorf
Sonicator	Sonopuls	Bandelin
Electroporation system	Gene Pulser® II	Bio-Rad

Heating block	Eppendorf or Kleinfeld
Vortexer	IKA-Works Inc.
Blotter	PeqLab
Power supplies	Bio-Rad or Pharmacia Biotech
DNA/Protein gel chambers	PeqLab/Hoefer
Gel-Doc system	MWG-Biotech

2.2 Reagents

2.2.1 Chemicals and reagents

Chemical/Reagent	**Supplier**
3-Aminopropyltriethoxysilane (APTES)	Pierce
3-(Glycidyloxypropyl)trimethoxysilane (GOPTES)	Sigma
4-(2-aminoethyl)-benzenesulfonyl fluoride (AEBSF)	AppliChem
4-(2-hydroxyethyl)-1-piperazineethanesulfonic acid (HEPES) buffer	Serva
Acetic acid	Roth
Acetone	Roth
Acrylamide/Bisacrylamide	Roth
AcTEV buffer (20X)	Invitrogen
Agar	Roth
Agarose	BioZym
Ammonium (NH_3)	Roth
Ammoniumperoxisulphate (APS)	Merck
Ampicillin	Roth
BenchMark™ Prestained Protein Ladder	Invitrogen
Biotin	Merck
Bromphenol blue	Serva
Bovine Serum Albumin (BSA)	Serva

Calcium chloride ($CaCl_2$)	Merck
Casein from bovine milk	Sigma
Cetyl trimethylammonium bromide (CTAB)	Sigma
Chloramphenicol	Roth
Coomassie® Brilliant blue G250	Roth
Dithiobis(sulfosuccinimidyl propionate) (DTSSP)	Pierce
Dithiothreitol (DTT) 0.1M	Invitrogen
DMEM	PAA
dNTP's	Invitrogen
DTT	Roth
Ethanol	Roth
Ethidiumbromide	Roth
Ethylendiamine-tetraacetic acid (EDTA)	Roth
Foetal Bovine Serum (FBS)	PAA
Formaldehyde	Roth
Fuming Nitric Acid (HNO_3)	Roth
Glutamine	PAA
Glutathione Sepharose™ 4B	GE Healthcare Life Sciences
Glycerol	Roth
Glycine	Roth
Guanidinium hydrochloride (GuaHCl)	Roth
Herring sperm DNA	Invitrogen
HPLC-grade water	Roth
Hydrochloric acid (HCl)	Roth
Hydrogen peroxide (H_2O_2)	Roth
Imidazol	Roth
Isopropanol	Roth
Isopropyl β-D-1-thiogalactopyranoside (IPTG)	Roth
Ligation Buffer (2X)	Promega

Magnesium Chloride ($MgCl_2$) 50 mM	Invitek
Methanol	Roth
Mg^{++} free PCR buffer (10X)	Invitek
N,N,N',N'-Tetramethylethylenediamine (TEMED)	Roth
Phosphate buffered saline (PBS)	PAA
Peptone/Tryptone	Roth
Polyethylene glycol (PEG)	Roth
Polyvinylpyrrolidone average mol weight 40,000 Da (PVP40)	Sigma
Ponceau S	Roth
Potassium chloride (KCl)	Merck
Potassium dihydrogenphosphate (KH_2PO_4)	Merck
Potassium hydroxide (KOH)	Roth
Protease inhibitors	Roche
Restriction endonuclease buffers	Invitrogen or Fermentas
Skimmed milk powder	Lasana
Sodium carbonate (Na_2CO_3)	Sigma
Sodium chloride (NaCl)	Roth
Sodium dodecyl sulphate (SDS)	Merck
Sodium hydroxide (NaOH)	Roth
ß-mercaptoethanol	Sigma or Roth
Tris base	Roth or Merck
Triton X-100	Roche or Roth
Trypsin	PAA
Tween 20	Roth
Yeast extract	Roth
λ phage DNA *Eco*RI/*Hind*III cut	Fermentas

2.2.2 Kit systems

Kit	Brand
D_C Protein Assay	Bio-Rad
ECL-Plus Kit™	GE Healthcare Life Sciences
Jetquick PCR Purification Spin Kit	Genomed
Nucleospin® Extract Kit	Macherey-Nagel
Nucleospin® Plasmid Quick Pure Kit	Macherey-Nagel
Wizard® SV Gel and PCR Clean-Up Kit	Promega

2.2.3 Enzymes and proteins

Enzyme/Protein	Supplier
AcTEV protease	Invitrogen
HA-eGFP and HA-CFP	kindly provided by Denise Walther, IfG
CombiZyme polymerase	Invitek
Lysozyme	Sigma-Aldrich
rPhiYFP	Evrogen
Restriction enzymes	Invitrogen or MBI Fermentas
T4 DNA ligase	Promega
Trypsin EDTA (1:250) 1X	PAA

2.2.4 Metallic Nanoparticles

Gold nanoparticles (60 nm diameter) British Biocell International

Gold nanoparticles and gold-silver alloyed nanoparticles (60 nm diameter; alloy NPs with a 23% Ag and 77% Au composition), synthesized by citrate reduction modified from Frins G. (1973) and according to El-Sayed (1999), respectively, were kindly provided by Mathias Lakatos (Institute of Materials Science, University of Technology Dresden).

Gold nanoparticles (2 nm diameter) synthesized by sodium borohydrate reduction [Zheng J., *et al.*, 2004] and embedded in polymeric dendrimers (Stp1831) [Appelhans D., et al., 2007] kindly provided by Mathias Lakatos and Dr. Dietmar Appelhans (Leibniz-Institut für Polymerforschung Dresden e. V).

2.2.5 Antibodies

2.2.5.1 For Western blot analysis

The antibodies were diluted as indicated in TBS-T buffer containing 5% (w/v) skimmed milk powder.

Primary antibodies:	
Mouse-anti-GFP	Roche (1:5000)
Goat-anti-GST	Roche (1:5000)
Secondary antibodies:	
Sheep-anti-mouse IgG-HRP-coupled	Amersham Biosciences (1:5000)
Donkey-anti-goat IgG-HRP-coupled	Amersham Biosciences (1:5000)

2.2.5.2 For coupling to Gold Nanoparticles

Mouse-anti-GFP	Roche
Anti-HA	Roche
Anti-HA high affinity	Roche
Anti-rPhiYFP	Evrogen

2.2.6 Media

Media for *E. coli*	**Recipe**
LB	1.0 % (w/v) Peptone/Tryptone
	0.5 % (w/v) Yeast Extract
	86 mM NaCl
For solid plates additional	2.0 % (w/v) Agar
pH adjusted to 7.4 by addition of NaOH	
For selection	100 mg/l Ampicllin

SOC	2.0 % (w/v) Peptone/Tryptone 0.5 % (w/v) Yeast Extraxt 10 mM NaCl 2.5 mM KCl 10 mM $MgCl_2$ x $6H_2O$ 10 mM $MgSO_4$ x $7H_2O$ 20 mM Glucose/Dextrose

Medium for HeLa cells	**Recipe**
DMEM cell culture medium	DMEM, high glucose (4.5 g/l) 10% ml FBS 2 mM L-Glutamine

2.2.7 Buffers

Buffer	**Recipe**
TBE	90 mM Tris base 90 mM Boric acid 2.5 mM EDTA
TBS (10X)	20 mM Tris-HCl (pH 7.4) 137 mM NaCl
TBS-T	1X TBS 0.9 mM Tween 20
PBS (pH 7.4)	137 mM NaCl 8 mM Na_2HPO_4 1.5 mM KH_2PO_4 2.7 mM KCl

DNA loading buffer (6X)	3.7 mM Bromophenol blue 9.7 M Glycerol
E.coli lysis buffer	50 mM Tris-HCl (pH 7.8) 0.05 % (w/v) Lysozyme 1 mM AEBSF

Potassium phosphate buffer

Solution A: KH_2PO_4 0.2M

Solution B: K_2HPO_4 0.2M

Solution A and B mixed in the ratios provided in table 2 in appendix; volume then completed to 200 ml

Potassium acetate buffer

Solution A: Glacial acetic acid 0.2M

Solution B: $KC_2H_3O_2$ 0.2M

Solution A and B mixed in the ratios provided in table 3 in appendix; volume then completed to 100 ml

2.2.7.1 Buffers and solutions for SDS-PAGE and Western blotting

Buffer	**Recipe**
Separating gel (12%)	375 mM Tris-HCl (pH 8.8) 1.7 M Acrylamide 20.8 mM Bisacrylamide 3.5 mM SDS 4.4 mM APS 8.6 mM TEMED

Stacking gel (4%)	125 mM Tris-HCl (pH 6.8) 0.6 M Acrylamide 6.5 mM Bisacrylamide 3.5 mM SDS 4.4 mM APS 8.6 mM TEMED
Running buffer	25 mM Tris 192 mM Glycin 3.5 mM SDS
6 x loading buffer	300 mM Tris-HCl (pH 6.8) 3.3 M Glycerol 350 mM SDS 1.5 mM Bromphenol Blue 600 mM DTT or 640 mM β-mercaptoethanol (freshly added)
Coomassie blue stain	45 % (v/v) Methanol 17 % (v/v) Acetic acid 1.2 mM Coomassie brilliant blue G250
Destaining solution	30 % (v/v) Methanol 7 % (v/v) Acetic acid
Transfer buffer	192 mM Glycine 25 mM Tris 5.0 % (v/v) Methanol 3.5 mM SDS
Ponceau S stain	6.6 mM Ponceau S 1.0 % (v/v) Acetic acid

Blocking solution	TBS-T 5 % (w/v) skimmed milk powder

2.3 Materials for genetic modification

2.3.1 Primers

Primers for the amplification of GST encoding sequence from pGEX-3 vector, addition of restriction endonuclease recognition sites, and introduction of the AcTEV protease target sequence were purschased from biomers.

Forward primer (5' to 3'):
TAT ATA CAT ATG TCC CCT ATA CTA GGT TAT TGG AAA ATT AAG GGC C
*Nde*I recognition site (underlined)

Reverse primer (5' to 3'):
TAT ATA CTC GAG **TCC CTG AAA ATA AAG ATT CTC** TTT TGG AGG ATG GTC GC
AcTEV protease target sequence (bold) and *Xho*I recognition site (underlined)

2.3.2 Plasmids

Plasmid	**Source**
pGEX-3X (used as source for GST)	GE Healthcare Life Sciences
pPhi-Yellow-B	Evrogen
pET17b-eGFP (used as vector for the cloning of GST-eGFP fusion protein)	Blecha A., 2005
pET17b-SbsCeGFP (used for over-expression of SbsC-eGFP)	Blecha A., 2005
pET17b-GSTeGFP (cloned GST-eGFP overexpression vector)	this work (see Fig. 13)

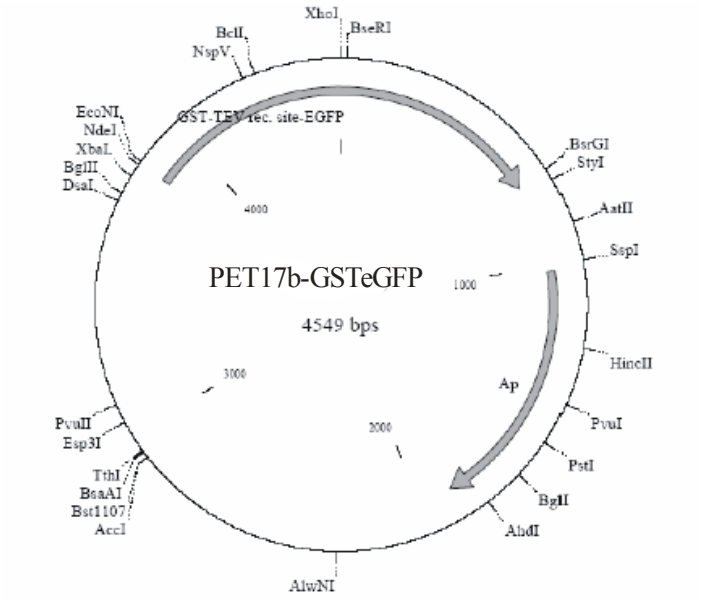

Figure 13. pET17b GST-eGFP expression vector (Ap: Ampicillin resistance gene).

2.3.3 Strains

Strain	Source
E.coli Bl21 (DE3) B, F$^-$, *omp*T, *gal*, [*dcm*], [*lon*], *hsdSB*(rB$^-$mB$^-$), galλ(DE3)	Novagen
HeLa human cervical carcinoma cell line	kindly provided by Andreas Ettinger (MPI-CBG, Dresden)

2.4 Methods

2.4.1 High yield production of eGFP

2.4.1.1 Amplification of DNA by polymerase chain reaction

The *GST* gene sequence was amplified from the commercially available pGEX-3X plasmid by standard PCR. The annealing temperature (T_A) for PCR reaction was calculated according to the following formula [MWG-BIOTECH], where n_{GC} represents the number of GC base pairs in the primer and n_{Total} is the total number of base pairs:

$T_A = 69.3ºC + 41(n_{GC}/n_{Total}l)ºC – (650/n_{Total})ºC - 5ºC$ (Eq. 8)

The mix for the PCR consisted of: 1 ng/µl of the template, 0.2 mM of dNTP mix (containing 10 mM of each dNTP), 1.5 pmol/µl of forward and reverse primers, 2.5 units of DNA polymerase, 1X PCR buffer. The total volume was completed up to 100 µl with distilled water. The cycles used in the amplification are as follows: 1 cycle of initial denaturation at 95ºC for 5 minutes, followed by 20 cycles of denaturation (1 min, 94ºC), annealing (1 min, T_A), elongation (2 min, 72ºC), and final elongation at 72ºC for 5 min. The resulting fragments were cleaned up by using the kits listed in 2.2.2.

2.4.1.2 Separation of DNA

DNA fragments were separated by agarose gel (1% (w/v) agar dissolved in TBE buffer and containing 1 µg/ml of ethidium bromide for visualisation) electrophoresis in TBE buffer at 100V. Standard ladder was commercially available λ phage DNA digested with *Eco*RI and *Bam*HI restriction endonucleases. After separation, the desired fragments were excised under UV light and cleaned up by using one of the kits listed in 2.2.2.

2.4.1.3 Restriction enzyme digestion of DNA

DNA was mixed with sterile bi-distilled water, the respective restriction enzyme buffer stock solution, and the restriction endonuclease with a final concentration of 1 unit per µg of DNA. The reaction mixture was incubated at 37ºC for 1 hour. The resulting fragments were cleaned up using one of the kits listed in 2.2.2.

2.4.1.4 Ligation of DNA fragments

Restriction endonuclease digested vector and insert DNA fragments were mixed in a 3:1 molar ratio in ligase buffer, and 2 units of T4 DNA ligase were added. The reaction mixture was incubated overnight at 4ºC.

2.4.1.5 Preparation of electrocompetent E. coli cells

An overnight grown *E. coli* BL21 (DE3) culture was diluted 1:100 in fresh LB medium and grown until an optical density at 600 nm of 0.5 to 0.8 was reached. Then the culture was chilled on ice for 15 min, followed by pelleting the cells by centrifugation at 4.000 x g for 15 min (4ºC);

and two subsequent washings with ice chilled sterile distilled water, and once with sterile glycerol (1.4 M). Finally cells were resuspended in 2 ml of 1.4 M of glycerol (aliquots stored at -80ºC).

2.4.1.6 Transformation of E. coli cells and isolation of plasmid DNA

7 µl of ligation mixture was dialysed against sterile distilled water for 15 min, then mixed with 40 µl of electrocompetent *E. coli* cells and transferred into a prechilled electroporation cuvette. Electroporation parameters were as follows: capacitance of 25 µF, resistance of 200 Ω, and voltage of 2.5 kV. After the pulse, the transformation mixture was diluted in 1 ml of SOC medium and transferred into an Eppendorf tube for incubation at 37ºC for 1 hour. The transformation mixture was pelleted at 6.000 x g at 4ºC or room temperature for 10 min and resuspended in LB medium. Transformants were selected on LB plates with ampicillin at 37ºC.

Plasmid DNA from the transformed cells was obtained from overnight grown 2-3 ml cultures by using the appropriate kits listed in 2.2.2.

2.4.1.7 Overexpression and extraction of GST-eGFP

Cells containing the respective plasmids were inoculated in 2-3 ml of LB and were grown for 8 hours to overnight, followed by diluting 1:1000 into 1L of LB. The cells were grown for 5-6 hours, until an OD_{600} of 0.5-0.8 was reached; afterwards synthesis of the respective proteins for 6 hours to overnight was induced by adding 50 mM of IPTG.

For the extraction of the overexpressed proteins, the cells were spun down at 6.000 x g for 10 min at 4ºC, washed with cold 50 mM Tris-HCl buffer pH 7.4 two times, and resuspended in 20 ml of *E. coli* lysis buffer and incubated for 1 hour at 30ºC with gentle shaking for the cell wall components to be digested by lysozyme. Finally, the cells were incubated on ice for about 15 minutes, followed by sonication for 6 cycles of 30 seconds with 70% - 80% of maximum power. Lysates were centrifuged at 12.000 x g for 30 min at 4ºC to separate the cytosolic fraction, containing the soluble GST-eGFP. GST-eGFP was purified by incubating the supernatant with Glutathione Sepharose™ 4B beads for 1 hour at 4ºC with gentle rotation, followed by 3 wash steps with PBS. The separation of GST-eGFP was carried out by incubating the beads with 50 mM reduced glutathione in 50 mM Tris-HCl, pH 8.0 for 10 min at room temperature and finally

centrifuging at 500 x g to separate the beads from GST-eGFP. The protein concentrations before and after isolation were measured by using the BIO-RAD DC-Protein Assay.

2.4.1.8 AcTEV protease digestion of GST-eGFP and isolation of eGFP

The clear GST-eGFP solution was digested with AcTEV protease according to the protocol provided by the manufacturer:

Fusion protein	20 µg
20X TEV buffer	7.5 µl
0.1 M DTT	1.5 µl
AcTEV Protease, (10 units)	1.0 µl
Water up to	150 µl

The reaction mixture was incubated at various temperatures for various time periods to determine the most optimum conditions. The efficiency of digestion was determined by running the digested samples on SDS-PAGE, followed by western blotting. After the cleavage GST was removed by incubating the mix with Glutathione Sepharose™ 4B beads and centrifuging at 500Xg to separate the GST bound beads from eGFP. eGFP was further purified from the AcTEV protease and other impurities via FPLC (using a Sephacryl™ S-300 column Pharmacia Biotech and degassed PBS or 50 mM Tris-HCl with varying pH as the running buffer).

2.4.2 Overexpression of SbsC-eGFP

2.4.2.1 Transformation

The already available pET17b-SbsCeGFP plasmid was electroporated into electrocompetent *E.coli* BL21 (DE3) cells as explained in 2.3.1.5.

2.4.2.2 Extraction of SbsC-eGFP

Extraction of SbsC-eGFP form the cells were performed in a similar fashion to that of GST-eGFP. The steps were the same until the first centrifugation after incubating on ice for 15 min. Due to the network structures formed by SbsC-eGFP already in the cell in the course of expression, the majority of the protein sediments to the pellet after centrifugation at 12000Xg for 30 min at 4ºC. Therefore, after centrifugation, the pellet fraction was retained, which was then resuspended in 5M guanidium HCl with gentle shaking at room temperature for 20 – 30 min, leading to reversible denaturation and monomerisation of SbsC-eGFP. The monomers were

separated from cell debris via centrifugation at 16000Xg for 30 min at 4ºC. The recrystallisation of SbsC-eGFP monomers was carried out by dialysing the supernatant against sterile distilled water, PBS, or Tris-HCl buffer with varying pH values overnight at 4ºC. (Preparation of the dialysis membrane: desired size of the membrane was cut and boiled in 189 mM Na_2CO_3 solution containing 1 mM EDTA, pH 8.0 for 10 min, then rinsed with water, and finally boiled for another 10 min in 1 mM EDTA, pH 8.0 and rinsed thoroughly with water.

2.4.3 Overexpression of rPhiYFP

Commercially available bacterial expression vector pPhi-Yellow-B was electroportaed into electrocompetent *E.coli* BL21 (DE3) cells as explained in 2.3.1.5. Transformants were selected by growing the cells on ampicillin (100 mg/ml) containing LB plates. A single colony was picked to start an overnight liquid culture, which was then diluted 1:1000 in a 1 L LB culture. The cells were grown until an OD_{600} of 0.5-0.8 is reached; afterwards the synthesis of the rPhiYFP was induced by adding 50 mM of IPTG and letting the cells grow overnight. The extraction of rPhiYFP was done in the same way as for eGFP until the sonication and following centrifugation step, as explained in 2.3.1.6. After centrifugation, cell debris was discarded, and the overexpressed rPhiYFP was separated from the rest of the supernatant by FPLC (using a Sephacryl™ S-300 column Pharmacia Biotech and degassed PBS or 50 mM Tris-HCl with varying pH as the running buffer).

2.4.4 Preparation of samples for microscopy

The inverse microscope Axiovert 200M (Zeiss) connected to a Cascade 512B camera (Roper Scientific) was employed for fluorescence microscopy. The filter sets (Zeiss) were as follows:

Filter set:	09	excitation:	450-490 nm	emission:	515 nm
	10		451-490 nm		515-565 nm
	15		546 nm		590 nm

Scanning microscopy was carried out by a digital SEM Leo 982 (Zeiss). The samples were analysed by changing magnification and acceleration voltage, typically 1-2 kV. The working distance was kept constant at 4 nm.

BioScope from Digital Instruments was used for analysis of surface structures in connection with fluorescence, the filter set for the fluorescence microscope was 09 (see above) and the AFM was used in the tapping mode. Unlike a conventional AFM, the samples were prepared on glass, for the possibility of fluorescence microscopy.

2.4.4.1 Cleaning of glass slides and silicon wafers

The substrate (glass slide or silicon wafer) was incubated in fuming nitric acid for 5 min, and then transferred into neutralisation solution ($ddH_2O:H_2O_2:NH_3$ in 5:1:1 volume ratio) for a 10 min neutralisation reaction. The substrate was then rinsed thoroughly with double distilled water and heat dried in an oven at 105ºC for at least 1 hour. When no surface modification was required, eGFP or SbsC-eGFP and/or metallic nanoparticles were adsorbed onto cleaned glass slides (for fluorescence microscopy or BioScope analysis) or onto silicon wafers (for SEM), adsorption time varying from 5 minutes to 30 minutes in a humid chamber in order to minimize the evaporation of the medium, and eventually rinsing and drying with a nitrogen gun.

2.4.4.2 Surface modifications

For APTES modification, glass slides (or silicon wafers) were cleaned as explained in 2.3.4.1; then submerged into a solution containing 0.4 ml of 1 M APTES, 1 ml of ddH_2O, and 19 ml of absolute EtOH for 2 min; followed by submerging into a beaker containing absolute EtOH for 20 min before rinsing thoroughly with ddH_2O and eventually heat drying at 105ºC for at least overnight. Adsorption onto APTES modified substrate was done the same way for unmodified substrate.

For GOPTES modification, glass slides (or silicon wafers) were cleaned as explained in 2.3.4.1; then submerged into a solution of 0.2 mM of GOPTES in absolute EtOH for 5 min, followed by immersing in absolute EtOH for 20 min. Afterwards, the substrates were thoroughly rinsed with ddH_2O and finally heat dryed at 105ºC for at least overnight. Adsorption onto GOPTES modified substrate was done the same way for unmodified substrate.

For plasma modification, the substrate was incubated in the Plasma-Prep™ II plasma etcher under a pressure of 200 µatm under a radiowave frequency of 13.56 MHz for 30 min. Afterwards

the sample was adsorbed onto plasma treated substrate in the same manner as unmodified substrate.

2.4.4.3 Maintenance, transfection, and preparation of HeLa cells for fluorescence microscopy

HeLa cells were grown to at least 75% confluence in T75 cell culture flasks in DMEM cell culture medium. The medium was removed and the cells were rinsed 3 times with PBS preheated to 37ºC, followed by incubating with 1 ml of 1X Trypsin at 37ºC until at least 75% of the cells looked round and floated under the light microscope. 9 ml of DMEM culture medium was added and the resulting cell suspension was transferred into a 50 ml reaction tube and the cells were spun down at 500Xg. The pellet was resuspended in DMEM cell culture, and total cell counting from the medium was performed using a Neubauer cell counting chamber with a grid. For further cultivation, the volume containing 500000 to 1000000 cells was completed up to 10 ml with DMEM growth medium and seeded into a T75 flask.

For transfection, prior to seeding 22x22 mm glass slides were sterilised by autoclaving, transferred into EtOH under sterile conditions, and finally dried and laid to the bottom of each well of a 6-well plate, still under sterile conditions. After trypsinization and counting, 100.000-200.000 cells were seeded in each well (total volume of 2 ml) and were grown overnight (to roughly 70% to 80% confluence). Afterwards 20 µl from of dendrimers (10 mg/ml) or dendrimers with embedded autofluorescent gold nanoparticles were added, so that a final concentration of 0.1 mg/ml was achieved. The structures were allowed to transfect cells for 4 hours, then the cells were rinsed thoroughly with PBS and finally fixed with 3.7% (v/v) formaldehyde. The glass slips with fixed cells were mounted onto glass slides and eventually analysed by confocal laser scanning microscopy (the excitation of autofluorescent nanoparticles was carried out at 750 nm by a fibre-coupled coherent mira 900 NIR-fs-laser and the fluorescein moiety of the dendrimer structures was excited at 488 nm with argon laser source).

2.4.5 Production of gold nanoparticles on SbsC-eGFP

For the production of gold nanoparticles the citrate tannin reduction [Oliver C., 1994] was used. 10 µl of 1 µg/µl of SbsC-eGFP was adsorbed onto a glass slide and a silicon wafer, incubated overnight with 3 mM of $HAuCl_4$ for the association of gold atoms with the protein to serve as growth nuclei for gold cluster growth. The reduction of Au salt, *i.e*. growth of gold clusters was

carried out in a solution containing: 46.7 mM Na-Citrate, 72.4 mM K_2CO_3, 58.8 mM Tannin, and 3 mM $HAuCl_4$ for 15 min to 1 hour (Note that all the incubations on glass or silicon substrates were carried out in a humidified Petri dish). After the reduction, the slides were rinsed, dried and observed with SEM and FM.

2.4.6 Conjugation of proteins to metallic nanoparticles

Two main approaches for the conjugation of proteins onto gold or gold/silver alloyed nanoparticles have been adopted: use of chemicals and electrostatic adsorption.

2.4.6.1 Crosslinking of eGFP to Au nanoparticles in solution

eGFP was isolated as outlined above in PBS buffer (by using PBS as the running buffer in FPLC). Gold nanoparticles (with 60 nm diameter) were incubated with 1.7 M DTSSP in PBS for 30 min at room temperature with gentle shaking. 5 mg/ml of eGFP was added and incubated for another 30 min at room temperature with gentle shaking. The reaction was stopped by adding 1 M Tris solution at pH 7.5. The conjugated nanoparticles were cleaned up from the crosslinker and unconjugated eGFP via centrifugation at 6.000 x g for 10 minutes and gentle resuspension in PBS. The efficiency of crosslinking was evaluated via UV/Vis spectroscopy.

2.4.6.2 Adsorption of eGFP (and rPhiYFP) onto Au nanoparticles at various pH values

eGFP was experimentally determined to have a pI value of 5.5 via isoelectric focusing followed by SDS-PAGE. The buffers of choice for generation of pH values near that value were potassium phosphate and potassium acetate buffers. Adsorption was carried out by incubating 5 mg/ml of eGFP with varying amounts of 60 nm-diameter gold nanoparticles at pH values varying around the pI value of eGFP, i.e. pH of 5.5, and at neutrality; followed by spinning down the nanoparticles at 6.000 x g for 10 min in order to separate them from unbound eGFP. The evaluation of the binding was confirmed by three methods.

Firstly, 5 mg/ml of eGFP was incubated with varying amounts of Au nanoparticles at pH 5.5 and 7.0 and spun down as explained above. Aliquots from the supernatants were run on 12% SDS-PAGE, transferred onto a polyvinyl membrane and finally detected using antiGFP antibodies. The lack of eGFP bands indicated pelleting down of eGFP together with Au nanoparticles. Secondly, the same procedure was applied at the pH range as indicated above and the shift in the

LSPR peak upon adsorption of eGFP onto Au nanoparticles was measured by UV/Vis spectroscopy. Thirdly, the efficiency of adsorption was tested by fluorescence spectroscopy, assuming a stronger influence on fluorescence upon stronger binding. Samples were prepared the same way as for UV/Vis spectroscopy. Additionally, another set was prepared under the same conditions except with Au/Ag alloyed nanoparticles with a different LSPR peak, in order to be able to relate the change in fluorescence to Au nanoparticles. A second control was carried out by exchanging eGFP with rPhiYFP, *i.e*. the fluorescence signal intensity of rPhiYFP was compared to signal intensity of rPhiYFP incubated with Au nanoparticles at pH 7.0, rPhiYFP buffered at pH 6.5 (its pI value), and rPhiYFP incubated with Au nanoparticles at pH 6.5. The sample preparation was the same as the above explained eGFP adsorption.

2.4.6.3 Attachment of antiGFP antibodies onto Au nanoparticles

Unlike the attachment of fluorophores onto Au nanoparticles, it is favoured to attach only a limited number of antibodies onto Au nanoparticles. For the determination of the most stable antibody to Au nanoparticle concentration salt test was applied. Dilution series from 0.4 mg/ml to $4x10^{-5}$ mg/ml for the antiGFP antibodies was prepared in water and then mixed with Au nanoparticles (kept constant). After an incubation of 30 min at room temperature with constant gentle shaking, NaCl was added to the final concentration of 1 M. The stability of the conjugates was evaluated visibly by observing the coloration of the suspension, whereby blue is indicative of precipitation and red is indicative of stability.

The adsorption of antiGFP antibodies onto Au nanoparticles was carried out at pH 8.0 (theoretical pI value calculated by SwissProt). The unbound antibodies were removed by spinning the Au nanoparticles at 6.000 x g for 10 min and resuspending the pellet, followed by blocking with 1% (w/v) BSA, Casein, or PVP40. The efficiency of the binding was evaluated by UV/Vis spectroscopy in terms of shifts in the LSPR peak and by incubating the bioconjugated Au nanoparticles and unconjugated ones with SbsC-eGFP adsorbed onto silicon wafer, and observing the distribution of each group by SEM. The ability of the antiGFP antibodies conjugated to Au nanoparticles to bind to eGFP was evaluated by further LSPR shifts and changes in the fluorescence signal intensity of eGFP.

2.4.7 Au nanoparticles functionalised with antiHA antibodies and replacement of bound HA-eGFP by HA-CFP

Solutions of varying concentrations of HA-eGFP and HA-CFP were prepared as follows:

Solution	[HA-eGFP] (mg/ml)	[HA-CFP] (mg/ml)
1	0.5	0
2	1.0	0
3	1.5	0
4	0	0.5
5	0	1.0
6	0	1.5
7	0.5	0.5
8	1.0	1.0
9	1.5	1.5

Afterwards, aliquots from each solution were pipetted on a 96-well plate and the fluorescent signal from each well was measured (i) at 490 nm excitation/520 nm emission, and (ii) at 434 nm excitation/474 nm emission.

60 nm-diameter nanoparticles were functionalised with standard antiHA antibodies and high affinity antiHA antibodies at concentrations of $4x10^{-5}$, $4x10^{-4}$, $4x10^{-3}$, $4x10^{-2}$, and $4x10^{-1}$ mg/ml, and then unoccupied Au nanoparticle surface was blocked with 1% (w/v) PVP40 (as explained in the previous section). The conjugates were incubated with 0.5 mg/ml of HA-eGFP at room temperature for 15 min with gentle shaking; the fluorescence signal at 520 nm was measured by exciting at 490 nm. This was followed by addition of 0.5 mg/ml HA-CFP and a further incubation at room temperature for 15 min with gentle shaking; and the fluorescence signal at 520 nm was measured by exciting at 490 nm.

2.4.8 Quantification of fluorescence signals of transfected HeLa cells

HeLa cells were trypsinized. After counting, 15.000 cells (per well) in DMEM cell growth medium were seeded in the wells of a 96-well plate, while an equal number of wells were only filled with DMEM growth medium and were grown overnight. Firstly, into two wells (one containing cells and one without) dendrimers conjugated to autofluorescent nanoparticles were added to a final concentration of 0.1 mg/ml; into another two wells (one with cells, one without)

only dendrimers were added (0.1 mg/ml final concentration). After 8, 10, 11, and 12 hours, 4 new sets of wells were treated the same way, so that the plate contained:

1. cells transfected with dendrimer-autofluorescent Au nanoparticles for 12, 4, 2, 1, and 0 hours
2. cells transfected with dendrimers for the same time periods
3. empty wells incubated with dendrimer-autofluorescent Au nanoparticles for the same time periods
4. empty wells incubated with dendrimers for the same time periods
5. untransfected cells as well as wells incubated with DMEM but not incubated with any of the structures.

Wells were rinsed with PBS and the fluorescence signal from the autofluorescent Au nanoparticles from each well was measured by the plate reader with excitation at 270 nm and emission at 610 nm.

3 Results

3.1 Formation of protein assemblies with SbsC-eGFP

For the ease of microscopic visualization of the effect of near-field enhancement around metallic nanoparticles on eGFP, the intrinsic property of SbsC to form a well defined tube-like structure was exploited. The SbsC-eGFP fusion protein was adsorbed onto various substrates under different conditions in order to find the most suitable adsorption method which would produce a surface covered with SbsC-eGFP tubes. For the details of high yield production of SbsC-eGFP and the other fluorescent proteins, please refer to the appendix

3.1.1 Adsorption of SbsC-eGFP and metallic nanoparticles onto unmodified glass and silicon

It should be noted that glass surface and silicon surface mimic each other in terms of surface charge and behaviour at the same pH values; although that does not necessarily mean that their surface characteristics are identical [Simões L.C., *et al.*, 2007]. The above mentioned similarity is simply due to the fact that both surfaces are silicon oxides.

Another component in the scheme of observing the effect of metallic nanoparticles on eGFP is naturally the metallic nanoparticles. Therefore, the optimization of surface properties for the binding of SbsC-eGFP should also take the binding of nanoparticles onto the surface into consideration. The main characteristic of nanoparticles which determines the interaction with a substrate is their surface charge, which in turn is determined mainly by the protective surfactant [Hauck T.S., *et al.*, 2008]. Both the commercially purchased gold nanoparticles and those synthesized in our group bear a net negative charge as shown by their migration towards the anode in agarose gel electrophoresis [Jiang X., 2006].

As explained in the methods part, guanidine hydrochloride prevents the SbsC-eGFP monomers from polymerizing, i.e. keeps them as monomers. The first approach was to dialyze the monomers to get rid of GuaHCl in order to allow them to polymerize in the dialysis tube, followed by adsorbing them onto glass slides for atomic force microscopy (Fig. 14).

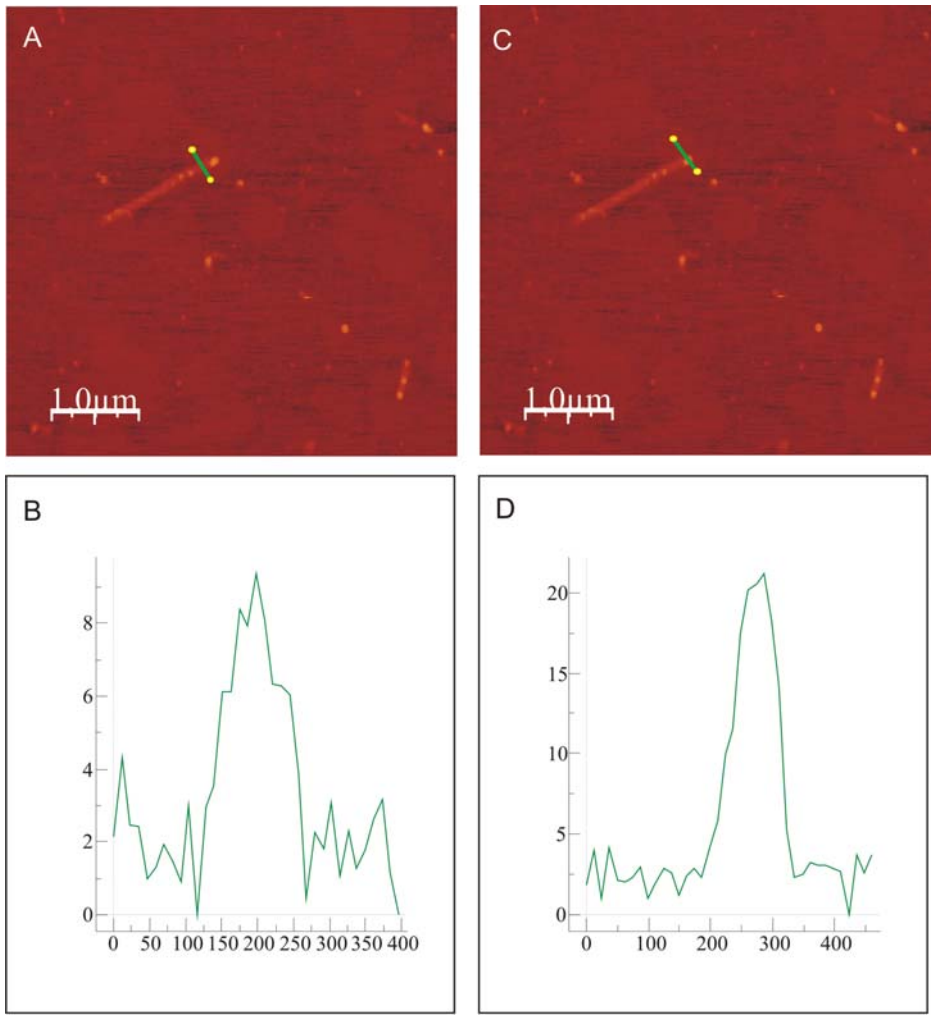

Figure 14. AFM analysis of SbsC-eGFP tubes and gold nanoparticles adsorbed onto glass. SbsC-eGFP tubes were adsorbed onto glass slides followed by incubation with gold nanoparticles of 60 nm diameter, and AFM images were taken (A and C). Height profiles were taken at two different points (indicated by green dashes in A andC): In a region that is devoid of nanoparticles (A and B), and in a region where SbsC-eGFP tube is interacting with a gold nanoparticle (C and D).

SbsC-eGFP forms the expected tube structures that are randomly distributed on the surface. Yet a certain amount interacts with the nanoparticles. The height of the SbsC-eGFP tubes (8 nm on average) is in the expected range [Blecha A., 2005]. However, the height of the nanoparticles seems to be less than 60 nm. This is due to the spherical shape of the nanoparticles: the AFM tip does not measure the maximum height of the nanosphere due to random contact. The size of the nanoparticles was confirmed to be 60 nm by SEM. Therefore, the average AFM measurement of 25 nm is accepted to be the internal error.

3.1.2 Surface modifications on glass and silicon

In the pH range of PBS, glass has an overall negative charge. In order to see the effect of charge of surface on the behaviour of SbsC-eGFP, glass slides and silicon wafers were treated with different chemicals and processes, which mostly give an overall positive charge, then incubated with the SbsC-eGFP and/or nanoparticles and finally analyzed by microscopic methods.

3.1.2.1 APTES treatment

3-aminopropyltriethoxysilane is a chemical commonly used to promote adhesion between glass or other siliceous surfaces and organic or metallic materials with applications ranging from advanced composites to biomolecular lab-on-a-chip applications [Howarter J.A. and Youngblood J.P., 2006]. APTES acts by creating positively charged aminopropyl groups on the surface onto which anionic matter can adsorb.

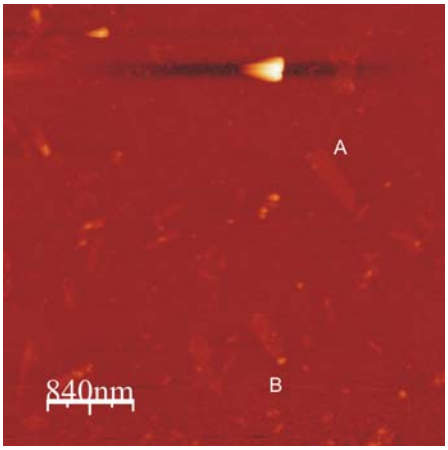

Figure 15. AFM image of SbsC-eGFP and gold nanoparticles adsorbed onto APTES functionalised glass. Patches formed by SbsC-eGFP with (A) and without gold nanoparticles (B).

Interaction of SbsC-eGFP with APTES treated glass seems to be different from that with untreated glass, as clearly evidenced by the formation of sheet like structures rather than the expected tubes. The patches and spots were determined to be SbsC-eGFP and nanoparticles respectively by height analysis (data not shown).

3.1.2.2 GOPTES treatment

(3-Glycidyloxypropyl)trimethoxysilane is another silane used as an alternative to APTES. The mechanism of action of GOPTES is the production of epoxy-silane groups on the surface of

choice. The main advantage of GOPTES over APTES is the fact that epoxysilane groups are more reactive as compared to aminopropyl groups [Tsukruk V.V., *et al.*, 2002].

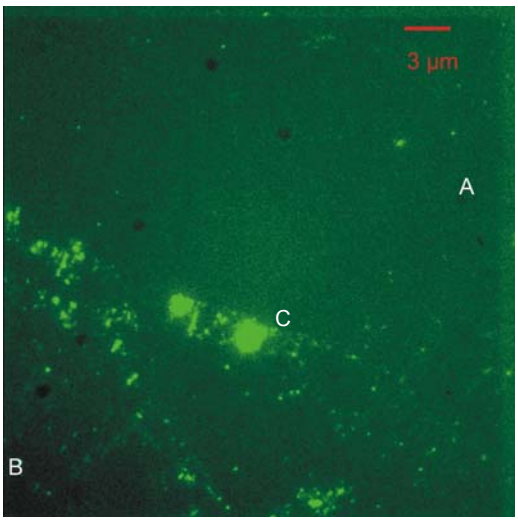

Figure 16. eGFP adsorbed on GOPTES treated glass. eGFP molecules attached to the epoxysilane groups (A), uncovered glass (B), and eGFP aggregates (C) (100x magnification)

As can be seen in Fig. 16, eGFP covers an epoxysilane functionalised glass quite uniformly, even though some aggregates can be observed. Covering is obvious when compared to the bottom left corner (uncovered). The adsorption behaviour of SbsC-eGFP on GOPTES treated glass was also analysed (please refer to fig 17). The typical tube-like structures, which provide a means for identification under the microscope, were formed on GOPTES treated glass.

3.1.2.3 Plasma treatment and poly-L-lysine coated glass

Gas plasma treatment is extensively used for chemical modification of a polymer surface. For example, nonpolymerizing gas plasma treatment may create reactive sites on the surface of polymers Wang D.Y., *et al.*, 2007]. It has been previously shown that during the course of oxygen plasma treatment the number of oxygen bonded to silicon gradually increases [Olander B., *et al.*, 2004], which increases the wettability, i.e. the hydrophilicity of the surface.

The oxygen plasma treatment did not confer any advantage over regular silicon wafer. However, on the other hand the adsorption of the nanoparticles seemed to be reduced. This is most probably due to the charge repulsion between negatively charged gold nanoparticles and the hydroxyl groups introduced by the oxygen treatment.

In addition to the above mentioned chemical surface modification methods, the adsorption behaviour of SbsC-eGFP and nanoparticles were tested on poly-L-lysine glass. Like aminopropyl and epoxysilane groups, lysine is positively charged due to its ε-amino group; so that it confers an overall positive charge to the surface. However, the main difference between lysine and the two other methods is that lysine is an amino acid. Therefore the main motivation to test it was to observe the efficiency of adsorption of SbsC-eGFP onto biological matter rather than a chemically modified surface.

Poly-L-lysine glass slides proved to be too rough for AFM analysis, no structure was visible on the slides (data not shown). Therefore, the usage of this type of slides was abandoned.

3.2 Effect of nanoparticles on eGFP fluorescence on a microscope slide

The aim of this study is to investigate the effect of nanoparticles on fluorescent proteins, i.e. to determine whether fluorescence is reduced or enhanced or unaffected. To this end, the most suitable surface modification was selected, which in our case turned out to be epoxysilanization by GOPTES treatment. In a sequential approach SbsC-eGFP was first deposited on epoxysilane functionalized glass, followed by deposition of gold nanoparticles. The following image (Fig. 17) shows the fluorescence and AFM images of such structures.

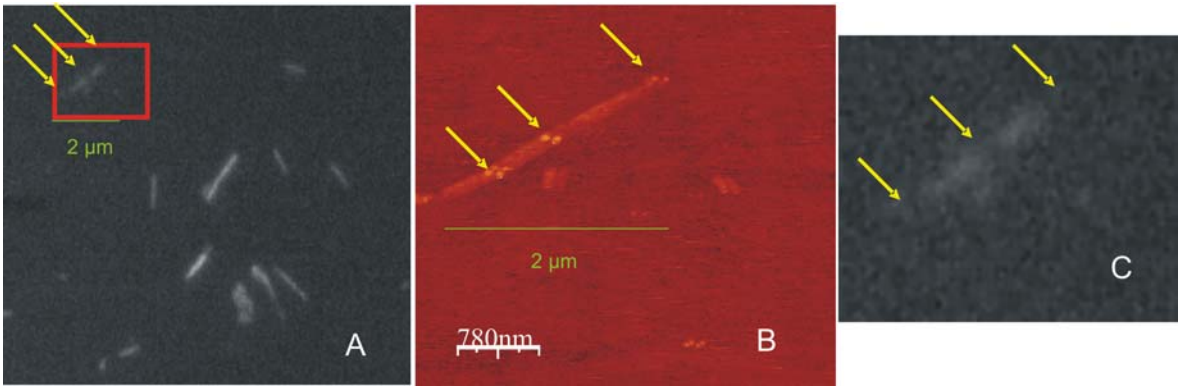

Figure 17. Effect of nanoparticles on the fluorescence of eGFP. (A) Fluorescence image of SbsC-eGFP and gold nanoparticles (60 nm) adsorbed onto GOPTES treated glass. (Magnification 100 x; for details see text. (B) AFM image of the area indicated by the red rectangle in (A). (C) Zoomed-in fluorescence microscopy image of the rectangled area of (A). Height profile is in agreement with Fig. 14 (data not shown). Yellow arrows indicate the positions of gold nanoparticles.

Firstly, it should be noted once again that SbsC-eGFP retains the characteristic tube-like appearance on an epoxysilane functionalized glass. Along the rod in the red rectangle of Fig. 17 A, fluorescence is discontinuous. When this SbsC-eGFP tube was analysed by AFM (B), all the structures are doubled due to a phenomenon called double tip (if the tip is broken, or contaminated, one can often get a "double tip" effect, where both the tip and the contamination are scanning the surface, so that the structures scanned have twins). In spite of this, three nanoparticles could clearly be observed and were identified by height measurement. In C, the same area is presented with a zoom. Upon comparing the AFM image with the fluorescence pictures, it becomes clear that the discontinuity of fluorescence is limited to the parts of SbsC-eGFP that interact with the gold nanoparticles.

3.3 Formation of nanoparticles on SbsC-eGFP

One of the well established easy, rapid, and cheap methods of producing gold nanoparticles is reducing gold complexes with the help of a reducing agent such as citric acid [Philip D., 2007]. It has been suggested that a very efficient method of conjugating nanoparticles to proteins is synthesizing nanoparticles via chemical reduction in aqueous solutions containing globular proteins, where the unreduced gold is first incubated with the globular proteins and then reduced. This method has been claimed to eliminate the necessity to use a linker, passivation of nanoparticles by protective agents, and to prevent nanoparticle aggregation [Burt J.L., *et al.*, 2004]. In our approach, SbsC-eGFP tubes were first adsorbed onto glass slides and silicon wafers, onto which then gold nanoparticles were deposited by chemical reduction of the gold complexes via citric acid. Formation and distribution of gold nanoparticles were observed by scanning electron microscopy. The effect of gold nanoparticles on the fluorescence behaviour of eGFP was analysed by fluorescence microscopy.

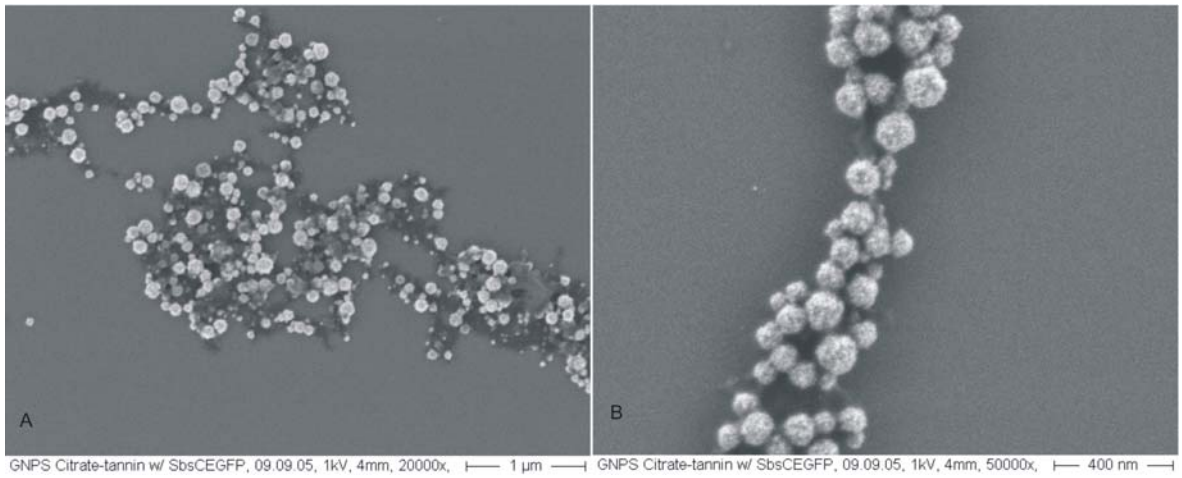

Figure 18. SEM image of SbsC-eGFP tubes bearing gold nanoparticles. Gold nanoparticles were synthesized on the SbsC-eGFP tubes which had been adsorbed on a silicon wafer prior to the gold nanoparticle synthesis.

First implication to be taken from the SEM image (Fig. 18) is that formation of the nanoparticles on the SbsC-eGFP by reduction is successful, resulting in the formation of uniformly sized nanoparticles on the SbsC-eGFP tubes. However, the technique seems to deform the tubes because the protein in the image no longer demonstrates the typical tube-like organization.

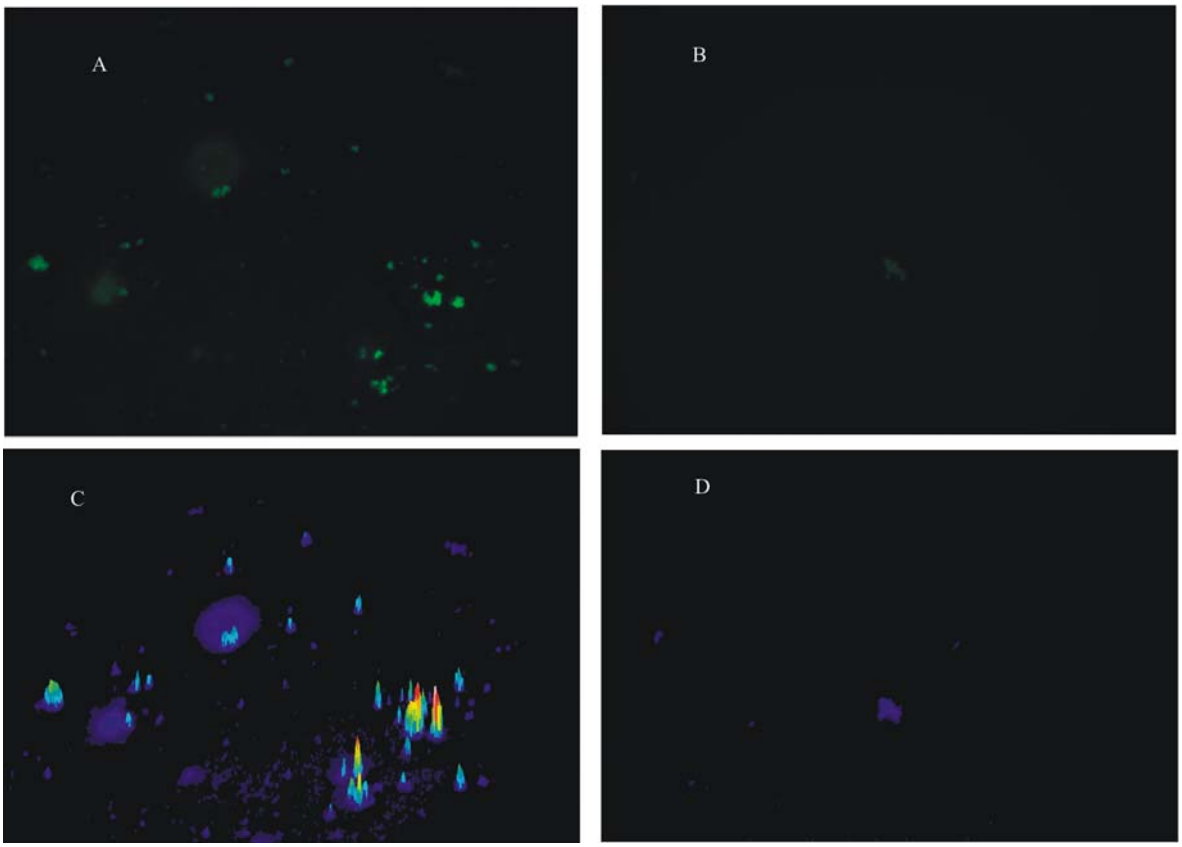

Figure 19. Fluorescence images and intensity profiles of SbsC-eGFP bearing gold nanoparticles. SbsC-eGFP adsorbed onto glass (A); gold nanoparticles were formed on the SbsC-eGFP as explained in the text and the resulting conjugates were adsorbed onto glass (B). The fluorescence signal intensity profiles of SbsC-eGFP (C) and of SbsC-eGFP-nanoparticle conjugates (D) (100 x magnification)

From the comparison of the fluorescence signals and intensity profiles (A and C to B and D, respectively), it seems that eGFP fluorescence signal is significantly reduced. This can be due to denaturation of eGFP or quenching of the signal.

3.4 Quantification of the effect of nanoparticles on eGFP in solution

Although the fluorescence and scanning electron microscopy images prove to be valuable tools not only for analysing the interaction of SbsC-eGFP with metallic nanoparticles, but also for the determining, how nanoparticles affect the fluorescence signal of eGFP, the images obtained due to changing parameters are difficult to compare. Moreover, for the images obtained by microscopy specimens were used, which were adsorbed onto various substrates, and this does not necessarily simulate the situation in a solution.

In the following chapters the conjugation and interaction of gold or silver nanoparticles or gold-silver alloy nanoparticles to eGFP or yellow fluorescent protein (rPhiYFP) by different methods and the effect they exert on fluorescence is described without the additional influence of a substrate.

3.4.1 Effect of pH on binding efficiency and change in fluorescence signal of fluorescent proteins onto nanoparticles

As explained before the nanoparticles utilised in this work bear a net negative charge. Therefore one of the most straightforward methods for conjugating proteins onto them is to cause an electrostatic attraction. Another advantage of such an electrostatic interaction is the stability of the binding [Brewer S.H., *et al.*, 2005; Tkachenko A. *et al.*, 2005].

Firstly, the optimum ratio between nanoparticles and eGFP was estimated by testing the stability of the conjugates containing different nanoparticle to eGFP ratios in a solution with a high salt concentration. Nanoparticles are negatively charged and the cations in the salt solution cause the aggregation of the nanoparticles. However, if they are stabilized by proteins, polymers etc., the salt bridges are not formed and the nanoparticles are stable in the saline solution [Rouhana L.L., *et al.*, 2007]. The destabilization of nanoparticles is observed by the colour of the suspension turning to blue. However, the results of this test are not definitive, just gives an idea about the optimum ratio between the nanoparticle concentration and adsorbed material concentration, because it is assumed that nanoparticle-protein conjugates which are stable at very high salt concentration are also stable at lower concentrations.

First proof to the successful binding of eGFP onto nanoparticles comes from Western blots. The same molar concentration of protein was incubated with equal amount of gold nanoparticles at neutral pH and pH 5.5. Afterwards the nanoparticles were spun down and aliquots from the supernatants were run on 12% SDS-PA gel, followed by Western blot transfer (Fig. 20).

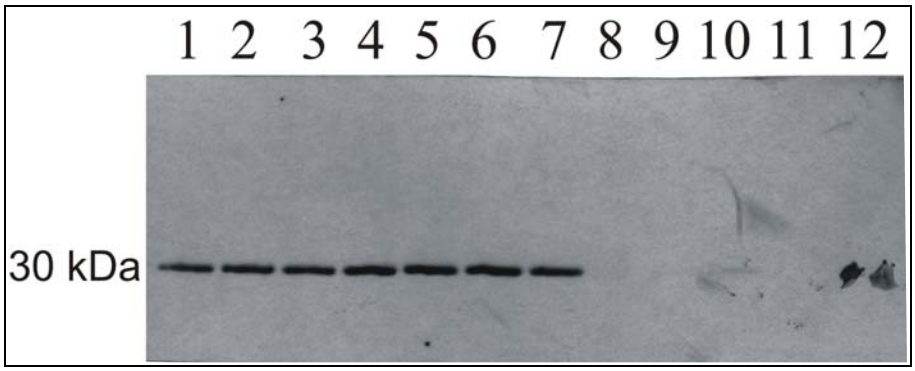

Figure 20. eGFP in the supernatant after adsorption onto gold nanoparticles. eGFP was adsorbed onto gold nanoparticles (60 nm diameter) at neutral pH (lanes 1-6) and pH 5.5 (lanes 7-12), and then the nanoparticles were spun down and the supernatant fractions were checked for eGFP content. Controls, i.e. eGFP without nanoparticles are the lanes 1 and 7. Lanes 2-6 and 8-12 represent an increasing nanoparticle to eGFP ratio, where NP amount was kept constant.

The supernatants from the samples incubated at neutral pH showed strong protein bands, whereas no protein band was visible in any of the aliquots taken from the samples incubated at the pI value of eGFP. This clearly hints to a far more effective adsorption at the pI value of the protein, since the protein precipitates with the nanoparticles in the pellet fraction upon centrifuging at a speed not high enough to precipitate unconjugated eGFP, *i.e.* 6.000 x g.

The efficiency of the binding was then evaluated then by UV/Vis spectroscopy. Due to the presence of localised surface plasmons the metallic nanoparticles possess a characteristic peak in the UV/Vis absorption spectrum. The wavelength of the peak is a function of the size, shape, and composition of the nanoparticles, as well as the dielectric constant of the surrounding medium [Lue J.-T., 2001]. The binding of a protein, polymer, etc. on the surface of a nanoparticle changes the dielectric medium of the environment and hence induces a shift in the position of the plasmon peak. Therefore, when using nanoparticles with the same size, shape, and composition, it is possible to measure the efficiency of binding by measuring the shift in the plasmon peak.

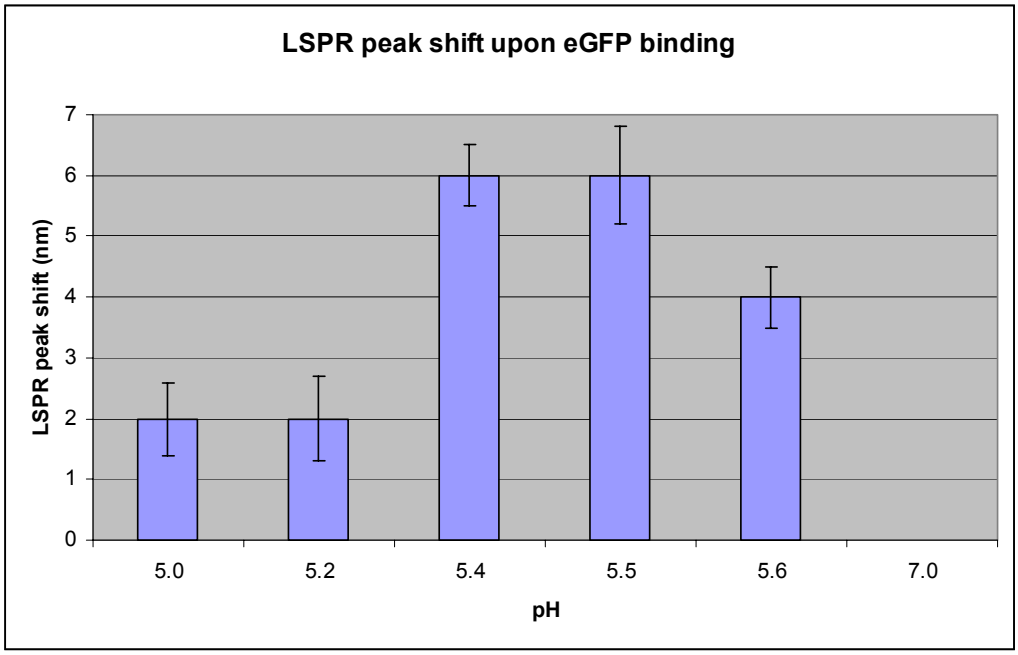

Figure 21. Shift in the plasmon peak of AuNPs upon eGFP adsorption at different pH values. eGFP was adsorbed onto 60 nm diameter gold nanoparticles at different pH values and their absorption spectra were measured. The size of the shift of the LSPR peak relative to unconjugated NPs is presented on the graph.

The graph (Fig. 21) illustrates that the shift in the plasmon peak is greater when eGFP is adsorbed onto nanoparticles at a pH value close to its pI value.

The third method for testing of the binding of nanoparticles to fluorescent proteins was to measure the change in their fluorescence signal upon binding to nanoparticles; inspired from existing literature and previous results. As explained above, binding of nanoparticles to SbsC-eGFP tubes diminish the fluorescence of the tubes at the contact points between nanoparticle and fluorescent protein. By taking that into account, it was expected to see a stronger reduction in the fluorescence signal of the fluorescent proteins upon a more efficient binding, *i.e.* a higher ratio of bound protein.

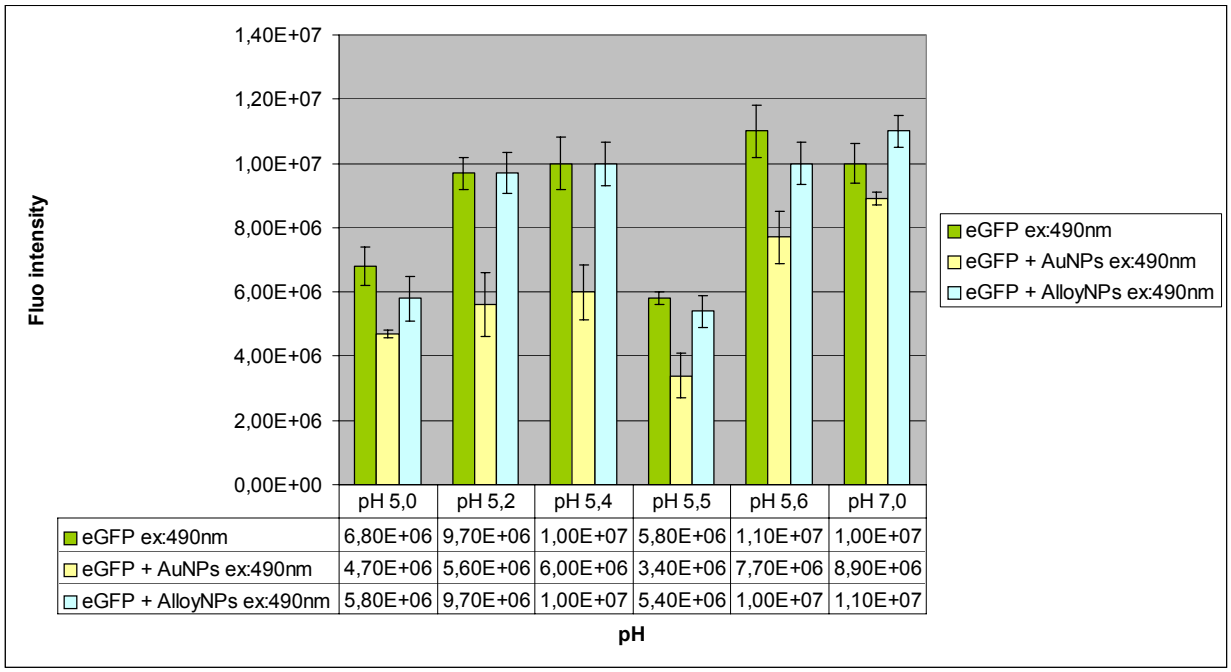

Figure 22. Dependence of eGFP fluorescence signal on the nanoparticles and pH. Same concentration of eGFP was adsorbed onto two types of nanoparticles: gold nanoparticles, and gold and silver alloyed nanoparticles, both with 60 nm diameter. Green columns: eGFP fluorescence signal at different pH values; yellow columns: eGFP signal upon adsorption to gold nanoparticles at various pH values; teal columns: eGFP fluorescence signal upon adsorption to alloyed nanoparticles at the same pH values (emission at 520 nm and excitation at 490 nm).

As can be observed from the graphs (Fig. 22) eGFP fluorescence signals are reduced when conjugated to gold nanoparticles, which have a plasmon peak around 520 nm. The extent of fluorescence reduction is more pronounced, when binding is carried out at the pI value of eGFP. On the other hand silver-gold alloyed nanoparticles, which have plasmon peak at 490 nm, seem not to strongly affect eGFP fluorescence. This is in accordance with the UV/Vis spectroscopy and Western blot data. The first conclusion that can be drawn from these results is that the most effective binding of eGFP onto nanoparticles takes place at its pI value. However, the main focus is the effect of the nanoparticles on fluorescence. What remains as a question is the reason for the observed reduction in the fluorescence signal. One possible explanation can be the denaturation of eGFP by the near field enhancement around the nanoparticles. Yet another and perhaps more likely explanation is the interaction of metallic nanoparticles with the fluorescence signal without denaturing the proteins. It is well documented in literature that metallic nanoparticles interact with fluorophores either by quenching or by enhancing their fluorescence signals [Kühn S., *et al.*,

2006; Anger P., *et al.*, 2006]. Same type of experiments were done by adsorbing rPhiYFP onto gold nanoparticles (Fig. 23)

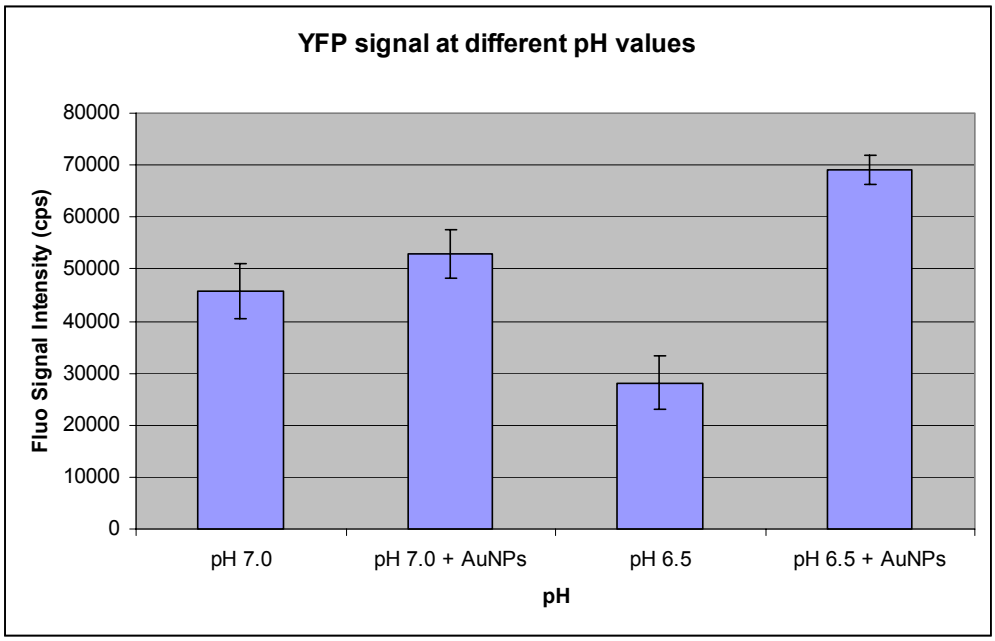

Figure 23. pH-dependence of rPhiYFP fluorescence. rPhiYFP was adsorbed onto 60 nm diameter nanoparticles at neutral pH and at pH 6.5 (*i.e.* the pI value of rPhiYFP). The graph shows the comparison of the fluorescence signal (emission at 535 nm and excitation at 525 nm) between non-adsorbed rPhiYFP at pH 7.0 (first column), rPhiYFP adsorbed onto nanoparticles at pH 7.0 (second), non-adsorbed rPhiYFP at pH 6.5 (third), and rPhiYFP adsorbed onto nanoparticles at pH 6.5 (fourth).

As in the case of eGFP, the adsorption of rPhiYFP onto nanoparticles seems to be most effective at the pI value. However, contrary to gold nanoparticles the fluorescence of rPhiYFP seems not to be reduced by the nanoparticles, rather an enhancement in fluorescence is observed. By tuning the plasmon peak of nanoparticles, which is possible by using gold-silver alloyed nanoparticles with different gold to silver ratio and hence different plasmon peaks, it is possible to reduce the extent of fluorescence reduction of the eGFP fluorescence signal. Taking into account that alloyed nanoparticles with a LSPR peak at 490 nm either do not quench eGFP fluorescence or do not quench as strong as gold nanoparticles with LSPR peak at 520, it seems likely that the effect of nanoparticles on the fluorescent proteins is not to due to denaturation, but either to enhance or to quench their signals, depending on the nature of the fluorophore and of the nanoparticles of choice.

3.4.2 Cross-linking of proteins onto nanoparticles

In order to compare the efficiency of cross-linking proteins onto nanoparticles with the efficiency of adsorbing them at their pI values, eGFP was cross-linked to gold nanoparticles by DTSSP; and the binding was monitored by UV/Vis and fluorescence spectroscopy (Fig. 24).

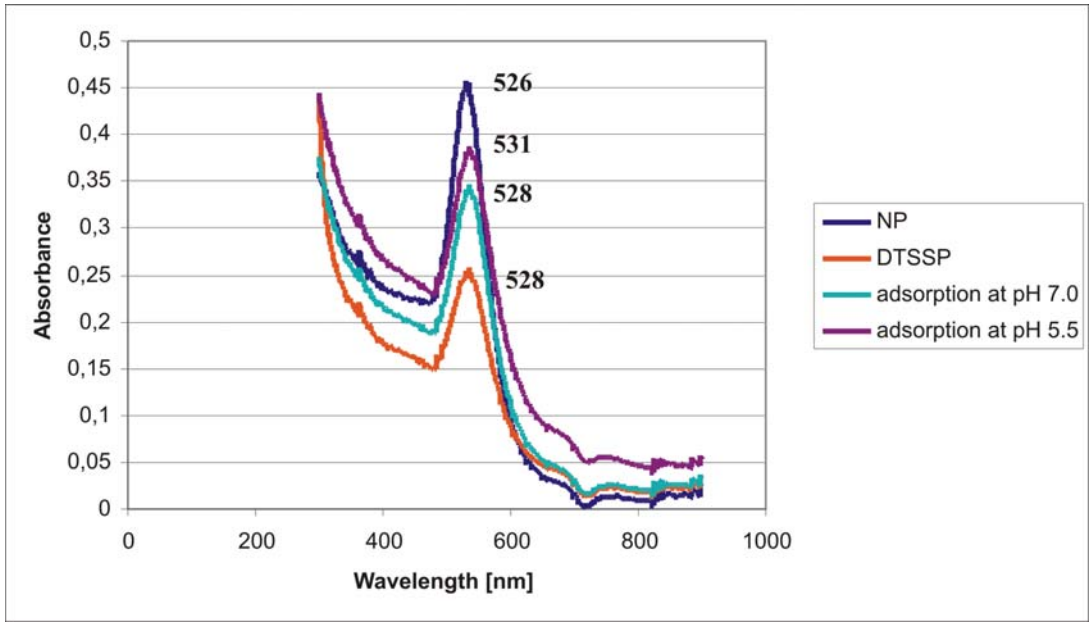

Figure 24. UV/Vis absorption spectrum of gold nanoparticles upon adsoption of eGFP by various methods. Unmodified, 60 nm diameter gold nanoparticles show a characteristic plasmon resonance peak at 526 nm (blue). The plasmon peak is 2 nm red-shifted upon adsorption of eGFP at pH 7.0 (turquoise) and upon cross-linking eGFP via DTSSP (orange). A shift to right of 5 nm is obtained, when eGFP is adsorbed onto nanoparticles at its pI value (pink).

When the shifts in the plasmon peak positions are compared, it is evident that the biggest shift takes place when eGFP is adsorbed onto nanoparticles at its pI value, exceeding even the shift in the case of DTSSP usage. The reductions in the peak sizes hint at greater particle aggregation as a result of functionalisation. Adsorption at pI value proves to be more effective than the two other cross-linking methods, since it demonstrates the smallest peak size reduction. It is noteworthy to mention that more efficient adsorption on the nanoparticle fits with the highest fluorescence quenching, as explained in the previous part.

3.5 Combining the LSPR shift with fluorescence quenching as the basis of a bioassay method

In the literature use of LSPR resonances in biosensors has been reported several times, as well as use of fluorescent reporters for the very same purpose. Both methods come with intrinsic advantages and disadvantages. The main disadvantage of LSPR based sensors is the reproducibility of the nanoparticle synthesis. Most nanoparticles are synthesized by using a competitive growth-and-passivation process to control the size of the particle. Such a control is very rough. As a result, most nanoparticle products synthesized from wet chemical methods are polydispersed, particles with a range of size distribution instead of one uniform size [Huo Q., 2007]. Since the LSPR peak (and many other properties) of nanoparticles depends strongly on size, this variation in the size might impose a problem. Therefore combination of LSPR based sensing with fluorescence as a second method might improve the sensitivity of the measurement.

3.5.1 Functionalisation of nanoparticles with antibodies

Based on the above-mentioned process, a simple scheme was devised. Gold nanoparticles were functionalised with antiGFP antibodies, and then their capability to bind to eGFP, the extent of plasmon peak shift as well as the fluorescence quenching was measured. As explained above, the most straightforward, simplest, and cleanest method for protein binding onto gold nanoparticles was determined to be adsorption at the pI value of the proteins. Therefore antibodies were adsorbed onto gold at pH 8, the general theoretical pI value for IgG class antibodies.

With a simple method, the functionalisation of nanoparticles with antiGFP antibodies was evaluated. Firstly SbsC-eGFP was adsorbed on a silicon wafer, and then the distribution of nanoparticles functionalised with antiGFP antibodies was compared with that of non-functionalised nanoparticles (Fig. 25).

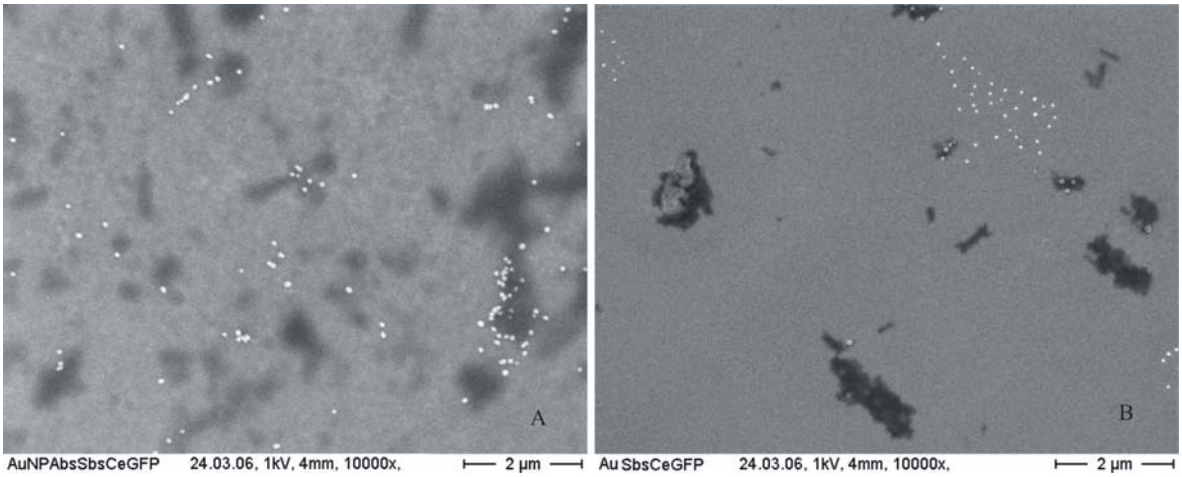

Figure 25. Distribution of bare and antibody-linked nanoparticles on a surface with an antigen. SbsC-eGFP was adsorbed onto silicon wafers (black patches on both SEM images). AntiGFP antibody adsorbed- (A) and non-functionalized (B) gold nanoparticles (white dots, 60 nm diameter) were incubated on the wafers.

Clearly, the distribution of the nanoparticles in the two images differs. On the right image, nanoparticles seem to be distributed randomly. On the left image nanoparticles demonstrate a bigger tendency to cluster on the proteins rather than random distribution; probably due to functionalisation with antiGFP antibodies.

Although the microscopy images suggest a successful functionalisation, UV/Vis spectroscopy measurements were also carried out, in order not only to provide further evidence to functionalisation but also to quantify the amount of antibodies associated with nanoparticles in terms of shifts in the plasmon peak. Firstly, the optimum ratio range between the antibodies and nanoparticles was inferred by the salt test, as explained previously. The binding was confirmed by UV/Vis spectroscopy (section 3.5.2.1).

As seen from the following UV/Vis spectroscopy data (Fig. 26) it is possible to attach antibodies onto nanoparticles by adsorbing them at their pI values. The conjugation by this way does not only seem to be stable, but also the antibodies seem to retain their functionality, as suggested by the SEM images in Fig. 25.

3.5.2 Binding capability of antibody-functionalised nanoparticles to respective fluorescent proteins in solution

As outlined, the two components of the bioassay system to be combined are PPR shift and the fluorescence change. To this end, the functionalized nanoparticles should be able to bind to the respective fluorescent proteins (as explained above they seem to be capable of binding to SbsC-eGFP on a silicon wafer), furthermore the binding should cause a further shift in the plasmon peak, i.e. in addition to the one caused by the adsorption of the antibodies onto nanoparticles, as well as a change in the fluorescence intensity of the fluorophore.

3.5.2.1 UV/Vis spectroscopy measurements

As explained in 3.3.1, the plasmon peak position of metallic nanoparticles depends on size, composition, shape, and the dielectric constant of the surrounding medium; and any kind of interaction the nanoparticles engage in, represents a change in the dielectric constant of the medium, and hence a shift in the plasmon peak. Furthermore this effect is cumulative, *i.e.* if nanoparticles go through a stepwise adsorption, a stepwise shift in the plasmon peak is observed, as long as the adsorbing matter is still in a critical distance from the surface of the nanoparticle. Therefore, functionalisation of nanoparticles with antibodies and the subsequent attachment to the respective antigen is expected to yield a two stepped shift in the plasmon peak.

According to the above mentioned scheme, gold nanoparticles were functionalised with antiGFP antibodies by adsorbing them at pH 8.0 and then incubated with defined amounts of the respective fluorescent protein.

Table 1. Plasmon peak position of gold nanoparticles after functionalisation with anti-GFP antibodies and subsequent incubation with increasing amounts of eGFP

Plasmon peak position		**Antibody concentration (mg/ml)**					
		0	$4*10^{-5}$	$4*10^{-4}$	$4*10^{-3}$	$4*10^{-2}$	$4*10^{-1}$
eGFP conc (mg/ml)	0	529.9	530.4	531.4	533.0	533.5	533.8
	0.4	531.3	532.2	533.2	533.0	533.2	533.6
	0.8	532.4	533.4	533.4	533.1	533.5	533.7
	1.2	533.1	533.8	534.2	533.5	533.7	533.8

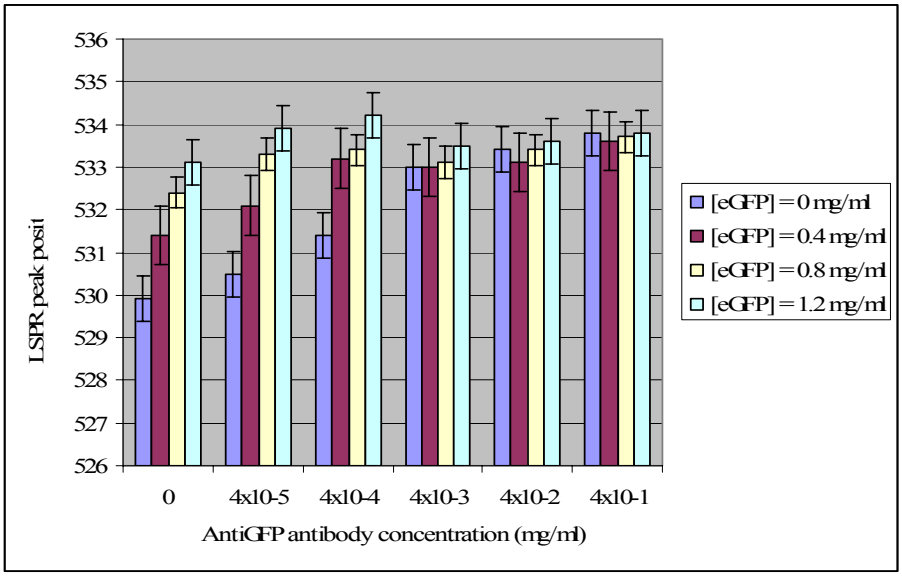

Figure 26. Shift in the plasmon peak of gold nanoparticles upon functionalisation with anti-GFP antibodies and subsequent incubation with increasing amounts of eGFP. 60 nm diameter gold nanoparticles were attached to various concentrations of anti-GFP antibodies (X axis) at pH 8.0 and the UV/Vis spectra were measured before the addition of eGFP (blue column) and after each addition of 0.4 mg/ml of eGFP in a stepwise fashion. The graph is constructed by plotting the peak positions of the plasmon peaks.

The expected two-stepped shift in the plasmon peak can be clearly observed in the above graphs, when the antibody concentration is within a certain range. According to the graphs this concentration is between 4 x 10^{-5} mg/ml and 4 x 10^{-4} mg/ml. It is possible that, when the antibody concentration is higher than 4 x 10^{-3} mg/ml, plasmon signal is already saturated, i.e. interaction of further material with the gold nanoparticles does not cause an additional shift. Therefore, the biggest shift in the first step does not necessarily represent the optimum ratio between the antibody concentration and sensor affectivity. Once again, the observed optimum antibody to gold nanoparticle ratio for the above mentioned case is around an antibody concentration of 4 x 10^{-5} mg/ml and 4 x 10^{-4} mg/ml.

The second subsequent shifts in the plasmon peak confirm not only the presence of bound antibodies on the gold surface, but also that the antibodies retain their functionality, provided that eGFP only binds to antibodies. One convenient way to prevent unspecific binding is to block the gold surface after the functionalisation with antibodies. Such a blocking agent should fulfil certain criteria: First of all, it should be inert, *i.e.* fluorescent proteins must not interact with the blocking agent, but only with the antibodies. Secondly, the plasmon shift caused by the blocking

agent must not be as big as that of antibodies as well as the fluorescent protein. Thirdly, it should not inhibit the binding of the fluorescent proteins to their respective antibodies. Among the blocking agents available and tested, polyvinylpyrrolidone (PVP40) proved to be the most suitable. Nanoparticles were first functionalized with antiGFP antibodies, then blocked with PVP40, and finally exposed to increasing concentrations of eGFP for the measurement of the plasmon peak shift.

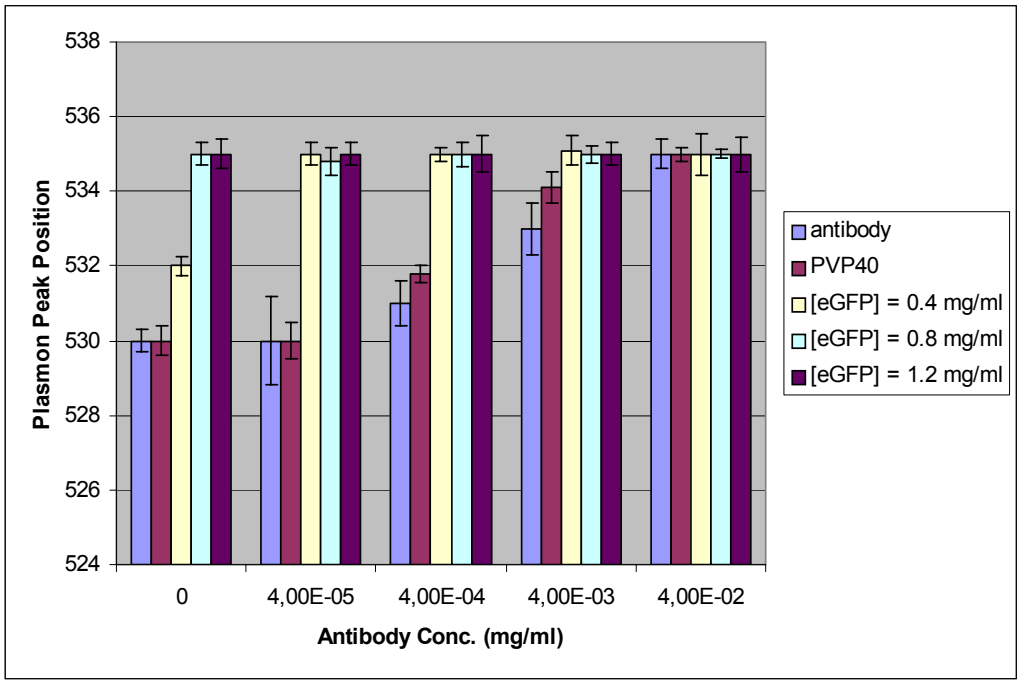

Figure 27. Shift in the plasmon peak of gold nanoparticles upon functionalisation with anti-GFP antibodies, blocking with PVP40, and incubation with increasing amounts of eGFP. 60 nm diameter gold nanoparticles were attached to various concentrations of anti-GFP antibodies (X axis) and the UV/Vis spectra were measured before blocking with PVP40 and the addition of eGFP (blue column) and after first blocking with PVP40 (pink column), and then each 0.4 mg/ml of eGFP were added in a stepwise manner. The graph is constructed by plotting the peak positions of the plasmon peaks.

As can be seen from Fig. 27, PVP40 fulfils the above mentioned criteria. Blocking with PVP40 does not cause a big plasmon shift, and the antibodies seem to retain their ability to bind to eGFP. Furthermore, as can be seen from the control column, eGFP demonstrates minimum adsorption on the PVP40 layer.

3.5.2.2 Fluorescence measurements

After the binding and the retaining of functionality of the antibodies were confirmed by UV/Vis spectroscopy in terms of plasmon peak shifts, the effect of nanoparticles on fluorescence was evaluated. The fluorescence signals of the previous constructs were measured using a fluorescence plate reader.

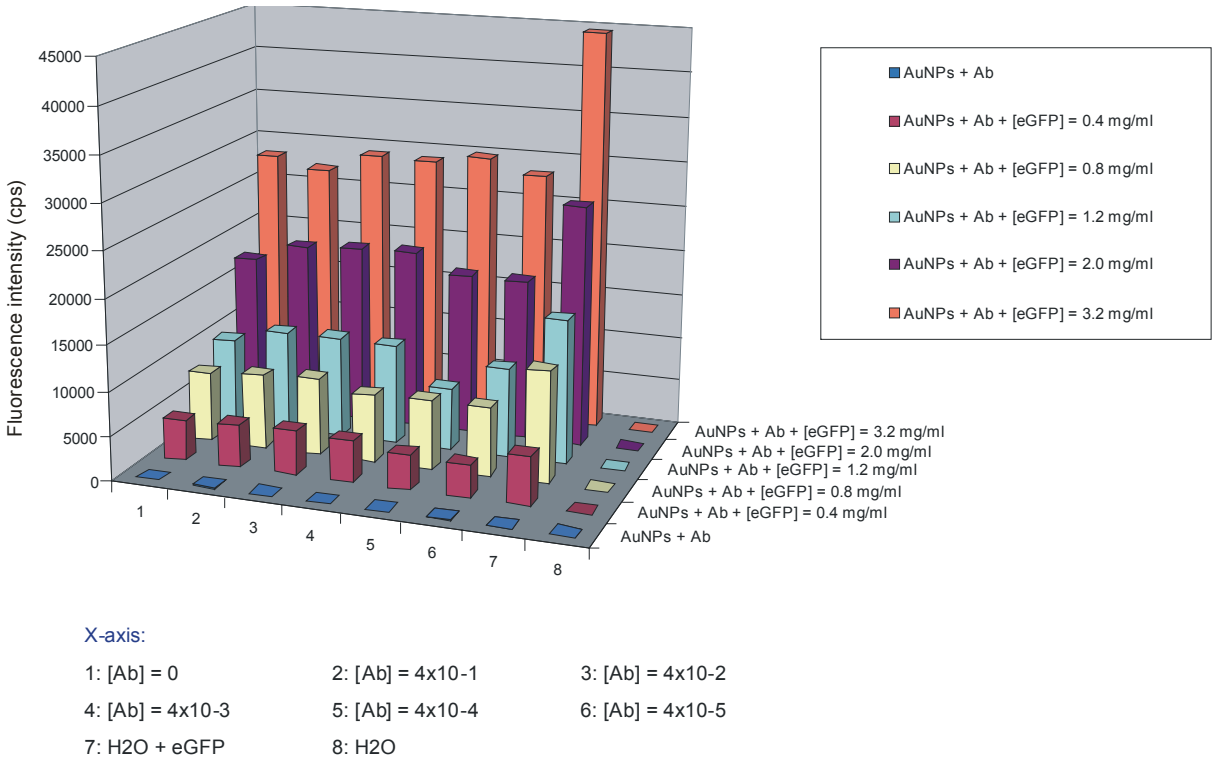

X-axis:

1: [Ab] = 0	2: [Ab] = 4x10-1	3: [Ab] = 4x10-2
4: [Ab] = 4x10-3	5: [Ab] = 4x10-4	6: [Ab] = 4x10-5
7: H2O + eGFP	8: H2O	

Figure 28. Change in the fluorescence signal of eGFP upon binding to 60 nm gold nanoparticles functionalised with antiGFP antibodies. Y-axis shows the fluorescence signal intensity.

Fig. 28 shows that the extent of quenching does not increase with increasing antibody concentration. This indicates that there is indeed a critical antibody to gold nanoparticle ratio, which yields not only the optimum plasmon peak shift but also the biggest fluorescence quenching.

3.6 Displacement assay with two different fluorophores

As explained in the previous part, it is possible to functionalise nanoparticles with antibodies and to measure the binding of the antibodies to their antigens via plasmon peak shift and fluorescence, provided that the antigen has autofluorescence or is coupled to a fluorescent tag.

Furthermore, various fluorophores show different behaviours when they are brought in the vicinity of nanoparticles, e.g. gold nanoparticles quench the fluorescence of eGFP, whereas the fluorescence of rPhiYFP seems to be enhanced (Part 3.3.1). This observation formed the basis for the bioassay model explained in the aim of the work.

The model consists of two fluorophores, namely eGFP and cyan fluorescent protein (CFP), both HA tagged; and gold nanoparticles functionalised with Roche low or high affinity antiHA antibodies. The motivating question was whether it is possible to replace the antigen in such a nanoparticle-antibody-antigen construct and to monitor the replacement (please refer to figure 1 in the Aim).

3.6.1 Interference of eGFP and CFP fluorescence signals

In order to use two different fluorescent proteins in an exchange type assay, which includes measuring fluorescence, it is necessary that the two fluorophores do not quench or enhance each other´s signal. In the fluorescent plate reader, the fluorescence emissions of both fluorescent proteins were measured at their respective excitation maxima (Fig. 29).

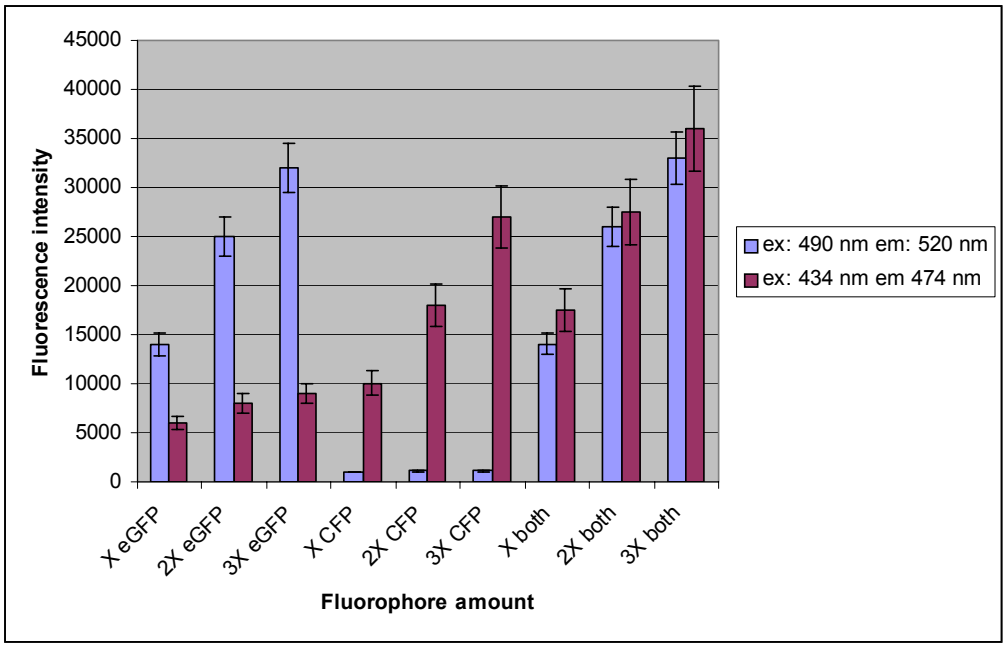

Figure 29. Interference of eGFP and CFP fluorescence signals. X stands for 0.5 mg/ml

As can be seen from Fig. 29, eGFP and CFP might be good reporter systems: CFP does not give a signal when excited at the excitation maximum of eGFP (490 nm). However, eGFP still emits when excited at the excitation maximum of CFP (434 nm).

3.6.2 The Assay

After determining (i) that it is possible to functionally cover nanoparticles with antibodies, (ii) that with PVP40 surfaces on nanoparticles that are not occupied with antibodies can be blocked, (iii) that depending on the choice of fluorescent reporters, interaction of the fluorophores can be minimized, and finally (iv) that all the modifications on the gold surface, i.e. functionalisation, blocking, binding of the antigen to the antibody, can be monitored by shifts in the plasmon peak, the capability of the assay system was tested.

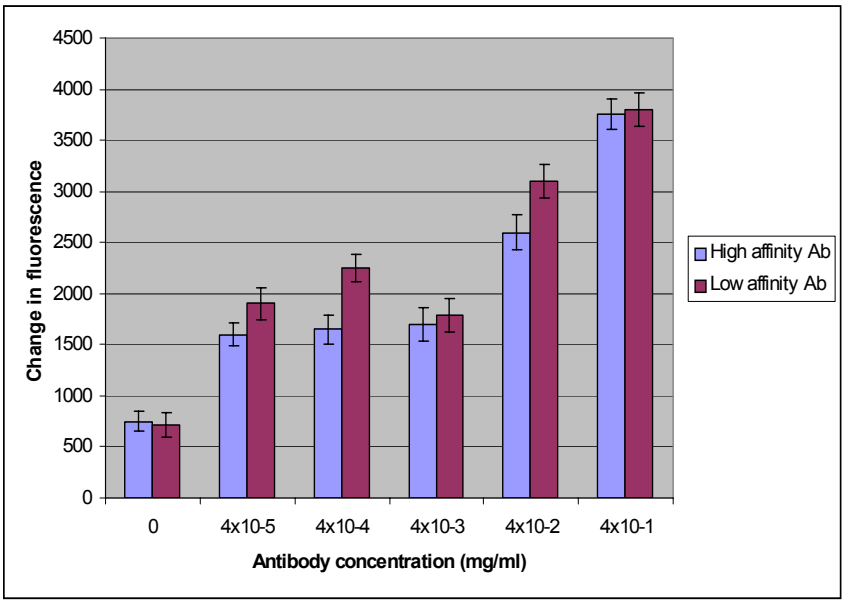

Figure 30. Change in the fluorescence signal upon replacement of HA-eGFP by HA-CFP. The change in the fluorescence signal (y-axis) of HA-eGFP bound to high affinity antiHA antibodies adsorbed onto 60 nm gold nanoparticles (blue) and lower affinity antiHA antibodies adsorbed onto 60 nm gold particles (purple) upon addition of HA-CFP, excited at 490 nm.

The replacement of HA-eGFP by HA-CFP is successful within the antibody concentrations of 4 x 10^{-5} and 4 x 10^{-4}, in line with the plasmon shifts described above. The increase in the fluorescence signal upon addition of HA-CFP, i.e. replacement of HA-eGFP and its subsequent "escape" from quenching is more pronounced when lower affinity antibodies are employed.

3.7 *In vivo* fluorescence studies

The effect of nanoparticles on certain fluorophores, and a potential use of this phenomenon in a bioassay system have been shown. As explained all these experiments were carried out *in vitro*; it is not known if the similar effects can be observed *in vivo* as well. In an *in vitro* system the interaction partners can be directly bound to each other and the effect can be observed (fluorescence and plasmon peak shift in our case), the only possible interference being the medium in which the measurements or tests are carried out. On the other hand, the situation is different *in vivo*. First of all, for a successful *in vivo* investigation, nanoparticles and the fluorophores have to be transfected, during which nanoparticles and fluorophore might detach from each other. Secondly, after successful transfection, the structures need to be addressed to correct compartments, which for instance can be done by targeting antibodies. Thirdly, within the cells, even if the structures find their target, they are subject to various ongoing processes within the living cells.

In our study, autofluorescent gold nanodots (1-2 nm in diameter) have been embedded in a polymeric dendrimer structure coupled to fluorescein (Stp1831). Both fluorescein and autofluorescent gold nanodots serve as the reporter for the monitoring of transfection. Fluorescein has excitation and emission maxima at 494 nm and 521 nm, respectively. On the other hand the autofluorescent gold nanodots have excitation and emission maxima at 270 nm and around 610 nm respectively. Therefore either no or minimal FRET between the two fluorescent reporters is expected. As explained in the introduction part the dendrimer structures have intrinsic transfection abilities. This removes the necessity to use an extra transfection reagent, making the transfection process simpler and cleaner.

3.7.1 Monitoring of transfection by fluorescence microscopy

As explained above the dendrimer structure used in these trials is coupled to fluorescein, so that it is possible to monitor the entry and intracellular fate of the dendrimer structures. Firstly bare dendrimer-fluorescein structures (referred to as PPI) were transfected into HeLa cells and observed under fluorescent microscope (fig 31) in order to see the transfection efficiency. Afterwards, the dendrimers were coupled to autofluorescent gold nanodots (referred to as PPI-AuND) and then were transfected into HeLa cells, which had been grown to confluence, simply

by adding the dendrimers with nanoparticles into the growth medium. Transfection was carried out at different concentrations and for different time periods for the optimisation of the process.

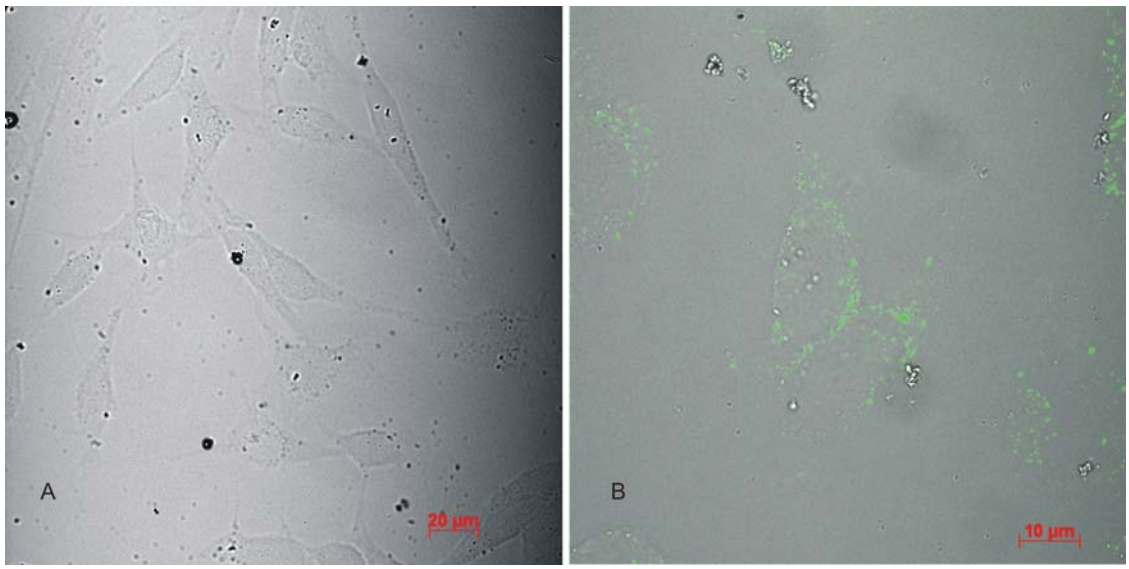

Figure 31. Transfection of HeLa cells with dendrimers. Fluorescence microscopy images of untransfected HeLa cells (A – 40 x magnification) and of HeLa cells transfected with PPI (B – 100 x magnification). Both images are merged with bright-field images.

Compared to untransfected HeLa cells, transfected cells clearly demonstrate green fluorescence, i.e. fluorescein signal (fig. 31). This, along with the observation that the green signal is distributed throughout the cytoplasm of the cells rather than the periphery, indicates successful transfection of the dendrimers into the cells. The distribution of fluorescein signal within the cytoplasm is further ilustrated by the images taken along the z-axis (fig. 33). As the scanning plane moves from top to the bottom of the cells, the distribution of fluorescence within the cells increases throughout the cell except for the nucleus, indicating that the PPI-AuND constructs are in the cytoplasm. Their capability to deliver the gold nanodots is documented in fig. 32. Cells which were transfected only with PPI, do not demonstrate any specific red fluorescence (D-F). However, although it is not as high as the green fluorescence, cells transfected with PPI-AuND show red fluorescence (A-C).

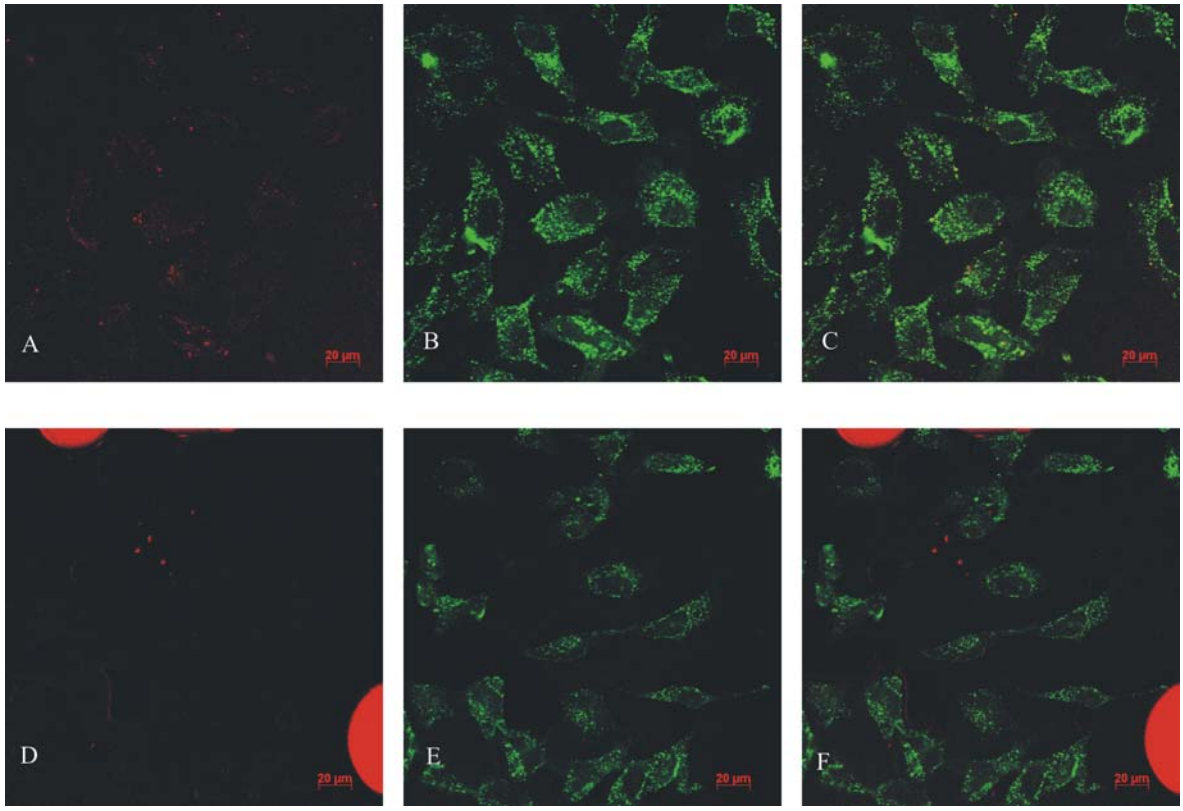

Figure 32. Confocal LSM of HeLa cells upon transfection with PPI-AuND. HeLa cells on glass slides were transfected with PPI-AuND and visualized with the red filter for the AuNDs (A), with the green filter for fluorescein (B), and both channels were merged (C). HeLa cells were also only transfected with PPI and was checked for AuND signal (D), fluorescein signal (E); and both signals were merged (E). All images 40 x magnified.

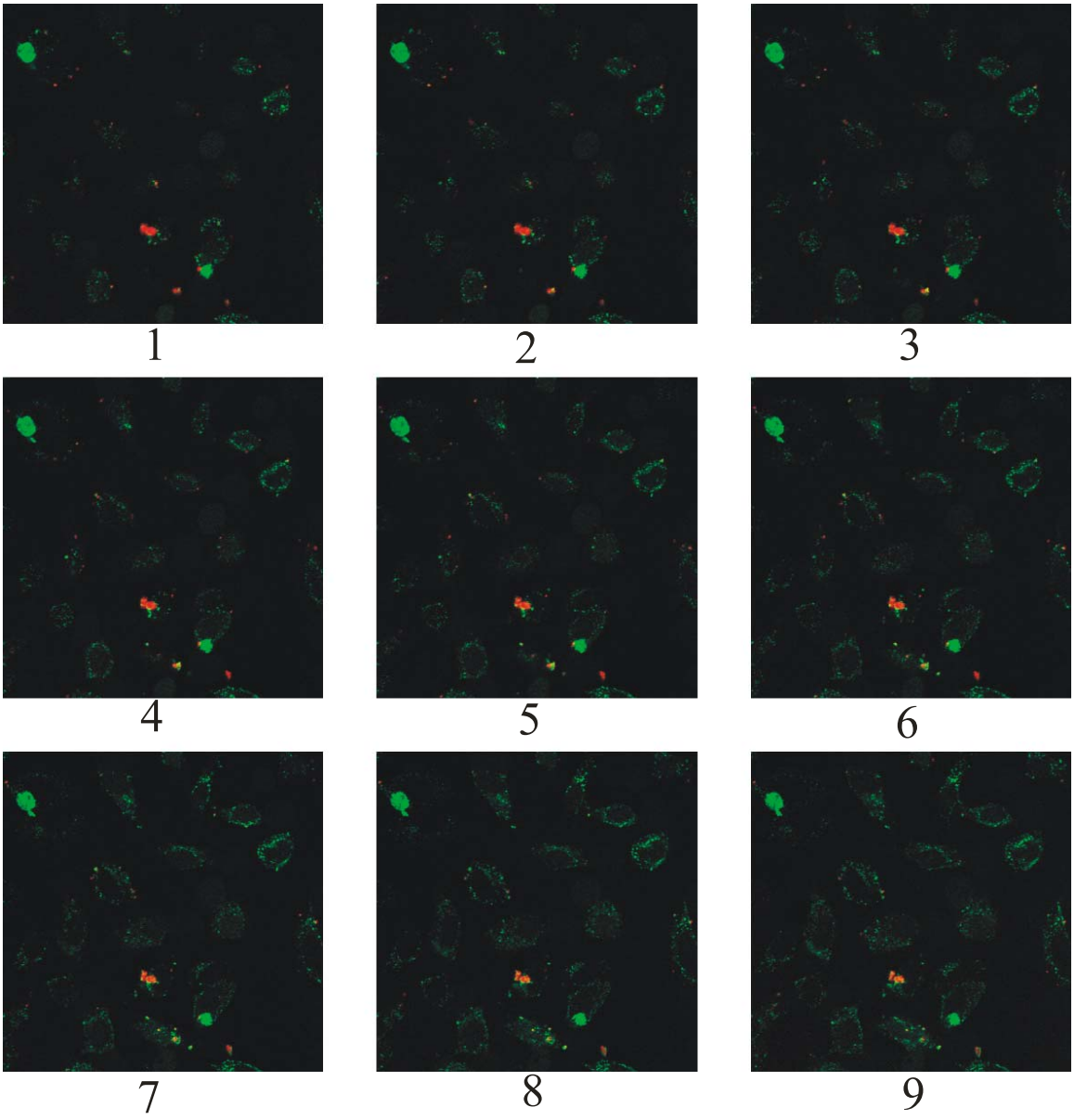

Figure 33. Distribution of fluorescence within HeLa cells along the z-axis. HeLa cells transfected with PPI-AuND were observed with the green and red filters and images were taken at different depths along the z-axis, from the top (1) to the middle of the cells (9). (Confocal LSM – 40 x magnification)

3.7.2 Measurement of the fluorescence signal from the nanoparticles

Next, HeLa cells were grown in 96-well plates and transfected with the same amount of PPI conjugated to autofluorescent gold nanodots for different time periods. The fluorescence of the dendrimer, i.e. that of fluorescein and the fluorescent signal of the nanodots were measured by a plate reader. The following graph (Fig. 34) shows the nanodot fluorescence signal after such a transfection.

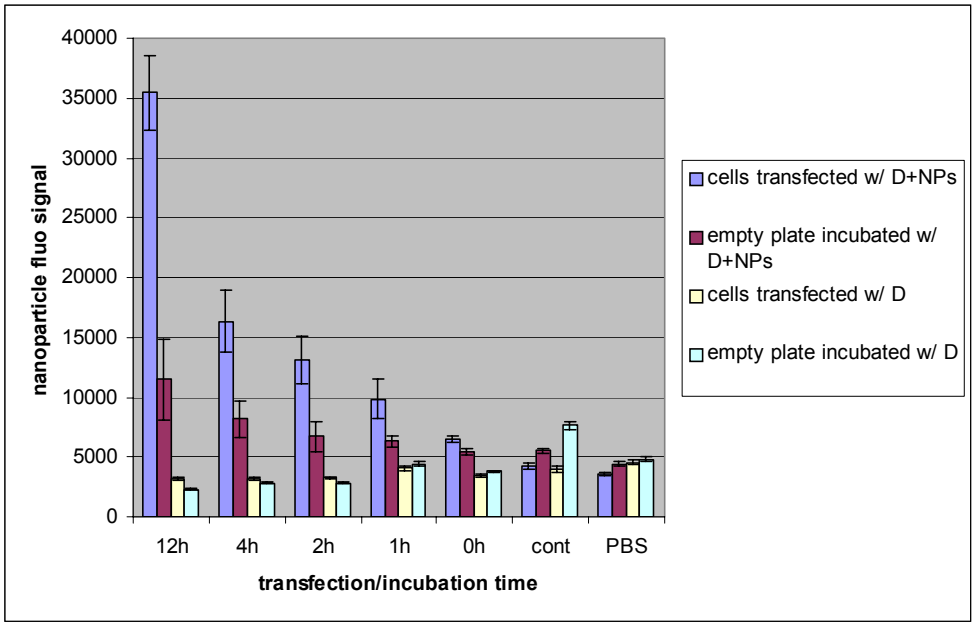

Figure 34. Quantification and comparison of the nanoparticle fluorescent signals. HeLa cells were incubated with the same concentration of PPI or with PPI-AuND, respectively. Cells were incubated for the time periods indicated in the x-axis. Cont refers to untransfected cells for blue and yellow columns, or wells incubated with DMEM for purple and light blue columns (excitation at 270 nm).

As can be seen from the graph, with increasing transfection time the nanoparticle signal increases. Nanoparticle signal obtained from samples treated with unconjugated dendrimer (yellow and light blue columns) shows only minimal signal. So it is plausible to assume that fluorescein does not interfere with the signal of the gold nanodots. More importantly, the fluorescence measurements provide a sound support for the above microscopy results. The signal obtained from cells incubated with PPI-AuND is higher than empty plate treated with the same structures, indicating that although some interaction between the well surface and the dendrimers take place, the interaction between the dendrimers and the cells is higher.

4 Discussion

In the previous chapter, results obtained from studies aiming to use gold nanoparticles as photonic markers were presented. What will be further discussed in this chapter are the requirements that need to be fulfilled for a successful use of gold nanoparticles and fluorescence of certain fluorescent proteins for such an aim. These necessary conditions required include:

- Determination of how a given type of nanoparticle affects the fluorescence signal of a given fluorophore, which depends heavily on the LSPR peak of the nanoparticles and on the excitation and emission spectra of the fluorophore.
- Efficient biofunctionalisation of the nanoparticles, *i.e.* making the nanoparticles capable of binding to biological structures. This includes not only the direct binding of fluorophores to nanoparticles, but also binding of antibodies onto nanoparticles for biospecific recognition.
- Determination of the potential of nanoparticles as *in vivo* reporters and methods of intracellular delivery of such nanoparticles.

4.1 Photonic interaction of gold nanoparticles with enhanced green fluorescent protein immobilized on a substrate

4.1.1 Obtaining a fluorescent surface

For the microscopic analysis of the effect of gold nanoparticles on the fluorescence pattern of eGFP, we decided to obtain a uniform distribution of eGFP on a microscope slide. It is well known that S-layer proteins self-assemble into monomolecular crystalline arrays on various artificial solid substrates [Horejs C., *et al.*, 2008]. Therefore, an S-layer/eGFP fusion protein, namely SbsC-eGFP, which was already available in the group, was chosen to form a surface with eGFP distributed evenly and uniformly. The above mentioned protein was over-expressed in bacteria, isolated, and finally adsorbed onto various types of substrates: unmodified glass and silicon, chemically modified glass and silicon. The pattern of SbsC-eGFP on those substrates was observed by FM, SEM, and AFM. As seen in fig. 14, the height of SbsC-eGFP is around 8 nm, which is in accordance with the height reported by Blecha [Blecha A., *et al.*, 2005]. However, the S-layer protein does not form a uniform monolayered crystal assembly, but it forms tube-like structures. It should be noted that the tubes formed by SbsC-eGFP served well in our

experiments, since the tubes are still regularly arranged units, which provide an ease in identification. The formation of the tubes is most probably because for the selected bacterial strain the monomers already assemble to curved patches in the solution before deposition on the substrate can start. There is a driving force for the formation of a curved patch, *i.e*. it is more favourable for the inner part of the tubes not to be exposed to the surface and not to adsorb onto glass or silicon [Horejs C., *et al.*, 2008].

In order to examine, how the surface charge and hydrophilicity influences tube formation, glass and silicon substrates were chemically modified. Surface modifications employed were functionalisation with APTES, GOPTES, and plasma treatment, and poly-L-lysine. APTES and GOPTES modified surface, and poly-L-Lys coated glass bear a positive charge. Plasma treatment, on the other hand increases the oxygen atoms on the surface, giving the surface an increased negativity and hence an increased hydrophilicity [Wang D.Y., *et al.*, 2007]. In none of the above mentioned methods, an entirely SbsC-eGFP covered surface was obtained. In each case the regular tube structures were formed. Poly-L-Lys covered glass proved to be too rough for AFM, making any structure on it virtually invisible to the AFM tip. Since the aim of the study is to observe the effect of nanoparticles on fluorescence, any surface modification should support the adsorption and homogenous distribution of nanoparticles on the surface and with the protein, as well. In that regard, plasma treatment reduced the number of nanoparticles adsorbing onto the surface, possibly due to charge repulsion between negative surface charge of the nanoparticles and the plasma treated surface. Therefore plasma treatment was not fitting with our motivations to prepare a homogenous distribution of gold nanoparticles and SbsC-eGFP complexes on a given substrate.

In addition to SbsC-eGFP, the adsorption behaviour of eGFP on various surfaces was also observed. As presented in fig. 16, it was possible to get a surface covering with eGFP on GOPTES modified glass, which was closest to uniform. However, regardless of the purity of the eGFP preparation, eGFP aggregates were always present. One possible way to get rid of such aggregates could be filtering the eGFP suspension with 30 kDa pore sized filters prior to adsorption on such treated surfaces. However, as explained above the tubes formed by SbsC-eGFP were preferred over eGFP because the tube-like structures make it easier for the recognition of the protein on the microscope slides.

4.1.2 Fluorescence interaction of nanoparticles with immobilized SbsC-eGFP complexes

Fig. 17 shows AFM and FM images of SbsC-eGFP and gold nanoparticles adsorbed onto GOPTES modified glass as discussed above. The SbsC-eGFP tubes and gold nanoparticles were identified by measuring their height from the AFM images. Although the association of gold nanoparticles with SbsC-eGFP is random, there is at least one SbsC-eGFP tube associated with gold nanoparticles at three points (see FM image fig. 17A and AFM image fig. 17B). Please refer to the results section for the explanation of the doubling of the structures on fig. 17B. As already stated in the beginning of this discussion, it is now well known that metal nanoparticles affect the fluorescence in various ways. Upon closer inspection of fig. 17A and B, it is clearly visible that the boxed SbsC-eGFP tube does not demonstrate fluorescence around the gold nanoparticles, unlike the other SbsC-eGFP tubes. Three reasons for the lack of the fluorescence around the nanoparticles can be envisaged: First possibility is the simple shadowing of the fluorescence signal by the nanoparticles. However, this is the least likely explanation, since in the experimental scheme, the adsorption of the nanoparticles was carried out after the adsorption of the SbsC-eGFP tubes, so that the nanoparticles resided on the tubes and FM was carried out from beneath. Secondly, using nanoparticles for thermal denaturation of proteins attached to them has also been reported in the literature [Takeda Y., *et al.*, 2006]. Therefore it is possible that the local heat caused by the strong light absorption by the gold nanoparticles causes the denaturation of SbsC-eGFP around the nanoparticles, leading to the observed effect. Thirdly, as detailed in the introduction, it is also known that nanoparticles interact with the fluorescence emission and excitation of many fluorophores without affecting the structure of the fluorophore, causing a quenching or enhancement of the fluorescence, depending on the characteristics of the given nanoparticle fluorophore couple. Although fig. 17 demonstrates a reduction in the SbsC-eGFP fluorescence signal, it does not suffice to explain whether it is due to denaturation of eGFP or to quenching. It should also be noted that, it is not clear from fig. 17 whether the fluorescence signal is only reduced to an amount that is below the detection limit of the FM camera or whether it is completely extinguished. It is very important to be able to determine the extent of the reduction, because a complete lack of fluorescence would hint at denaturation of eGFP around the nanoparticles. On the other hand, a partial reduction of the signal would support the hypothesis that the signal is only quenched. Therefore, in the next steps, it was decided to work only with eGFP in solution and to bind it onto gold nanoparticles under various conditions in order to measure the change in the fluorescence signal using fluorescence spectroscopy.

An interesting feature of the reduction or diminishing of the eGFP signal of the SbsC-eGFP tubes is its localization in a very small area only around the gold nanoparticles, not throughout the entire tube. This shows that the effect, regardless of its underlying mechanism, is connected with some near field enhancement around the gold nanoparticles and hence limited to a small volume around the nanoparticles. It was already reported by Härtling that such an effect is limited to a certain area around the nanoparticles [Härtling T., *et al.*, 2007]. Another group reported very recently that it is possible to shape the emission spectra of fluorescent molecules by using gold nanoparticles and varying the distance between the nanoparticle and the fluorophore [Ringler M., *et al.*, 2008].

A more controlled approach for the interaction of nanoparticles with SbsC-eGFP was to produce the nanoparticles on the protein itself. As explained in the methods part, the protein was incubated with the non reduced gold atoms, and then the growth solution and reducing agent were added in order to grow the gold complexes on SbsC-eGFP into gold nanoparticles. The resultant structures were adsorbed onto silicon wafers for SEM (fig. 18) and onto glass slides for FM (fig. 19). The SEM images show successful production of uniformly sized nanoparticles on SbsC-eGFP. FM images show a strong reduction in the fluorescence signal (fig. 19B) as compared to the signal observed from the same amount of SbsC-eGFP without gold nanoparticles. Images C and D of fig. 19 demonstrate the fluorescence intensity profiles of A and B respectively; made by the MetaVue software, where the fluorescence intensities from images which were taken under the same parameters of illumination and recording of emission were transformed into numerical values. Each pixel of the fluorescence picture is appointed to such number, and an intensity profile is produced according to the values, resulting in a profile with higher fluorescence values having greater heights. The observed reduction and no total destroying of the fluorescence could be interpreted, that quenching and not denaturation is the relevant mechanism. However, it should also be noted that this type of synthesis of nanoparticles causes a strain on the protein leading to a deformation as can be observed from the SEM image, i.e. the previously observed phenomenon might be caused by a different mechanism than this particular case.

4.2 Fluorescence interaction of nanoparticles with eGFP in solution

Due to the above-mentioned reasons, and in order to see the difference, if any, between solution systems or adsorbed-on-substrate based systems, eGFP was adsorbed onto nanoparticles under different conditions. Afterwards the fluorescence signal as well as the shifts in LSPR upon binding were measured.

4.2.1 Adsorption of eGFP onto AuNPs

One of the simplest and most straightforward methods for attaching proteins to nanoparticles is to adsorb them at their pI value [Takeda Y., *et al.*, 2006]. To this end, the pI value of 5.5 was calculated for eGFP and experimentally confirmed using isoelectric focusing. The same was carried out for rPhiYFP, and a pI of 6.5 was measured.

The efficiency of binding eGFP onto nanoparticles at pH 5.5 and 7.0 was tested. As shown in fig. 20, the supernatant fractions of the samples incubated at pH 5.5 does not produce an eGFP band on the Western blot. Considering that the centrifugation speed was enough to sediment nanoparticles but not high enough to sediment eGFP alone, it is concluded that eGFP molecules must have been adsorbed onto nanoparticles and sedimented together with them. However, this does not necessarily mean that no eGFP is bound on the nanoparticles at pH 7.0. In order to determine the amount of the eGFP adsorbed onto nanoparticles, nanoparticles sedimented by centrifugation need to be resuspended and detached from the eGFP, e.g. by treatment with SDS. The nanoparticles used in this study, however, could not be completely resuspended upon centrifugation. Moreover, when samples containing nanoparticles were loaded and run on polyacrylamide gels, nanoparticles either prevented the entry of the proteins into the gel matrix, or interfered with their running pattern and the results were not reproducible.

As explained in the introduction part, one of the factors that determine the position of the LSPR peak is the dielectric constant of the medium of the nanoparticles. Binding of any type of molecule (e.g. capping agent, polymer, protein, etc.) to the nanoparticle surface represents a change in the dielectric constant and therefore manifests itself as a change in the plasmon peak. The change comes in various forms, either as peak broadening and/or reduction in the height of the peak, which is indicative of nanoparticle aggregation upon protein binding, or as a red shift, or both. Therefore, we monitored the changes in the plasmon peak upon adsorption of eGFP at

various pH values in terms of changes in the LSPR peak (Fig. 21). The most prominent shift is obtained when eGFP is adsorbed onto gold nanoparticles at pH 5.5, in accordance with the results explained above. Therefore, the most effective adsorption of eGFP onto gold nanoparticle takes place at pH 5.5 and refers to biggest number of eGFP molecules adsorbed. It should be noted that for all of the pH values the change in the LSPR peak pattern was a red-shift, lack of a significant peak broadening indicates that there was no significant agglomeration.

In another trial we compared the efficiency of adsorbing eGFP versus cross-linking eGFP onto gold nanoparticles. Equal amounts of eGFP were incubated with gold nanoparticles at neutral pH, at the isoelectric point of eGFP, and cross-linked to gold nanoparticles by a commercially available cross-linker, namely DTSSP. Fig. 24 shows the changes in the LSPR peak positions. The biggest shift is obtained when eGFP is adsorbed onto nanoparticles at pH 5.5. This confirms that proteins not bearing a net charge adsorb more efficiently onto nanoparticles because charge repulsion is not present. The shifts in the case of neutral pH and DTSSP cross-linking were the same and less than that of pH 5.5. Furthermore, there was a clear reduction in the height of the LSPR peak in the case of DTSSP, suggesting agglomeration. This is most probably because more than one DTSSP can bind to one eGFP molecule leading to the formation of nanoparticle-protein complexes, which agglomerate.

Therefore, it is more straightforward, cleaner, simpler, and more efficient to bind globular proteins, such as eGFP onto gold nanoparticles at their pI values rather than using DTSSP, which is not only less efficient but also leads to the aggregation of nanoparticles. Furthermore, as the number of reagents used in the binding process increases, the risk of creating a shift in the LSPR peak due to a change in the refractive index or dielectric constant of the medium increases.

4.2.2 Evaluation of the effect of nanoparticles on eGFP and rPhiYFP in solution

The measurement of the change in the fluorescence signal of the fluorophores upon adsorption onto gold nanoparticles was carried out in order to confirm and quantify the effect discussed in chapter 4.1. Furthermore, in addition to the confirmation of that effect, the change in the extent of fluorescence reduction upon adsorbing the fluorophores at different pH values would confirm the efficiency of binding at pI value.

In these measurements two fluorescent proteins, namely eGFP and rPhiYFP and two different types of nanoparticles, namely gold nanoparticles and gold/silver alloyed nanoparticles were used. Please refer to the appendix for the respective emission and excitation spectra of the fluorophores and the absorption spectra of the metal nanoparticles.

Fig. 22 shows the results of an experiment, where the fluorescence of eGFP was measured at different pH values (blue columns), then at the same pH values after adsorbing onto gold nanoparticles (red columns), and finally again at the same pH values after adsorbing onto gold/silver alloyed nanoparticles (yellow columns). First of all, there were changes in the eGFP fluorescence signal at varying pH values, which is a normal event considering that the pH of the medium is one of the main factors affecting the fluorescence of a fluorophore [Kneen M., *et al.*, 1998]. Secondly, at each pH value, when gold nanoparticles were present, the eGFP fluorescence signal was reduced. This suggests that even at pH 7.0 a certain amount of eGFP is bound to the nanoparticles. However, the greatest reduction was at the pI value of eGFP, *i.e.* at pH 5.5. This observation fits well with the expectation that the most efficient adsorption of eGFP onto gold nanoparticles was at its pI value and therefore the biggest change in its fluorescence signal would be observed at that pH.

The conclusion to be drawn from that experiment is not only the adsorption behaviour of eGFP. The fluorescence signal of eGFP was either not reduced at all, or not reduced as much when it was adsorbed onto gold/silver alloyed nanoparticles. Even a slight enhancement could be observed at pH 7.0. This observation rules out the denaturation of eGFP being the cause of the reduction in fluorescence. eGFP has an excitation maximum at 490 nm and an emission maximum at 520 nm, which means that the excitation wavelength for the above explained experiment was 490 nm. As stated in the appendix, the gold nanoparticles and alloyed nanoparticles have LSPR peak at 520 nm and 490 nm, respectively. As explained in the introduction, the LSPR peak corresponds to the wavelength, at which the surface electrons of nanoparticles absorb the most. Therefore, theoretically alloyed nanoparticles absorb more than gold nanoparticles and have a higher capacity of releasing the absorbed energy as heat. If the reason for the reduction in fluorescence had been heat denaturation of eGFP by nanoparticles, the reduction would have been more pronounced in the case of alloyed nanoparticles, with their higher absorbance at 490 nm. It is more likely, that the reduction was due to a FRET-like energy

transfer, where the fluorescence emitted by eGFP at 520 nm was absorbed by the gold nanoparticles which absorb strongly at that wavelength.

In order to support the above conclusion, the behaviour of rPhiYFP upon adsorbing onto gold nanoparticles was investigated. The fluorescence signal of rPhiYFP was measured at neutral pH and at its pI value (pH 6.5). Then it was incubated with gold nanoparticles at neutral pH and at its pI, and its fluorescence signal was measured. The outcome is presented in fig. 23. As in the case of eGFP, rPhiYFP fluorescence signal was reduced at its pI value. However, contrary to the eGFP case, addition of gold nanoparticles led to an enhancement of the rPhiYFP fluorescence signal, with the extent of enhancement being higher at pH 6.5. Please refer to the appendix for the excitation and emission spectra of eGFP and rPhiYFP, as well as the plasmon peak positions of the nanoparticles. If the underlying reason of reduced eGFP signal had been denaturation by gold nanoparticles, a similar behaviour would have been observed here, as well. Therefore, it was concluded that the reduction is mainly due to a FRET-like energy transfer between the fluorophore and nanoparticle.

Although the conclusion drawn from above mentioned experiments is favouring an interaction mechanism between a fluorescent proteins and nanoparticles other than protein denaturation, this possibility cannot completely be ruled out. Light absorption and heat dissipation by a nanoparticle possibly takes more time. In order to rule out denaturation, parameters required for such a phenomenon could be determined by exposing the conjugates longer to irradiation times and/or higher intensity, e.g. by changing the laser. However, with increasing irradiation time the risk of bleaching the fluorophore increases. Therefore, it would make sense to use for such measurements either bleaching-resistant fluorescent proteins, or proteins that are not fluorescent at all; for instance enzymes, of which the activity can easily be monitored.

While being able to denature proteins locally offers a great promise in medicine; modifying fluorescence of fluorescent tags without denaturing or causing damage to the surroundings can prove to be valuable, especially in bioimaging and biosensing applications employing fluorescence. In such measurements, the sensitivity of the approach is a direct function of the signal obtained from the fluorescent reporter. Therefore, being able to enhance, e.g. the enhancement of rPhiYFP fluorescence by gold nanoparticles, or to quench, e.g. the quenching of

eGFP fluorescence by gold nanoparticles, the fluorescence of tags can prove to be important for instance for increasing the signal to noise ratio or to switch off one reporter whilst switching on another.

4.3 Functionalisation of nanoparticles with antibodies

As stated in the introduction of the thesis, one of the aims of this study is to demonstrate the potential of nanoparticles and the effect they have on fluorescence of certain fluorophores in biosensing. For that purpose, one of the crucial steps is to attach antibodies onto gold nanoparticles. Additionally, during this process antibodies need to retain their functionality.

For the functionalisation of gold nanoparticles, an approach similar to the adsorption of eGFP onto gold nanoparticles was adopted. Commercially available antiGFP antibodies were incubated at 8.0, the general theoretical pI value for IgG class antibodies [Hamilton, R.G., 1990]. The functionality of gold nanoparticle attached antibodies was tested on SbsC-eGFP adsorbed onto silicon wafers. SbsC-eGFP was adsorbed onto silicon wafers and treated with gold nanoparticles functionalized with antiGFP antibodies and with non-functionalised nanoparticles. Afterwards, the distribution of the nanoparticles was observed by SEM (fig. 25). Fig. 25 shows a distribution difference between functionalised and non-functionalised nanoparticles, where functionalised nanoparticles seemed to bind to SbsC-eGFP patches on the silicon wafer and non-functionalised ones did not.

In order to support the SEM images and to quantify the antibody binding onto gold nanoparticles, LSPR peak shifts were measured (fig. 26). There, we see that the shift in the LSPR peak is greater for higher antibody concentrations. Furthermore, upon addition of eGFP further shift is achieved. However, it is not possible to ascertain the increase in the other cases to binding of antiGFP antibodies to eGFP because there is an LSPR shift when eGFP is added to nanoparticles not functionalized with antibodies. In order to prevent that, the same structures were prepared with an additional step of blocking immediately after the addition of antibodies (fig. 27). Among the tested blocking agents PVP40 turned out to be the best suited to our needs, because it did not cause a big shift in LSPR peak in most of the cases (lack of LSPR peak shift after blocking for the antibody concentrations 0 mg/ml and 4×10^{-5} mg/ml). eGFP did not seem to adsorb onto it very strongly (note the difference between the shift after addition of eGFP to naked nanoparticles

and to the nanoparticles functionalised with 4 x 10^{-5} mg/ml of antiGFP antibodies). It should be noted that antibody concentrations higher that 4 x 10^{-4} mg/ml and an eGFP concentration of 0.4 mg/ml were enough to saturate the LSPR peak shift. However, the system can still be used for detection of eGFP at concentration less than 0.4 mg/ml, with PVP40 as a safe blocking agent.

In the next step, the procedures for functionalisation of the gold nanoparticles were repeated and the change in eGFP fluorescence was measured. As stated earlier, as the amount of gold-bound eGFP increases, a reduction in the fluorescence signal is expected. Figure 28 shows the results of such a measurement where the degree of quenching did not increase linearly with increasing antibody concentration, which supports the conclusion that there is a critical antibody concentration; and in our case that ratio turned out to be 4 x 10^{-5} mg/ml. Note that the columns at the first lane in x-axis do not contain nanoparticles.

4.4 Utilisation of the above systems in an exchange type assay

As the name suggests, for an exchange type assay at least two antigens are required. Two HA-tagged fluorescent proteins, namely HA-CFP and HA-eGFP, were already available in the group. Therefore the FRET between the two fluorophores was investigated as the first step. The excitation and emission spectra and maxima of both proteins are supplied in the appendix part. Three solutions containing HA-eGFP, HA-CFP, and both were excited at their excitation maximum and at each other's excitation maxima, followed by measuring their emissions (figure 29). According to the graph, there is a FRET between CFP and eGFP if the mixture is excited at 434 nm and emission is recorded at 520 nm, which is expected considering emission maximum of CFP lies close to the excitation maximum of eGFP. On the other hand if excitation is carried out at 490 nm, there is no FRET between the two fluorophores.

The assay was performed in a very similar way to the gold nanoparticle functionalisation experiments explained above. Gold nanoparticles were functionalised with commercially available antiHA antibodies and commercially available high affinity antiHA antibodies from the same supplier, followed by blocking the surfaces with PVP40. Then the functionalised nanoparticles were incubated with HA-eGFP, and the fluorescence signal was measured. Finally, the complexes were incubated with HA-CFP and the fluorescence signal was measured once again. Fig. 33 shows the change in HA-eGFP after addition of HA-CFP. First of all, after addition

of HA-CFP, HA-eGFP signal increases at each antibody concentration as compared to the signal coming from the control. This suggests that the displacement of HA-eGFP by HA-CFP takes place. The fluorescence signal is expected to increase when HA-eGFP is replaced by HA-CFP, because eGFP is no longer quenched by the nanoparticles. This is further supported by the fact that at antibody concentrations 4×10^{-5} mg/ml and 4×10^{-4} mg/ml the increase is higher for the lower affinity antiHA antibodies. The very high increase in the fluorescence signal for the higher antibody concentrations and a lack of difference between the lower affinity and higher affinity antibodies suggest saturation.

Together with the results from functionalisation studies, antibodies seem to retain their functionality and specificity when conjugated to nanoparticles. Also, as exemplified by the HA-eGFP and HA-CFP exchange system, it is possible to use the quenching of a fluorophore as a reporter for an exchange type assay, where the exchange of antigens leads to the release of a quenched fluorophore from the nanoparticle and a concomitant increase in the fluorescence signal. However, before this basic observation can be integrated into a bioassay, parameters such as kinetics of the exchange and stability of gold-antibody complexes need to be determined. Once such a system is fully characterised, it can be advantageous to many current systems because the gold nanoparticles also offer LSPR shifts as reporters of binding events, and theoretically the combination of fluorescence measurements with LSPR peak measurements can increase the sensitivity of the assay.

4.5 *In vivo* fluorescence studies

As stated in the introduction part, autofluorescent metal nanoparticles offer numerous advantages over classical fluorescent proteins and dyes. First step in the usage of autofluorescent gold nanoparticles is their intracellular delivery. As explained in the introduction, one of the newly emerging intracellular delivery agents is the dendrimers. Autofluorescent gold nanoparticles, with an excitation max at 270 nm and emission maximum at 610 nm (for respective spectra, please refer to the appendix) were embedded into PPI dendrimers. Furthermore, for an additional means for monitoring the intracellular delivery complex, dendrimer molecules were labelled with fluorescein, a fluorescent dye that has excitation max at 494 nm and emission max at 521 nm.

Results of the transfection experiments carried on the 96-well plate (figure 34) indicate that the delivery structure interacts with the surface of the wells, because a signal is also obtained from the wells that did not contain any HeLa cells, but were incubated with PPI-AuNDs. However, at every time point, the signal obtained from the wells containing cells is higher than that of the empty wells, which does not necessarily indicate a successful transfection. Yet, it is clear that the delivery complex interacts with the cells more than it adsorbs to the walls of the 96-well plate.

In order to confirm the intracellular delivery of the structures, a series of confocal LSM experiments were carried out. Firstly, HeLA cells were incubated with fluorescein labelled dendrimer (PPI), and the fluorescein signal from the treated cells was compared with that of untreated cells (fig. 31). Since the images were taken from a middle plane of the cells, it can be concluded from fig. 31, that the PPI enters the cell and is distributed in the cytoplasm. Secondly, HeLa cells were transfected with PPI-AuND and only PPI. The fluorescence images of AuND and PPI were separately taken and then merged (fig. 32). In the red channel there was a clear AuND signal coming from the cells transfected with PPI-AuND. In the case of the cells transfected with PPI, the only red signal is due to back-scattering from the glass surface and is definitely not associated with the cells. The fluorescence signal from the green channel shows the distribution of the dendrimer within the cytoplasm. Nuclei of the cells both transfected with PPI-AuND and PPI are distinguishable, once again supporting the fact that the dendrimers are successful in internalisation. Furthermore, the green signal is distributed throughout the cytoplasm, indicating a minimum aggregation of the delivery complexes. When the images from both channels are merged, it is clear that the red signal and the green signal from the cells transfected with PPI-AuND overlap. On the other hand the two signals, namely the red signal coming from back-scatter and green coming from fluorescein, for the cells transfected only with PPI do not overlay. This leads to the conclusions, that the dendrimers are successful in transfection and the autofluorescent gold nanoparticles are good candidates for being used as inorganic fluorophores *in vivo*. Fig. 33 provides more support to the fact that the fluorescence signal is coming from the cytoplasm, but not from the cell surface, i.e. the structures are internalised.

In addition to the internalization of the PPI-AuND, the success of the transfection also depends on the stability of the complexes within the cells. It should be noted that all the images presented

here were from cells transfected for 4 hours. In almost all of the cases the cells started dying after 5 to 6 hours of transfection. This makes this particular dendrimer suitable for short-term transfection studies. It should be also noted that the structures did not lose stability during 4 hours.

Although the above described and discussed experiments show that nanoparticles are promising intracellular markers, it is still important to determine numerous parameters regarding their efficiency and safety. As addressed above, one of the most critical questions is the stability of the dendrimer nanoparticle complexes. Additionally, especially in the case of live imaging, modes of transfection, intracellular fate, and toxicity of the nanoparticles and the dendrimers need to be determined before applications. However, once such questions are answered and safety issues are resolved, nanoparticles seem to be promising alternatives to conventional fluorescent dyes and proteins. Dendrimers on the other hand provide a good link to biofunctionalisation for nanoparticles, since they can be linked to antibodies or other specific biological recognition elements for targeting nanoparticles to intracellular locations.

5 Summary

Metal nanoparticles have recently gained popularity in many research areas due to their nanosize-related properties. Depending on the size of the metal nanoparticle, their mode of interaction with electromagnetic radiation and the outcome of this interaction vary; in turn the effect exerted on a protein which is conjugated to a nanoparticle varies, because different sized nanoparticles demonstrate different modes of energy transfer with electromagnetic radiation and molecules conjugated to them. This versatility opens the way for various different applications (shortly summarized in fig. 35). Very small cluster with sizes around 1 – 1.2 nm tend to get excited by incident light and emit fluorescence, whereas larger nanoparticles absorb the incoming light very strongly due to their LSPR.

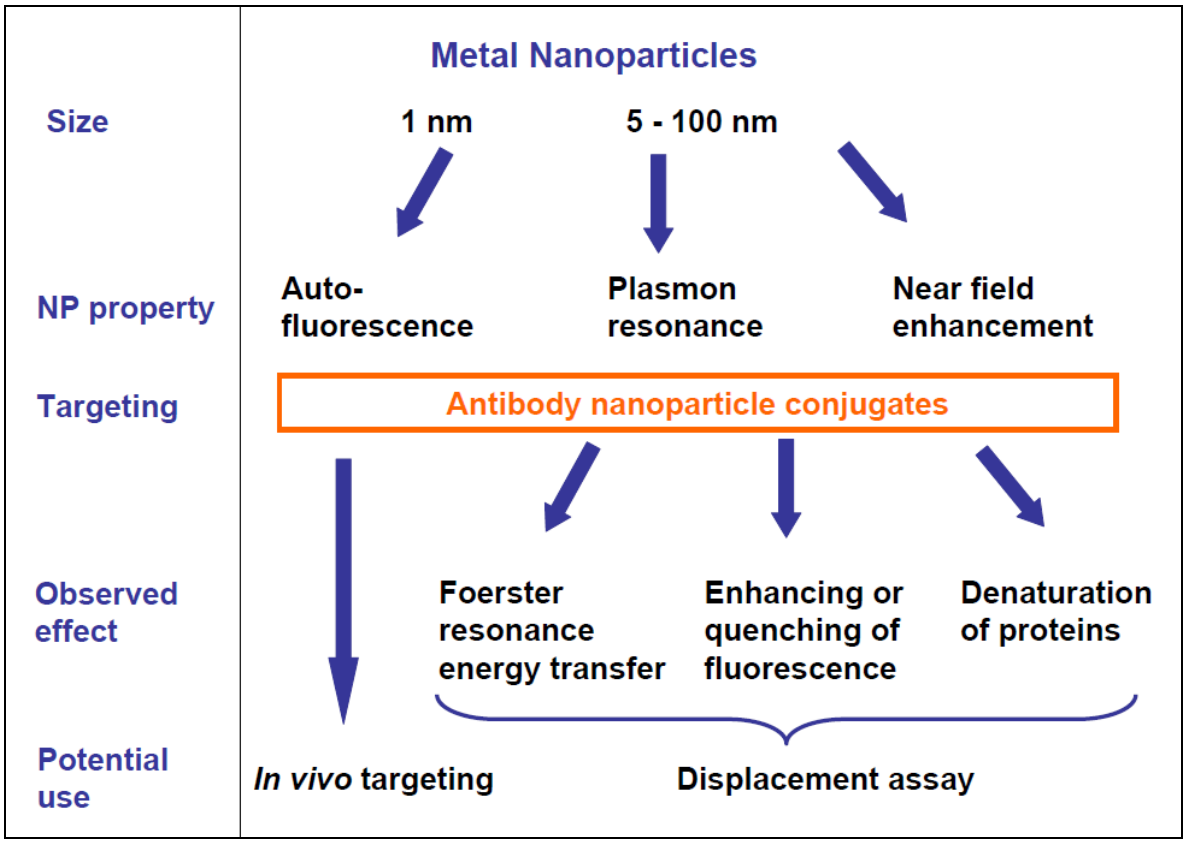

Figure 35. Size-dependent properties of metal nanoparticles, and their uses within the frame of this work.

In this study we observed the outcomes of the interaction between two types of nanoparticles, namely gold and gold/silver alloyed nanoparticles with the fluorescence emission of two fluorophores, namely eGFP and rPhiYFP. The first observed effect of gold nanoparticles on the

fluorescence emission of eGFP was a reduction of eGFP signal around the nanoparticles verified by fluorescence and atomic force microscopy. In order to determine whether the observed effect was due to quenching of the eGFP fluorescence by the gold nanoparticles or due to local denaturation of the eGFP molecules around nanoparticles (in turn caused by heat production due to absorbed light), the fluorescence emission of eGFP adsorbed onto gold nanoparticles was measured in solution. In addition to verifying the efficiency of adsorbing proteins onto gold nanoparticles at their isoelectric point as a simple means for protein-nanoparticle conjugate preparation, the measurements confirmed a reduction of eGFP fluorescence. The same reduction, however, was not observed, when either eGFP was adsorbed onto gold/silver alloyed nanoparticles, or rPhiYFP was adsorbed onto gold nanoparticles. Therefore, we conclude that the reason for the reduced fluorescence is not denaturation of the protein species by the heat produced due to the strong absorption of nanoparticles at their LSPR peaks, since rPhiYFP fluorescence is not reduced when adsorbed onto gold nanoparticles (on the other hand it was enhanced to a certain extent). Furthermore, since the same reduction is not observed with eGFP adsorbed onto gold/silver alloyed nanoparticles, we conclude that the reason of the reduction is quenching by a FRET-like mechanism, where light emitted by eGFP at around 520 nm is absorbed strongly by the neighbouring gold nanoparticles.

The above mentioned quenching/enhancement phenomenon can be utilised in various areas ranging from microscopy to biosensing. In order to exemplify one such application, a bioassay was designed, in which the replacement of an eGFP tagged antigen bound to gold-antibody conjugates was replaced by the addition of the antigen with a different tag lead to an increase in the eGFP fluorescence as a result of the exchange of antigen and subsequent separation of eGFP from the gold nanoparticle to stop quenching. We were able to get such an assay working, i.e. we could observe an increase in the eGFP fluorescence when eGFP-HA bound to antiHA antibody-gold nanoparticle conjugates was replaced by another HA tagged protein. This type of an assay provides another advantage: It is possible to monitor the replacement and binding events using the shifts in LSPR peak position as the gold bound species interchange. This observation can be further utilised as the basis of a proper biosensor combining the change in fluorescence and shifts in LSPR peak for an increased sensitivity.

In order to demonstrate the versatility of gold nanoparticles in biological research, we also tried to use gold nanoparticles as intracellular markers. For that end, autofluorescent gold nanoparticles were delivered into cultured HeLA cells by using oligosaccharide-modified poly(propyleneimine) dendrimers (PPI). Gold nanoparticles were embedded in the dendrimer structures and then transfected. By using confocal laser scanning microscopy, we were able to visualize gold nanoparticles within the cells, which seemed to be widely distributed, i.e. not confined to a certain organelle. Therefore, as a future prospect, antibodies targeted with such gold nanoparticles present a great potential for *in vivo* targeting studies. Furthermore, these experiments also presented the efficiency of the above mentioned dendrimers as intracellular carriers of various molecules.

6 References

Andrews M.P. and O'Brien S.C., 1992, Gas-phase "molecular alloys" of bulk immiscible elements: iron-silver (FexAgy), *J. Phys. Chem.*, 96(21), 8233–41

Anger P., Bharadwaj P., Novotny L., 2006, Enhancement and quenching of single-molecule fluorescence, *Phys. Rev. Letters*, 96(11), 113002

Appelhans D., Zhong Y., Komber H., Friedel P., Oertel U., Scheler U., Morgner N., Kuckling D., Richter S., Seidel J., Brutschy B., Voit B., 2007, Oligosaccharide-modified poly(propyleneimine) dendrimers: synthesis, structure determination, and Cu(II) complexation, *Macromol. Biosci.*, 7(3), 373-83

Aslan K., Lakowicz J.R., Geddes C.D., 2005, Metal-enhanced fluorescence using anisotropic silver nanostructures: critical progress to date, *Anal. Bioanal. Chem.*, 382(4), 926-33

Aslan K., Lakowicz J.R., Geddes C.D., 2005, Plasmon light scattering in biology and medicine: New sensing approaches, visions and perspectives, *Current Opinion in Chemical Biology*, 9, 538-44

Baigude H., Katsuraya K., Okuyama K., Hatanaka K., Ikeda E., Shibata N., Uryu T., 2004, Synthesis of spherical and hemispherical sugar-containing poly(ornithine) dendrimers, *Journal of Polymer Science Part A: Polymer Chemistry*, 42(6), 1400 - 14

Bakshi M.S., Sharma P., Banipal T.S., Kaur G., Kanjiro T., Petersen N.O., Possmayer F., 2007, Lamellar phase supported synthesis of colloidal gold nanoparticles, nanoclusters, and nanowires, *J. Nanosci. Nanotechnol.*, 7(3), 916-24

Barnes W.L., Dereux A. and Ebbesen T.W., 2003, Surface plasmon subwavelength optics, *Nature*, 424(6950), 824-30

Berlier J.E., Rothe A., Buller G., Bradford J., Gray D.R., Filanoski B.J., Telford W.G., Yue S., Liu J., Cheung C.Y., Chang W., Hirsch J.D., Beechem J.M., Haugland R.P., Haugland R.P., 2003, Quantitative comparison of long-wavelength Alexa Fluor dyes to Cy dyes: fluorescence of the dyes and their bioconjugates, *J. Histochem. Cytochem.*, 51(12), 1699-712

Bhattacharya R. and Mukherjee P., 2008, Biological properties of "naked" metal nanoparticles, *Adv. Drug Deliv. Rev.*, 60(11), 1289-306

Biju V., Itoh T., Anas A., Sujith A., Ishikawa M., 2008, Semiconductor quantum dots and metal nanoparticles: syntheses, optical properties, and biological applications, *Anal Bioanal Chem.*, 391(7), 2469-95

Blecha A., 2005, Gentechnisches Design bakterieller Hüllproteine für die Technische Nutzung, PhD Thesis, TU Dresden

Blecha A., Zarschler K., Sjollema K.A., Veenhuis M., Rödel G., 2005, Expression and cytosolic assembly of the S-layer fusion protein mSbsC-EGFP in eukaryotic cells, *Microb. Cell Fact.*, 4(28)

Boyd G.T., Yu Z.H., Shen Y.R., 1986, Photoinduced luminescence from the noble metals and its enhancement on roughened surfaces, *Phys. Rev. B Condens. Matter*, 33(12), 7923-36

Brewer S.H., Glomm W.R., Johnson M.C., Knag M.K., Franzen S., 2005, Probing BSA binding to citrate-coated gold nanoparticles and surfaces, *Langmuir*, 21(20), 9303-7

Bruzzone S., Arrighini G.P., Guidotti C., Electromagnetic response behavior of binary metallic nanoparticles: a comparison of results from a few models of different schematicity, *Mat. Sci. and Eng. C*, 23(2), 191-200

Burt J.L., Gutiérrez-Wing C., Miki-Yoshida M., José-Yacamán M., 2004, Noble-metal nanoparticles directly conjugated to globular proteins, *Langmuir*, 20(26), 11778-83

Canepa M., Fox M.A, Whitesell J.K., 2003, The influence of core size on electronic coupling in shell-core nanoparticles: gold clusters capped with pyrenoxylalkylthiolate, *Photochem. Photobiol. Sci.*, 2(11), 1177-80

Cody C.W., Prasher D.C., Westler W.M., Prendergast F.G., Ward W.W., 1993, Chemical structure of the hexapeptide chromophore of the Aequorea green-fluorescent protein, *Biochemistry*, 32(5), 1212-8

Cubbitt A.B., Woollenweber L., Heim. R., 1999, Understanding structure-function relationships in the Aequorea victoria green fluorescent protein, *Methods Cell Biol.*, 58, 19-30

Dulkeith E., Morteani A.C., Niedereichholz T., Klar T.A., Feldmann J., Levi S.A., van Veggel F.C., Reinhoudt D.N., Möller M., Gittins D.I., 2002, Fluorescence quenching of dye molecules near gold nanoparticles: radiative and nonradiative effects, *Phys. Rev. Lett.*, 89(20), 203002

Dulkeith E., Ringler M., Klar T.A., Feldmann J., Muñoz Javier A., Parak W.J., 2005, Gold nanoparticles quench fluorescence by phase induced radiative rate suppression, *Nano Lett.*, 5(4), 585-9

Egelseer E.M., Schocher I., Sleytr U.B., Sára M., 1996, Evidence that an N-terminal S-layer protein fragment triggers the release of a cell-associated high-molecular-weight amylase in Bacillus stearothermophilus ATCC 12980, *J. Bacteriol.*, 178(19), 5602-9

Elghanian R., Storhoff J.J., Mucic R.C., Letsinger R.L., Mirkin C.A., 1997, Selective colorimetric detection of polynucleotides based on the distance-dependent optical properties of gold nanoparticles, *Science*, 277(5329), 1078-81

Englebienne P., 1998, Use of colloidal gold surface plasmon resonance peak shift to infer affinity constants from the interactions between protein antigens and antibodies specific for single or multiple epitopes, *Analyst*, 123, 1599-603

Englebienne P., Van Hoonacker A., Valsamis J., 2000, Rapid homogeneous immunoassay for human ferritin in the Cobas Mira using colloidal gold as the reporter reagent, *Clin. Chem.*, 46(12), 2000-3

Frangioni J.V., 2003, *In vivo* near-infrared fluorescence imaging. *Curr. Opin. Chem. Biol.*, 7(5), 626-34

Gannon C.J., Patra C.R., Bhattacharya R., Mukherjee P., Curley S.A., 2008, Intracellular gold nanoparticles enhance non-invasive radiofrequency thermal destruction of human gastrointestinal cancer cells, *J Nanobiotech.*, 6:2

Hamilton R.G., 1990, Engineered human antibodies as immunologic quality control reagents, *Ann. Biol. Clin.*, 48(7), 473-7

Härtling T., Reichenbach P., Eng L.M., 2007, Near-field coupling of a single fluorescent molecule and a spherical gold nanoparticle, *Optics Express*, 15(20), 12806-17

Hauck T.S., Ghazani A.A., Chan W.C., 2008, Assessing the effect of surface chemistry on gold nanorod uptake, toxicity, and gene expression in mammalian cells, *Small*, 4(1), 153-9

Hawker C. and Fréchet J.M.J., 1990, A new convergent approach to monodisperse dendritic macromolecules, *J. Chem. Soc., Chem. Commun.,* 1010 - 13

Hernandez F.E., Yu S., Garcia M., Campiglia A.D., 2005, Fluorescence lifetime enhancement of organic chromophores attached to gold nanoparticles, *J. Phys. Chem. B*, 109(19), 9499-504

Hirsch L.R., Jackson J.B., Lee A., Halas N.J., West J.L., 2003, A whole blood immunoassay using gold nanoshells, *Anal. Chem.*, 75(10), 2377-81

Horejs C., Pum D., Sleytr U.B., Tscheliessnig R., 2008, Structure prediction of an S-layer protein by the mean force method, *J Chem. Phys.*, 128(6), 0651061-11

Howarter J.A. and Youngblood J.P., 2006, Optimization of silicon silanization by 3-aminopropyltriethoxysilane, *Langmuir*, 22(26), 11142-7

Huang T., and Murray R.W., 2001, Visible luminescence of water-soluble monolayer-protected gold clusters, *J. Phys. Chem. B*, 105(50), 12498-502

Huang X., Jain P.K., El-Sayed I.H., El-Sayed M.A., 2008, Plasmonic photothermal therapy (PPTT) using gold nanoparticles, *Lasers Med. Sci.*, 23(3), 217-28

Huo Q., 2007, A perspective on bioconjugated nanoparticle and quantum dots, *Colloids Surf. B Biointerfaces*, 59(1), 1-10

Imahori H., Kashiwagi Y., Hanada T.,Endo Y., Nishimura Y., Yamazaki I., Fukuzumi S., 2003, Metal and size effects on structures and photophysical properties of porphyrin-modified metal nanoclusters, *J. Mater. Chem.*, 13, 2890 - 8

Jarosch M., Egelseer E.M., Mattanovich D., Sleytr U.B., Sára M., 2000, S-layer gene sbsC of Bacillus stearothermophilus ATCC 12980: molecular characterization and heterologous expression in *Escherichia coli*, *Microbiology*, 146(2), 273-81

Jiang X., 2006, Investigation of the Properties of DNA-Gold-Nanostructure Conjugates, Diploma thesis, TU Dresden

Kain S.R., 1999, Green fluorescent protein (GFP): applications in cell-based assays for drug discovery, *Drug Discov. Today*, 4(7), 304-12

Kannan S., Kolhe P., Raykova V., Glibatec M., Kannan R.M., Lieh-Lai M., Bassett D., 2004, Dynamics of cellular entry and drug delivery by dendritic polymers into human lung epithelial carcinoma cells, *J Biomater Sci. Polym. Ed.*, 15(3), 311-30

Kariuki N.N., Luo J., Maye M.M., Hassan S.A., Menard T., Naslund H.R., Lin Y., Wang C., Engelhard M.H., Zhong C.J., 2004, Composition-controlled synthesis of bimetallic gold-silver nanoparticles, *Langmuir*, 20(25), 11240-6

Kitson S.C., Barnes W.L., Sambles J.R., 1995, Surface-plasmon energy gaps and photoluminescence, *Phys. Rev. B Condens. Matter*, 52(15), 11441-5

Kneen M., Farinas J., Li Y., Verkman A.S., 1998, Green fluorescent protein as a noninvasive intracellular pH indicator, *Biophys. J.*, 74(3), 1591-9

Kolhe P., Khandare J., Pillai O., Kannan S., Lieh-Lai M., Kannan R., 2004, Hyperbranched polymer-drug conjugates with high drug payload for enhanced cellular delivery, *Pharm. Res.*, 21(12), 2185-95

Kreibig U. and Vollmer M., 1995, Optical properties of metal clusters, Springer-Verlag, Berlin

Kubo R., 1962, Electronic properties of metallic fine particles, *J. Phys. Soc. Jpn.*, 17, 975-986

Kühn S., Hakanson U., Rogobete L., Sandoghar V., 2006, Enhancement of single-molecule fluorescence using a gold nanoparticle as an optical nanoantenna, *Phys. Rev. Letters*, 97(1), 017402.1-4

Lee K.-S. and El-Sayed M.A. 2006, Gold and silver nanoparticles in sensing and imaging: Sensitivity of plasmon response to size, shape, and metal composition, *J. Phys. Chem. B*, 110(39), 19220-5

Lévy R., Thanh N.T., Doty R.C., Hussain I., Nichols R.J., Schiffrin D.J., Brust M., Fernig D.G., 2004, Rational and combinatorial design of peptide capping ligands for gold nanoparticles, *J. Am. Chem. Soc.*, 126(32), 10076-84

Li X.-B., Wang H.-Y., Yang X.-D., Zhu Z.-H., Tang Y.-J., 2007, Size dependence of the structures and energetic and electronic properties of gold clusters, *J. Chem. Phys.*, 126(8), 0845051-8

Liou K.-N., 1977, A Complementary theory of light scattering by homogeneous spheres, *Applied Mathematics and Computation*, 3, 331-58

Lowery A.R., Gobin A.M., Day E.S., Halas N.J., West J.L., 2006, Immunonanoshells for targeted photothermal ablation of tumor cells, *Int. J. Nanomedicine.*, 1(2), 149-54

Lue J.-T., 2001, A review of characterization and physical property studies of metallic nanoparticles, *J of Phys. and Chem. of solids*, 62(9), 1599-612

Marinakos S.M., Chen S., Chilkoti A., 2007, Plasmonic detection of a model analyte in serum by a gold nanorod sensor, *Anal. Chem.*, 79(14), 5278-83

Mooradian A., 1969, Photoluminescence of Metals, *Phys. Rev. Lett.*, 22(5), 185-7

Mukherjee P., Bhattacharya R., Wang P., Wang L., Basu S., Nagy J.A., Atala A., Mukhopadhyay D., Soker S., 2005, Antiangiogenic properties of gold nanoparticles, *Clin. Cancer Res.*, 11(9), 3530-3534

Mulvaney P., 1996, Surface Plasmon spectroscopy of nanosized metal particles, *Langmuir*, 12, 788-800

Najlah M. and D'Emanuele A., 2006, Crossing cellular barriers using dendrimer nanotechnologies, *Curr. Opin. Pharmacol.*, 6(5), 522-27

Olander B., Wirsén B., Albertsson A.-C., 2004, Oxygen microwaveplasma treatment of silicon elastomer: Kinetic behavior and surface composition, *J. Appl. Polym. Sci.*, 91(6), 4098-104

Orendorff C.J., Sau T.K., Murphy C.J., 2006, Shape-dependent plasmon-resonant gold nanoparticles, *Small*, 2(5), 636-9

Painter O., Lee R.K., Scherer A., Yariv A., O'Brien J.D., Dapkus P.D., Kim I., 1999, Two-dimensional photonic band-Gap defect mode laser, Science, 284(5421), 1819-21

Pal A., Ghosh S.K., Esumi K., Pal T., 2004, Reversible generation of gold nanoparticle aggregates with changeable interparticle interactions by UV photoactivation, *Langmuir*, 20(3), 575-8

Pastoriza-Santos I., Pérez-Juste J., Carregal-Romero S., Hervés P., Liz-Marzán L.M., 2006, Metallodielectric hollow shells: optical and catalytic properties, *Chem. Asian J.* 1(5), 730-36

Patterson G.H., Knobel S.M., Sharif W.D., Kain S.R., Piston D.W., 1997, Use of the green fluorescent protein and its mutants in quantitative fluorescence microscopy, *Biophys J.*, 73(5), 2782-90

Pavkov T., Egelseer E.M., Tesarz M., Svergun D.I., Sleytr UB., Keller W., 2008, The structure and binding behavior of the bacterial cell surface layer protein SbsC, *Structure*, 16(8), 1226-37

Penn D.R. and Apell P., 1988, Free-electron-like Stoner excitations in Fe, *Phys. Rev. B Condens. Matter*, 38(7), 5051-4

Penn S.G., He L., Natan M.J., 2003, Nanoparticles for bioanalysis, *Curr. Opin. Chem. Biol.*, Vol. 7, Issue 5, 609-615

Philip D., 2008, Synthesis and spectroscopic characterization of gold nanoparticles, *Spectrochim Acta A Mol Biomol Spectrosc.*, 71(1), 80-5

Phillips K.S. and Cheng Q., 2007, Recent advances in surface plasmon resonance based techniques for bioanalysis, *Anal. Bioanal. Chem.*, 837(5), 1831-40

Prendergast F.G. and Mann K.G., 1978, Chemical and physical properties of aequorin and the green fluorescent protein isolated from *Aequorea forskålea*, *Biochemistry*, 17(17), 3448-53

Ravoo B.J., 2008, Nanofabrication with metal containing dendrimers, *Dalton Trans.*, 12, 1533-7

Ringler M., Schwemer A., Wunderlich M., Nichtl A., Kürzinger K., Klar T.A., Feldmann J., 2008, Shaping emission spectra of fluorescent molecules with single plasmonic nanoresonators, *Phys. Rev. Lett.*, 100(20), 203002

Rossi G., Ferrando R., Rapallo A., Fortunelli A., Curley B.C., Lloyd L.D., Johnston R.L., 2005, Global optimization of bimetallic cluster structures. II. Size-matched Ag-Pd, Ag-Au, and Pd-Pt systems, *J. Chem. Phys.*, 122(19), 194309

Rouhana L.L., Jaber J.A., Schlenoff J.B., 2007, Aggregation-resistant water-soluble gold nanoparticles, *Langmuir*, 23(26), 12799-801

Ruban A.V., Skriver H.L., Nørskov J.K., 1999, Surface segregation energies in transition-metal alloys, *Phys. Rev. B*, 59(24), 15990 - 16000

Sára M., Pum D., Schuster B., Sleytr U.B., 2005, S-layers as patterning elements for application in nanobiotechnology, *J. Nanosci. Nanotechnol.*, 5(12), 1939-53

Sharma P., Brown S., Walter G., Santra S., Mougdil B., 2006, Nanoparticles for bioimaging, *Adv. Colloid Interfaces Sci.*, 123-126, 471-485

Shaw C.F., 1999, Gold-based medicinal agents, *Chem. Rev.*, 99(9), 2589-600

Simões L.C., Simões M., Oliveira R., Vieiria M.J., 2007, Potential of the adhesion of bacteria isolated from drinking water to materials, *J Basic Microbiol.*, 47(2), 174-83

Singer J.M. and Plotz C.M., 1956, The latex fixation test. I. Application to the serologic diagnosis of rheumatoid arthritis, *Am. J. Med.*, 21(6), 888-92

Sleytr U.B., Sára M., Messner P., Pum D., 1994, Application potential of 2D protein crystals (S-layers), *Ann. N.Y. Acad. Sci.*, 745, 261-9

Sleytr UB, Huber C, Ilk N, Pum D, Schuster B, Egelseer EM., 2007, S-layers as a tool kit for nanobiotechnological applications, *FEMS Microbiol. Lett.*, 267(2), 131-44

Sokolova V. and Epple M., 2008, Inorganic nanoparticles as carriers of nucleic acids into cells, *Angew. Chem. Int. Ed.*, 47(8), 1382-95

Srnová-Sloufová I., Vlcková B., Snoeck T.L., Stufkens D.J., Matějka P., 2000, Surface-enhanced Raman scattering and surface-enhanced resonance Raman scattering excitation profiles of Ag-2,2'-bipyridine surface complexes and of $[Ru(bpy)3]^{2+}$ on Ag colloidal surfaces: manifestations of the charge-transfer resonance contributions to the overall surface enhancement of Raman scattering, *Inorg. Chem.*, 39(16), 3551-9

Stuart D.A., Haes A.J., Yonzon C.R., Hicks E.M., Van Duyne R.P., 2005, Biological applications of localized surface plasmonic phenomenae, *IEE Proc.-Nanobiotechnol.*, 152(1), 13-32

Szmacinski H., Lakowicz J.R., Johnson M.L., 1994, Fluorescence lifetime imaging microscopy: homodyne technique using high-speed gated image intensifier, *Methods Enzymol.*, 240, 723-748

Takeda Y., Kondow T., Mafuné F., 2006, Degradation of protein in nanoplasma generated around gold nanoparticles in solution by laser irradiation, *J Phys. Chem. B*, 110(5), 2393-7

Talley C.E., Jackson J.B., Oubre C., Grady N.K., Hollars C.W., Lane S.M., Huser T.R., Nordlander P., Halas N.J., 2005, Surface-enhanced Raman scattering from individual au nanoparticles and nanoparticle dimer substrates, *Nano Lett.*, 5(8),1569-74

Tam F., Goodrich G.P., Johnson B.R., Halas N.J., 2007, Plasmonic enhancement of molecular fluorescence, *Nano Letters*, 7(2), 496-501

Templeton A.C., Cliffel D.E., Murray R.W., 1999, Redox and fluorophore functionalisation of water-soluble, tiopronin-protected gold clusters, *J. Am. Chem. Soc.*, 121(30), 7081–9

Templeton A.C., Pietron J.J., Murray R.W., Mulvaney P., 2000, Solvent refractive index and core charge influences on the surface Plasmon absorbance of alanethiolate monolayer-protected gold clusters, *J. Phys. Chem.*, 104, 564-70

Thomas K.G. and Kamat P.V., 2000, Making gold nanoparticles glow: enhanced emission from a surface-bound fluoroprobe, *J. Am. Chem. Soc.*, 122 (11), 2655–6

Thomas K.G., Zajicek, J., Kamat P.V., 2002 Surface Binding Properties of Tetraoctylammonium Bromide-Capped Gold Nanoparticles, *Langmuir*, 18(9), 3722-7

Tkachenko A., Xie H., Franzen S., Feldheim D.L., 2005, Assembly and characterization of biomolecule-gold nanoparticle conjugates and their use in intracellular imaging, *Methods Mol. Biol.*, 303, 85-99

Tomalia, D.A., Baker, H., Dewald, J., Hall, M., Kallos, G., Martin, S., Roeck, J., Ryder, J. and Smith, P., 1985, A new class of polymers: starburst-dendritic macromolecules, *Polymer J.*, 17(1), 117–132

Tsukruk V.V., Sidorenko A., Yang H., 2002, Polymer nanocomposite coatings with non-linear elastic response, *Polymer*, 43(5), 1695-9

VanEngelenburg S.B. and Palmer A.E., 2008, Fluorescent biosensors of protein function, *Curr. Opin. in Chem. Biotech.*, 12(1), 60-5

Voisin C., Christofilos D., Del Fatti N., Vallee F., Prevel B., Cottancin E., Lerme J., Pellarin M., Broyer M., 2000, Size-dependent electron-electron interactions in metal nanoparticles, *Phys. Rev. Lett.*, 85(10), 2200-3

Wang D.Y., Huang Y.C., Chiang H., Wo A.M., Huang Y.Y., 2007, Microcontact printing of laminin on oxygen plasma activated substrates for the alignment and growth of Schwann cells, *J. Biomed. Mater. Res. B Appl. Biomater.*, 80(2), 447-53

Weiss S., 1999, Fluorescence spectroscopy of single biomolecules, *Science*, 283(5408), 1676-83

Wilcoxon J.P., Provencio P.P., Samara G.A., 2001, Synthesis and optical properties of colloidal germanium nanocrystals, *Phys. Rev. B*, 64(3), 035417-035426

Willets K.A. and Van Duyne R.P., 2007, Localized surface plasmon resonance spectroscopy and sensing, *Annu. Rev. Phys. Chem.*, 58, 267-97

Wolinsky J.B. and Grinstaff M.W., 2008, Therapeutic and diagnostic applications of dendrimers for cancer treatment, *Adv. Drug Deliv. Rev.*, 60(9), 1037-55

Xu Z.P., Zeng Q.H., Lu G.Q., Yu A.B., 2006, Inorganic nanoparticles as carriers for efficient intracellular delivery, *Chem. Eng. Sci.*, 61(3), 1027-40

Yguerabide J. and Yguerabide E.E., 1998, Light-scattering submicroscopic particles as highly fluorescent analogs and their use as tracer labels in clinical and biological applications, *Anal Biochem.*, 262(2), 137-56

Zhang Q., Myint A., Liu L., Ge X., Cui H., 2004, Flow injection-chemiluminescence determination of puerarin in pharmaceutical preparations, J *Pharm. Biomed. Anal.*, 36(3), 587-92

Zheng J., Zhang C., Dickson R.M., 2004, Highly fluorescent, water soluble, size-tunable gold quantum dots, *Phys. Rev. Letters*, 93(7), 0774021-4

Zhu J., 2005, Theoretical study of the optical absorption properties of Au-Ag bimetallic nanospheres, *Physica E*, 27(2), 296-301

Appendix

Preparation of 0.1 M potassium phosphate buffer

Table 2. Volume ratio of solution A and B for the desired pH

pH	Solution A (ml)	Solution B (ml)	pH	Solution A (ml)	Solution B (ml)
5.7	93.5	6.5	6.9	45.0	55.0
5.8	92.0	8.0	7.0	39.0	61.0
5.9	90.0	10.0	7.1	33.0	67.0
6.0	87.7	12.3	7.2	28.0	72.0
6.1	85.0	15.0	7.3	23.0	77.0
6.2	81.5	18.5	7.4	19.0	81.0
6.3	77.5	22.5	7.5	16.0	84.0
6.4	73.5	26.5	7.6	13.0	87.0
6.5	68.5	31.5	7.7	10.5	90.5
6.6	62.5	37.5	7.8	8.5	91.5
6.7	56.5	43.5	7.9	7.0	93.0
6.8	51.0	49.0	8.0	5.3	94.7

Preparation of 0.1 M potassium acetate buffer

Table 3. Volume ratio of solution A and B for the desired pH

pH	Solution A (ml)	Solution B (ml)
3.6	46.3	3.7
3.8	44.0	6.0
4.0	41.0	9.0
4.2	36.8	13.2
4.4	30.5	19.5
4.6	25.5	24.5
4.8	20.0	30.0
5.0	14.8	35.2
5.2	10.5	39.5
5.4	8.8	41.2
5.6	4.8	45.2

LSPR peak of the gold and gold/silver alloyed nanoparticles

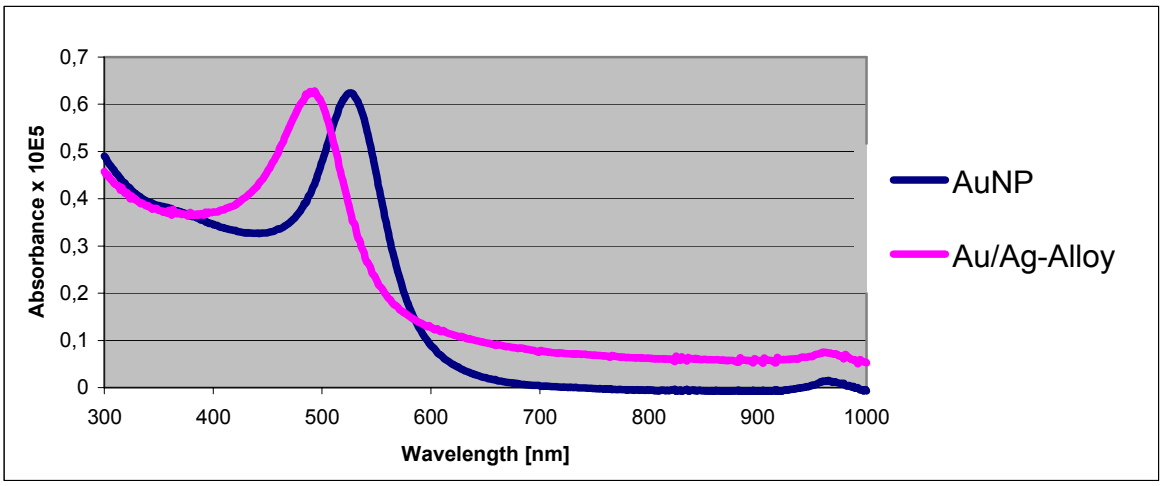

Figure 36. LSPR peak of 60 nm diameter Au nanoparticles (blue) at 520 nm and of 30 nm diameter Au/Ag alloyed nanoparticles (pink).

Emission and excitation spectra of the autofluorescent Au nanoparticles and fluorescein

Note that these nanoparticles have an average diameter of 2 nm and therefore do not exhibit LSPR peak. Therefore, only the fluorescence spectra are provided. Also, the dendrimer structures are labelled with fluorescein, so the green fluorescence signal measured from the dendrimers actually refer to the signal from fluorescein.

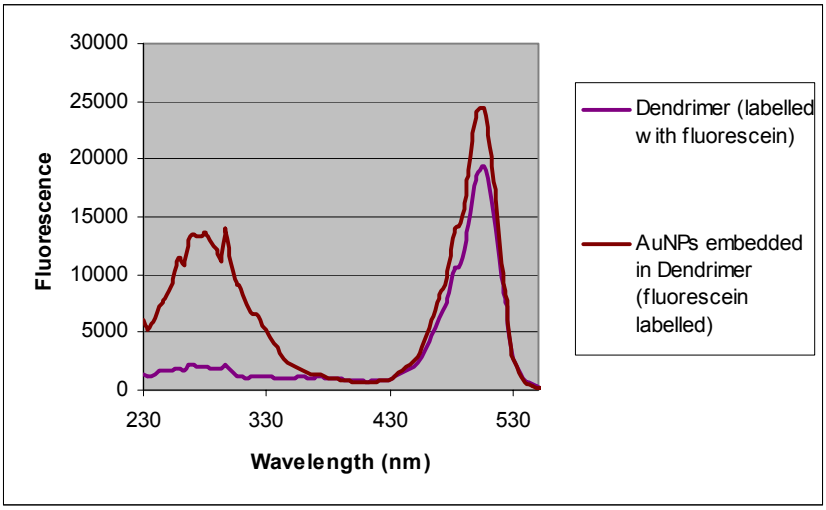

Figure 37. Excitation spectra of the autofluorescent Au nanoparticles embedded in dendrimer (dark red line) and of dendrimer (purple line). The peak at 270 nm corresponds to the excitation peak of AuNPs and the peak around 490 to the fluorescein.

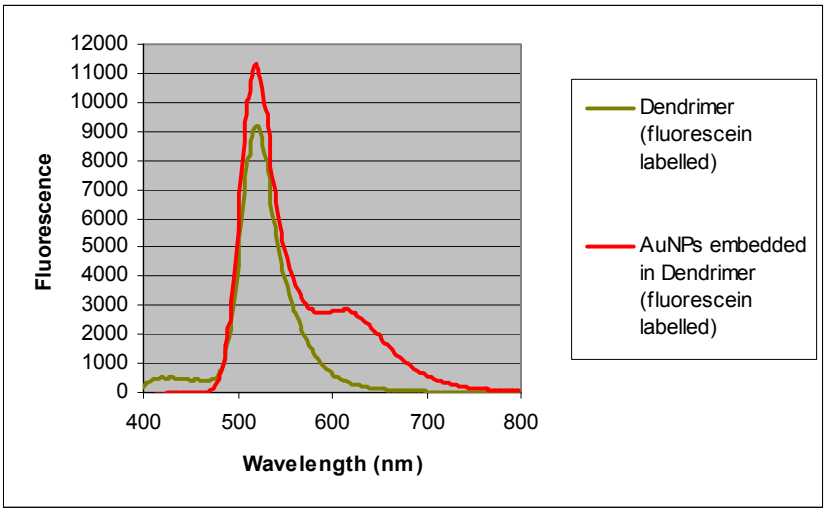

Figure 38. Emission spectra of the autofluorescent Au nanoparticles embedded in dendrimer (green line) and of dendrimer (red line). The peak at 610 nm corresponds to the emission peak of AuNPs and the peak around 520 to the fluorescein.

Emission and excitation spectra of the fluorescent proteins

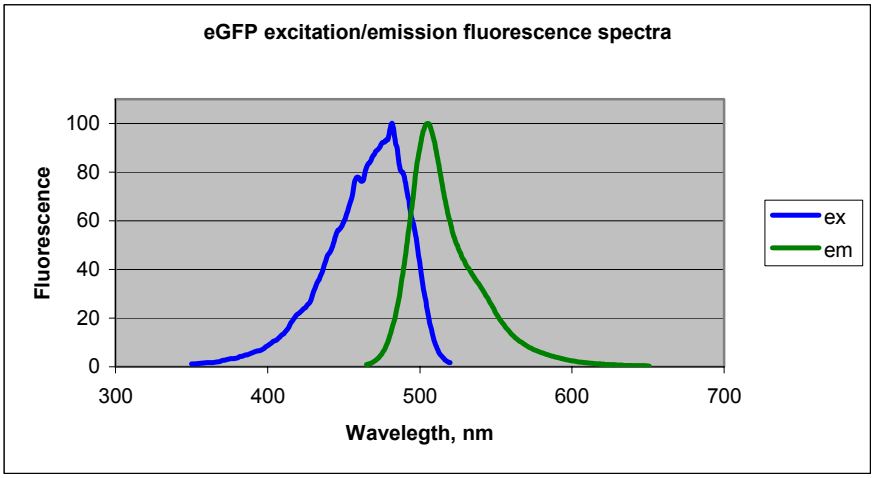

Figure 39. Excitation (blue line) and emission spectra (green line) of eGFP.

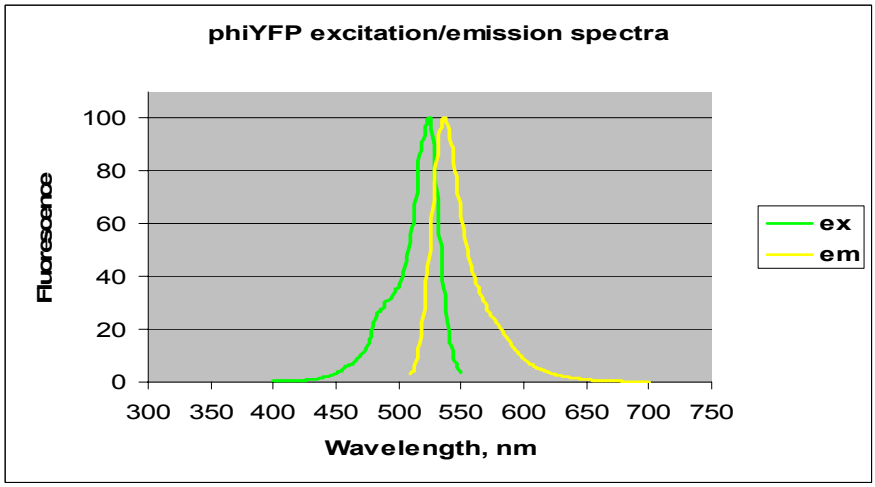

Figure 40. Excitation (green line) and emission spectra (yellow line) of rPhiYFP.

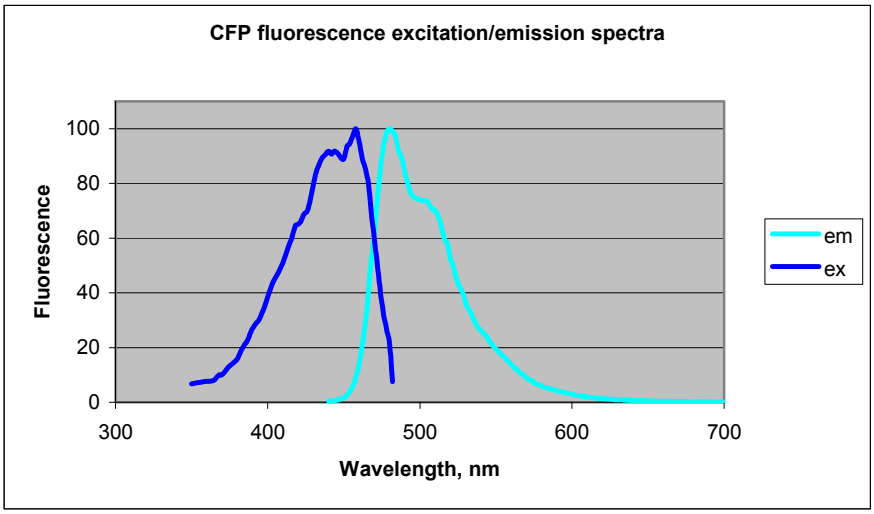

Figure 41. Excitation (navy blue line) and emission spectra (turquoise line) of CFP

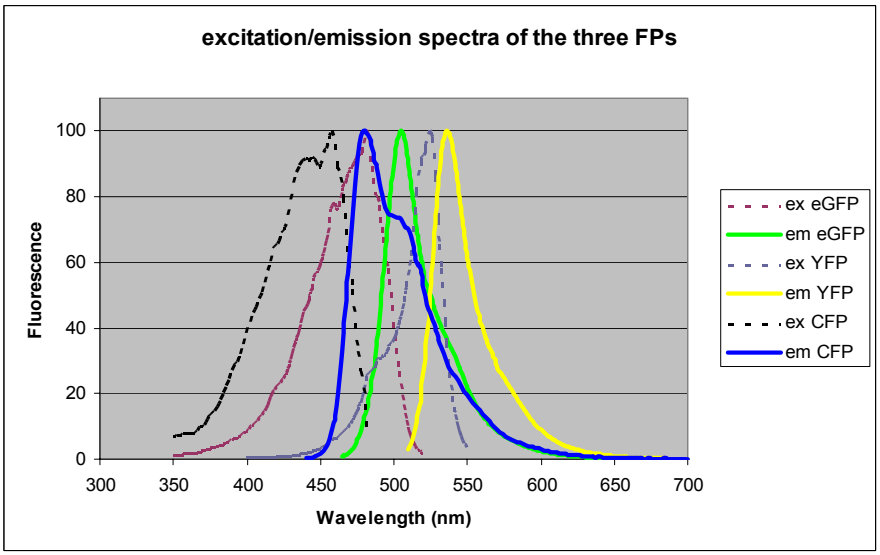

Figure 42. Overlayed excitation and emission spectra of the three fluorophores used. Normalisation of the relative intensities was carried out by Origin (OriginLab Corporation).

Table 4. Excitation and emission maxima of fluorescent proteins

Protein	excitation max (nm)	emission max (nm)
eGFP	490	520
rPhiYFP	515	527
CFP	434	474

High yield production of fluorescent proteins

For the analysis of the effect of metallic nanoparticles on biological matter, eGFP was chosen as the initial model. In order to produce eGFP in high yield a glutathione-S-transferase (GST)-eGFP hybrid protein was engineered. The GST tag allows easy isolation of the fusion protein by use of glutathione beads, as explained previously. Another eGFP fusion protein, namely SbsC-eGFP, was chosen as a second model because of the intrinsic ability of this S-layer protein to form uniform tube-like structures on surfaces *in vitro* [Blecha *et al.*, 2005]. By taking advantage of this property of SbsC, it should be possible to obtain a protein assembly on a surface with uniformly distributed eGFP molecules for microscopic analysis.

Cloning of GST-eGFP

DNA sequence of GST was PCR amplified from a pGEX3 vector and then cloned into the pET-17b expression vector which contains the *eGFP* gene under the control of the T7 promoter. The resulting construct was cloned into *E.coli* strain BL21 DE3α. Transformants were selected on LB medium containing Ampicillin.

Expression of GST-eGFP and isolation of eGFP

A correct transformant was grown overnight in a pre-culture and then inoculated into LB, whereby expression was induced by IPTG. To find the optimum induction time aliquots from the cell suspension at different incubation times were taken at time intervals, protein was isolated, and analysed by electrophoresis on a 12% SDS gel. The presence of the fusion protein was verified by Western blot analysis. The highest expression was observed after overnight incubation, as evidenced by the strongest eGFP band (fig 43). eGFP was separated from GST via acTEV protease digestion (fig 44).

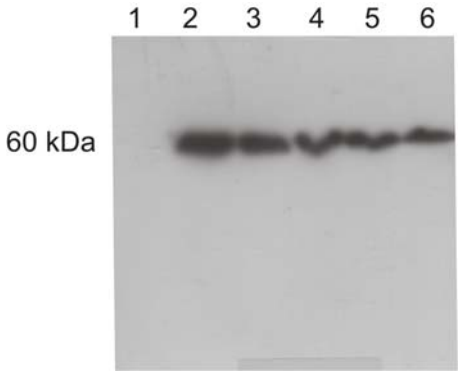

Figure 43. Kinetics of GST-eGFP expression. Lysates from uninduced culture (lane 1), o/n grown culture (lane 2), cultures grown for 8 (lane 3), 6 (lane 4), 4 (lane 5), and 2 (lane 6) hours were analysed by SDS-PAGE and detected with antiGFP antibodies.

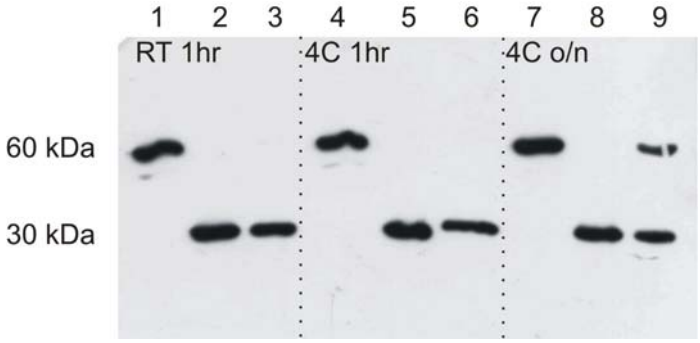

Figure 44. Efficiency of AcTEV protease digestion under different conditions for the isolation of eGFP. GST-eGFP fusion protein was digested at room temperature for one hour (RT 1hr), at 4ºC for one hour (4ºC 1hr), and at 4ºC overnight (4ºC o/n). Lanes 1, 4, and 7: undigested samples. Samples digested with protease in the presence (lanes 2, 5, and 8) or absence (lanes 3, 6, and 9) of protease inhibitor (AEBSF).

Theoretical pI value of eGFP was calculated using Swissprot to be 5.2. A pI value of 5.1 was verified experimentally via 2D-SDS-PAGE, with isoelectric focusing in the 1st separation (data not shown).

Expression and isolation of SbsC-eGFP

E.coli strain BL21 DE3α was transformed with the expression vector pet-17b containing SbsC-eGFP[Blecha A., 2005] and used for the expression of the respective protein. The isolation of the correct protein was verified by 12% SDS-PAGE followed by Western blotting and detection with antiGFP antibodies (data not shown).

Acknowledgements

I am very grateful to Prof. W. Pompe and Prof. G. Rödel for giving me the opportunity to work on this thesis in such an exciting area of science, as well as for all the support and motivation they have provided.

To Jörg for the valuable discussions and support.

To Kai and Udo for the critical and helpful comments.

To Msau, Nuriye, Karolina, Pavel, Kevin and Veronika not only for the warm and friendly atmosphere in the lab and in the office but also for all the nice time we had outside work.

To Mathias for providing the nanoparticles, the backbone of this thesis; and Dr. Appelhans for the dendrimers and for the related discussions.

To Anja Blüher and Thomas Hanke for the excellent various microscopy images.

I would like to thank Marlis and to all the members of the Rödel lab for support and good working atmosphere.

To Ebru and Emral for making living in Dresden so much fun.

To my mother for strong motivating support and understanding.

Curriculum Vitae

Personal	**Adress:**	Siebekingstr. 10, 01309 Dresden, Germany
	Phone:	+49 (0)176 237 111 51
	e-mail:	fyigita@gmail.com
	Date and place of birth:	17.01.1982, Ankara
	Nationality:	Turkish
Education	**2004 – Present:**	PhD at the University of Technology Dresden under supervision of Prof. W. Pompe and G. Rödel, Dresden/Germany
	2000 – 2004:	B.Sc., Molecular Biology and Genetics, Middle East Technical University, Ankara/Turkey
	1996 – 2000:	Gazi Anatolian High School, Ankara/Turkey
Experience	**Sept 2004 – Present:**	PhD thesis project, University of Technology Dresden: Interaction of metal nanoparticles with fluorophores and their effect on fluorescence
	Oct 2003 – June 2004:	Bachelor's thesis project: Middle East Tech. University, Dept. of Mol. Biol. and Genetics: Isolation and characterization of yeast killer protein K10
	Jul 2003 – Aug 2003:	Summer Practice in the Basic Oncology Dept. Hacettepe University, Ankara/Turkey
Conferences	**Oct 2006:**	Nanotechnology Research Forum, Middle East Technical Universtiy, Ankara/Turkey
	March 2005:	Abstract and paper presentation in the Biophotonik Symposium, Jena/Germany: Bioconjugated metal nanoparticles for biophotonic studies, Aksoy F.Y., Gorbunoff A., Krause-Buchholz, U., Lakatos M., Pompe W., Rödel G.

Selbständigkeitserklärung

Hiermit versichere ich, dass ich die vorliegende Arbeit ohne unzulässige Hilfe Dritter und ohne Benutzung anderer als der angegebenen Hilfsmittel angefertigt habe; die aus fremden Quellen direkt oder indirekt übernommenen Gedanken sind als solche kenntlich gemacht. Die Arbeit wurde bisher weder im Inland noch im Ausland in gleicher oder ähnlicher Form einer anderen Prüfungsbehörde vorgelegt.

Die vorliegende Arbeit wurde am Institut für Genetik der TU Dresden unter wissen-schaftlicher Betreuung von Herrn Prof. Dr. rer. nat. habil. G. Rödel angefertigt.

Die Promotionsordnung wird anerkannt.

Dresden, den 19.12.2008